Geophys. J. R. astr. Soc. (1977) **50**, 495–552

Free–air gravity anomalies in the world's oceans and their relationship to residual elevation

James R. Cochran and Manik Talwani *Lamont-Doherty Geological Observatory and the Department of Geological Sciences, Columbia University, Palisades, New York 10964, USA*

Received 1977 February 7; in original form 1976 August 16

Summary. Surface-ship gravity measurements were used to obtain 5 × 5° average free–air gravity anomalies over much of the world's oceans. Comparison of the surface data with the recent GEM 6 'combination' field shows the combination solution to be in reasonable agreement with the surface data in most areas in the general location and amplitude of major features of the Earth's gravity field. There is, however, significant disagreement on the location of extrema and on the exact values at specific points. It is thus necessary to use surface data to make detailed studies of the relationship of the gravity field to surface features at wavelengths of less than 4000 km. Mid-ocean ridges are consistently characterized by a gravity maximum. The gravity anomaly across mid-ocean ridges can be described by an empirical 1 × 1° average gravity–age relationship which shows a positive gravity anomaly of about 25 mgal falling off to zero by about 40 my. The observed gravity–age relationship is generally compatible with current thermal models of the lithosphere. The empirical gravity–age curve was removed from the free–air anomalies to produce residual gravity anomalies which can be compared to similarly obtained residual depth anomalies. A correlation between the two is found over some features. The most prominent of these are intermediate wavelength positive features associated with areas of extensive off-ridge volcanism. This applies not only to recently active areas but also to inactive areas such as Bermuda and aseismic ridges. On the other hand, areas of unusual elevation and volcanic activity located at a mid-ocean ridge crest such as Iceland and the Azores do not have a corresponding gravity amomaly at intermediate wavelengths. The long-wavelength component of the Earth's gravity field is characterized by large areas in which significant anomalies of constant sign are found. There is no apparent relationship between the long-wavelength gravity anomalies and oceanic depths. If the gravity anomalies have their origin within the asthenosphere, the lithosphere must in effect be decoupled from the main body of the asthenosphere. This could result from the effects of a strongly depth-dependent viscosity on the convection pattern under the elastic plates.

1 Introduction

It is convenient to think of the gravity field in the oceans as consisting of short wavelength (up to a few hundred kilometres), intermediate wavelength (a few hundred to a few thousand kilometres) and long wavelength (larger than those described by spherical harmonic coefficients of degree and order 10) components. The short-wavelength components are generally associated with bottom, or where the bottom is covered with sediments, basement, topography (Talwani, Poppe & Rabinowitz 1972) and there is little argument that these anomalies are supported by the strength of the lithosphere.

Our study will be concerned largely with the intermediate and long wavelength component of the Earth's gravity field as obtained from surface-ship gravity measurements.

In order to justify such a study, it is necessary to examine whether or not satellite-determined gravity data and the so called 'combination' solutions provide an adequate description of the gravity field and thus whether it is necessary to perform the laborious task of compiling surface ship gravity data. It is also necessary to demonstrate that the gravity values at these intermediate and long wavelengths are large enough to be tectonically significant.

Studies of satellite orbits can provide spherical harmonic coefficients up to degree and order 10 (wavelength > 4000 km) as well as certain higher order resonant terms (Gaposhkin & Lambeck 1971; Khan 1974) and the Earth's gravity field at these very long wavelengths appears to be well determined. Combination solutions have been constructed which are complete to sixteenth degree and order (Gaposchkin & Lambeck 1970, 1971; Lerch *et al.* 1974) or eighteenth degree and order (Gaposchkin 1973, 1974). The higher order harmonics in these solutions are largely determined from surface measurements (Gaposchkin & Lambeck 1971) and there are significant differences between the various solutions (Khan 1974). The surface data coverage available for the combination solutions is not uniform and is particularly sparse in the southern oceans. Thus, while satellite solutions can give an accurate picture of the very long wavelength field, it is necessary to use surface data to study features with wavelengths of less than about 4000 km. In studying the gravity data we have principally used values of free–air gravity averaged over $5 \times 5^\circ$ squares. Wavelengths larger than about 1000 km can be represented by this method. Where adequate surface ship gravity data exist, these values yield considerably more detail than the present 'combination' solutions.

The second point concerns the question of whether the intermediate and long wavelength gravity anomalies are significant in magnitude. One of the earliest results of gravity measurements at sea was the existence of large regions in which the isostatic anomalies are consistently of one sign (Vening Meinesz 1934, 1948). Vening Meinesz argued that another of the early discoveries of gravity exploration, the general prevalence of isostasy, along with the low finite strength of the asthenosphere, required these isostatic anomalies to be small and that anomalies of more than 10–20 mgal cannot generally exist over areas of 10° on a side (Vening Meinesz 1961; Heiskanen & Vening Meinesz 1958). The earliest regional treatments of gravity data on an ocean-wide basis (Talwani, Heezen & Worzel 1961; Talwani & Le Pichon 1969; Le Pichon & Talwani 1969) and satellite studies (Kaula 1966; Rapp 1968; Gaposchkin & Lambeck 1970, 1971) have, however, shown that large free–air and isostatic anomalies do exist over wide regions. Kaula (1969a, 1972a) has catalogued the major features in the satellite gravity field and has pointed out (Kaula 1969b) that there are at least 20 features in the Earth's gravity field which imply an anomalous mass greater than that of Mare Imbrium, the largest of the lunar mascons.

The large density inhomogeneities implicit in the presence of large gravity anomalies will result in large shear stresses, probably greater than can be supported by the lithosphere (McKenzie 1967; Lambeck 1972). Bott (1971) has suggested that the observed long-

wavelength anomalies could result from small undulations in the depth to the olivine–spinel phase transition at about 400 km depth in the mantle. He also proposed that the mantle beneath the phase transition has sufficient strength to maintain the undulations for 10–100 my. The more widely held view, however, is that the anomalies have their origin within the asthenosphere and, since the asthenosphere has no long-term strength, that they are maintained by convective flow.

If the long-wavelength gravity anomalies are an indication of flow in the asthenosphere, then it has been argued (McKenzie 1967) that the flow would exert stresses on the lithosphere producing surface deformations and that some correlation would exist between the gravity anomalies and surface deformations. McKenzie, Roberts & Weiss (1974) have carried out two-dimensional numerical experiments in which the mantle is modelled as a constant viscosity Newtonian fluid heated from within and/or below and in which parameters were chosen to simulate their best estimate of conditions in the mantle. They found that this highly simplified model predicted that surface deformation and free–air gravity anomalies are directly correlated and that the relationship has a slope of 30 mgal/km.

Anderson, McKenzie & Sclater (1973) have attempted to demonstrate the correlation of the satellite gravity field and topography by examining the variation of the two parameters along the crest of the mid-ocean ridge system using the Gaposchkin & Lambeck (1971) SE II combination solution which gives gravity values corresponding to $10 \times 10^\circ$ averages, and $1 \times 1^\circ$ depth averages from various sources averaged over 5° lengths of ridge crest. They claimed to have found a dependence between free–air gravity anomalies and crestal depth with the slope predicted by the numerical models of McKenzie *et al.* (1974). They considered their findings to be evidence supporting flow in the asthenosphere.

Sclater, Lawver & Parsons (1975) considered convection at a smaller scale and attempted to demonstrate the two-dimensional correlation of free–air gravity anomalies and 'residual depth anomalies' in the North Atlantic. They compared $5 \times 5^\circ$ average free–air gravity anomalies and residual depth anomalies and claimed a good visual correlation and satisfactory statistical correlation, again with the slope predicted by McKenzie *et al.* (1974). They interpreted this result as providing support for a proposal by Richter (1973) that convection occurs on two scales in the mantle, a larger scale necessary to conserve mass and a smaller scale needed to maintain the nearly constant heat flow found in the deep ocean basins.

We will attempt, in this study, to use the available surface ship gravity data to examine the relationship between gravity anomalies and elevation more intensively and extensively than was possible in previous studies. Specifically, we have two major objectives in this study:

(1) We wish to examine the gravity anomalies associated with the mid-ocean ridge system, one of the most prominent topographic features on the Earth. In particular, we wish to determine whether it is possible to empirically establish a general relationship between gravity anomaly and age similar to the manner in which Sclater, Anderson & Bell (1971) established an empirical relationship between depth and age. If such an anomaly exists and is found to be associated with the evolution of the lithosphere as it is transported away from the spreading centre, then it is sensible to remove it from the observed gravity field before comparisons are made between gravity anomalies and deviations from the empirical depth–age relationship (residual elevation or depth anomalies).

(2) We wish to study in detail the relationship between the residual gravity anomalies and residual elevation using the surface gravity data. We will examine the data in all of the oceans in order to determine, first of all, whether there is a relationship between the two data sets and, secondly, if so, at what wavelengths and in what geological and tectonic settings it is manifested.

2 Free–air gravity anomaly map

We have compiled 5 x 5° average free–air gravity anomalies over much of the world's oceans and present this data in Fig. 1 in the form of a map contoured at 10 mgal intervals. The 5 x 5° averages in the various oceans are tabulated in Appendix 3. This map represents the first map of the regional gravity field in the eastern Pacific, south-eastern Indian and south-western Indian Oceans, and a substantial increase in the amount of data in the South Atlantic Ocean to that available for the gravity anomaly map given by Talwani & Le Pichon (1969). The gravity anomalies in Fig. 1 and throughout this study are referred to the hydrostatic figure of the Earth (flattening 1/299.7). This ellipsoid was chosen because it represents the stress free figure of the Earth and departures from it must be supported in some manner. The 1 x 1° and 5 x 5° anomalies given in Appendices 1 and 3 are, however, referred to the International Ellipsoid (flattening 1/297) in order that they be compatible with previously published data sets. A reference ellipsoid is defined by the J_2 and J_4 terms in a harmonic expansion and so the choice of a particular ellipsoid will effect only the very longest wavelength anomalies. At the wavelengths with which we are primarily concerned, the difference between two ellipsoids appears as a slowly varying level change. It is not difficult to transform anomalies from one ellipsoid to another and Talwani *et al.* (1972) present a plot of the difference between the hydrostatic, best fitting and International ellipsoids as a function of latitude.

It may be argued that 5 x 5° averages are a poor way to represent the gravity field. Instead, for instance, the available data could have been used to obtain spherical harmonic coefficients to, say, degree and order 36 and then gravity anomalies corresponding to various spherical harmonics degrees can be conveniently determined. While such a procedure would undoubtedly be more elegant, we doubt that, in view of the present incomplete state of mapping of the gravity field of the Earth, it would yield any great advantage over simple 5 x 5° averages in areas of limited extent.

2.1 SOURCES OF DATA AND CONSTRUCTION OF MAP

The procedures that we have adopted to obtain 5 x 5° averages are somewhat arbitrary but are probably best suited to the data sets we had at our disposal.

We started by obtaining free–air anomaly averages over 1 x 1° squares. Wherever existing gravity maps were available or the density of data allowed the gravity field to be easily mapped, 1 x 1° averages were obtained from free–air gravity anomaly maps. In other areas, they were obtained by averaging gravity data along ships' tracks. There are several advantages to obtaining averages from maps. First, the process of making a map reveals segments of track along which the data are in error and quite often, due to the systematic nature of errors in gravity measurements, analysis of track crossings allows errors to be corrected and the data to be used. Talwani *et al.* (1972) discuss this procedure in some detail. In addition, maps have the advantage of giving the areal pattern more accurately since bathymetric data can be used to extend the contours away from the track and to interpolate between tracks. There is also a natural tendency for individual cruises to concentrate on unusual features and thus not necessarily be representative.

Talwani *et al.* (1972) compiled 1 x 1° free–air gravity anomalies over much of the western North Atlantic, Caribbean Sea, Gulf of Mexico, and North America. These values, with an improved set of values in Mexico from Woollard, Machesky & Caldera (1969), were generally adopted. However, comparison with more recent data resulted in changing some of the Talwani *et al.* (1972) values, particularly on the Mid-Atlantic Ridge flank where their data were rather sparce.

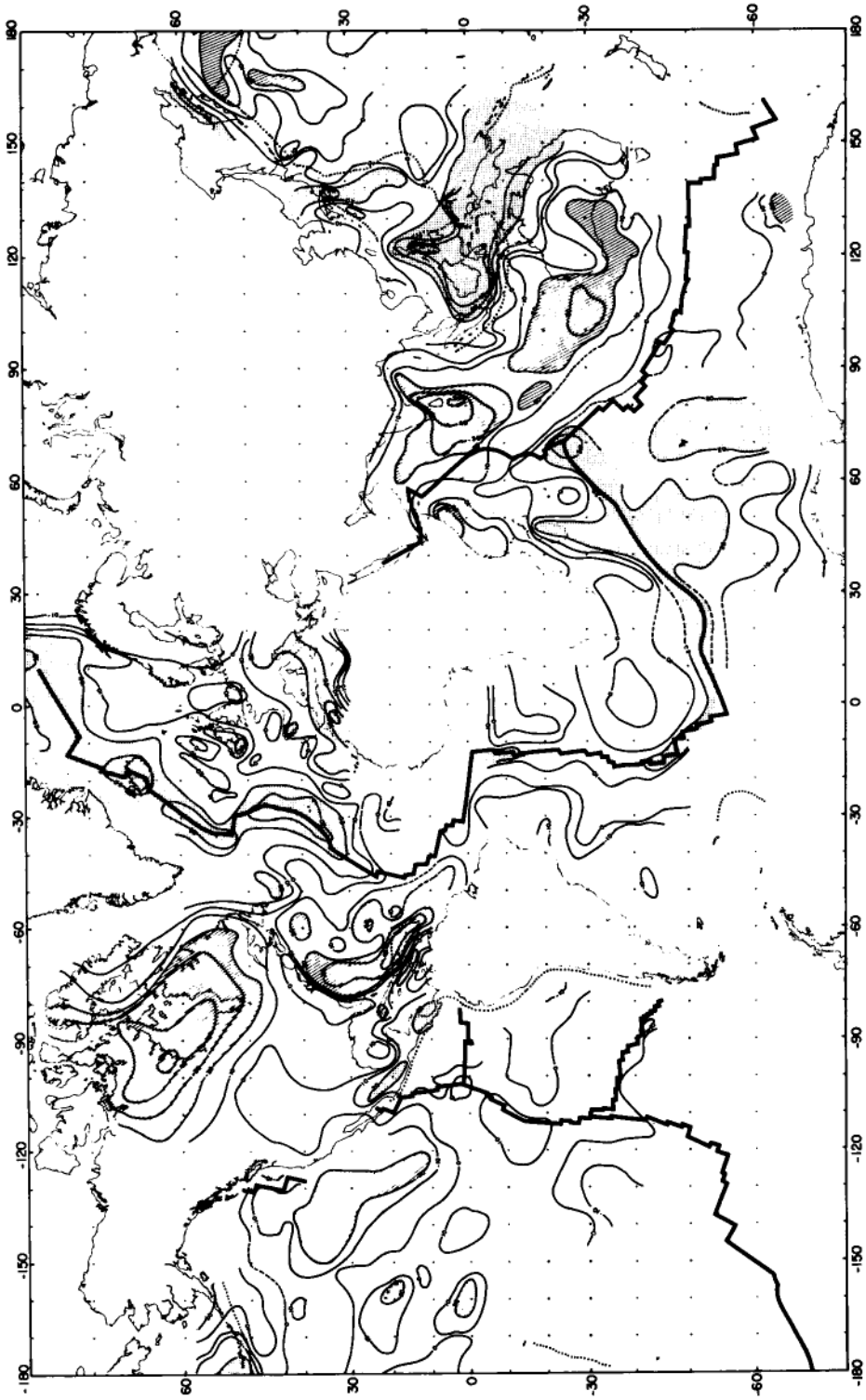

Figure 1. 5 × 5° average free–air gravity map of the Earth, contoured at 10-mgal intervals. Anomalies are referred to the hydrostatic figure of the Earth (flattening = 1/299.7). The method of preparing averages and sources of data are discussed in the text. The heavy solid line marks the location of the mid-ocean ridge system and dotted lines the location of deep-sea trenches. Areas with anomalies greater than 20 mgal are stippled. Areas with anomalies more negative than −20 mgal are ruled.

One degree averages were obtained north of 60° N from the free–air gravity map of Talwani & Grønlie (1976), and from 15° N to 6° S in the western basin of the Atlantic Ocean from a revised version of the map in Cochran (1973) (Rabinowitz & Cochran 1977). Both of these maps have a 25 mgal contour interval with frequent spot values.

A free–air gravity map of the northern Reykjanes Ridge is given by Talwani, Windisch & Langseth (1971), of the southern Reykjanes Ridge by Fleischer (1971) and of the Bedford Institute survey area near 45° N by Woodside (1972). Averages were obtained from their maps in the same manner as in other areas.

Coron (1973) compiled 1 x 1° averages in the region 20° W–20° E, 30° N–70° N using various sources of data available to the International Gravity Bureau. Most of the values over the Atlantic Ocean were evaluated as having a uncertainty of from 5 to 10 mgal. These values were adopted in the region east of 20° W from 30°N to 60°N.

1 x 1° averages were obtained in remaining areas of the North Atlantic by using all of the available data to construct preliminary contour maps which were used, along with the annotated values, to obtain averages in the same manner as where finished maps were available. The areas treated in this manner are the southern Labrador Sea and the central portion of the North Atlantic (roughly 20° W–45° W) from 15° N to 60° N. No value was obtained for 1° squares for which sufficient data was not available. The 1 x 1° average free–air gravity anomalies are tabulated in Appendix 1.

A free–air gravity map of the Indian Ocean north of about 30° S has been prepared by Talwani & Kahle (1975) and 1 x 1° averages were determined from the map by Kahle & Talwani (1973). These 1 x 1° averages were converted to 1 x 1° averages referred to the hydrostatic figure of the Earth.

All of the 1 x 1° averages obtained as above were then averaged to obtain the 5 x 5° average free–air gravity anomalies shown in Fig. 1. No 5 x 5° average was calculated for squares which did not have a minimum of thirteen 1 x 1° values.

In other areas 5 x 5° averages were obtained as follows:

A series of free–air gravity maps of the central and north-western Pacific Ocean have been constructed (Watts & Talwani 1975; Watts 1975, 1976b; Watts & Kogan, in preparation) and 5 x 5° averages which were constructed in a manner similar to that described above for these areas were provided by A. B. Watts. The IDOE Surveyor SEAMAP data (Elvers *et al.* 1971) were used along with Lamont-Doherty data to construct 5 x 5° averages in the north-eastern Pacific. The 5 x 5° gravity anomalies shown over Australia in Fig. 1 were obtained from 1 x 1° averages compiled by Mather (1969).

It was necessary to follow a somewhat different procedure in the South Atlantic, South-east Indian Ocean, and in the eastern Pacific where data are more meager. A 1° (110 km) running average was calculated along the ship profiles and these values were smoothed and averaged over 500 km to approximate 5° averages. The procedure of obtaining averages from profiles has obvious difficulties, but in these areas the data did not allow any other procedure. Fortunately, many of the long profiles used were run nearly perpendicular to the regional topographic trends. The 5 x 5° averages are tabulated in Appendix 3.

3.2 COMPARISON OF SURFACE AND 'COMBINATION' FIELDS

Several global gravity combination solutions employing satellite data and limited surface data have recently been developed. They are expressed mainly by spherical harmonic coefficients of degree and order 16 and under. We show, in Fig. 2, the gravity anomalies referred to the hydrostatic figure calculated from the coefficients of one of these solutions, the Goddard Space Flight Center GEM 6 (Lerch *et al.* 1974).

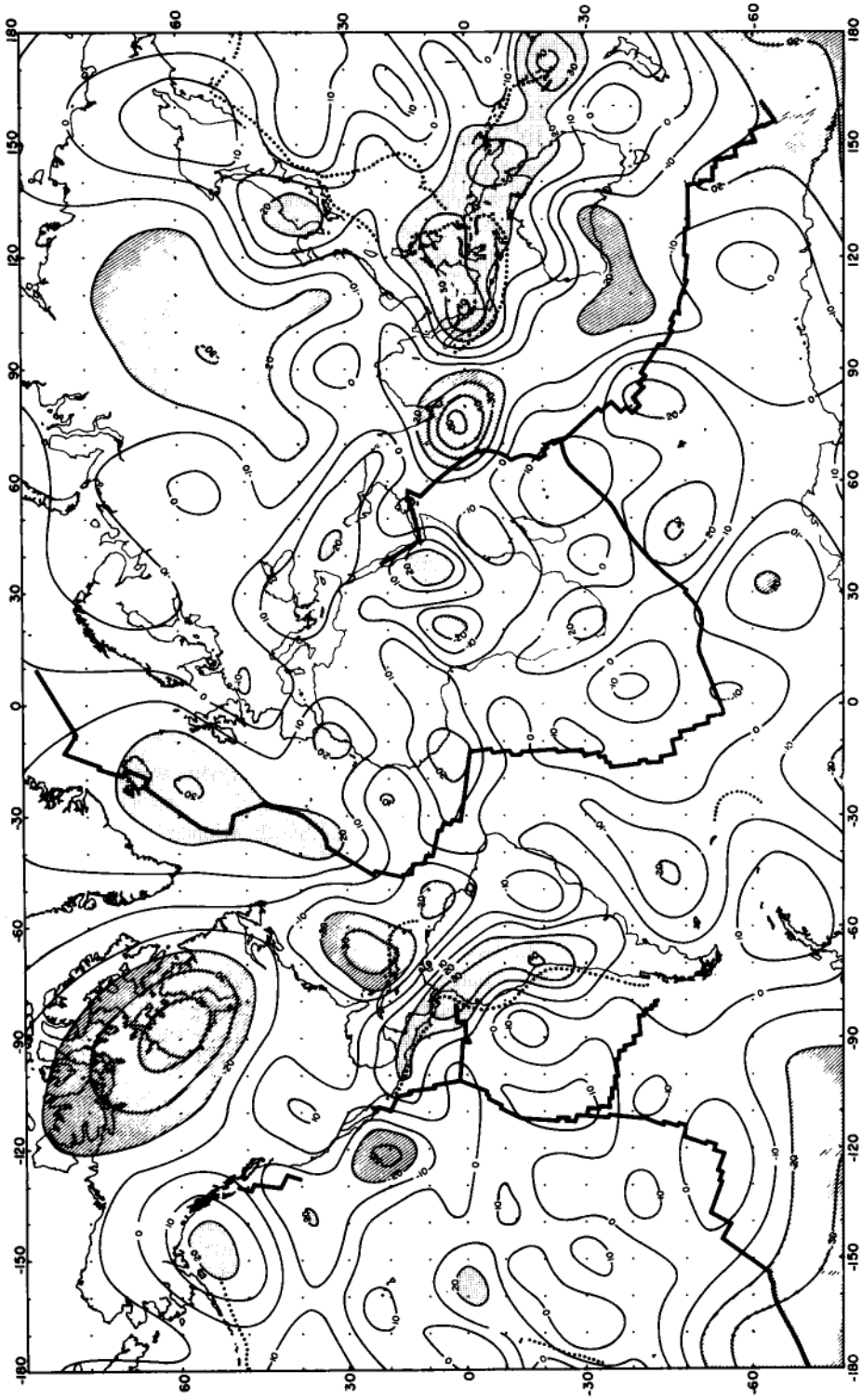

Figure 2. Free–air gravity anomalies calculated from the Goddard Space Flight Center's GEM-6 gravity field model (Lerch *et al.* 1974). The contour interval is 10 mgal and the anomalies have been referred to the hydrostatic figure of the Earth. GEM-6 is a 'combination' solution which is complete to sixteenth order and degree and thus can resolve features with wavelengths greater than about 2500 km. Areas with anomalies greater than 20 mgal are stippled, areas with anomalies more negative than −20 mgal are ruled.

There is a good general agreement between the surface and satellite fields in the position and amplitude of major features although the values at a specific location often disagree by as much as 15–20 mgal. Both gravity fields show highs over the mid-ocean ridges in the Atlantic Ocean and in portions of the eastern Pacific south of the equator. They also agree on the position of gravity highs over the Hawaiian and Line Islands. Watts (1976a) compared the GEM 6 solution to surface $10 \times 10^{\circ}$ averages in the area around Hawaii and found very good agreement both in the magnitude and position of the gravity high.

The agreement between the observed surface gravity field and the GEM 6 combination solution is not as good in the southern as in the northern hemisphere, but even there it is in much better agreement than the older, widely used SE II solution (Gaposchkin & Lambeck 1971).

The GEM 6 combination solution generally agrees with the surface field in the position of most of the major features in the Earth's gravity field that are expressed by longer wavelengths. In this respect it appears to be a substantial improvement on the SE II (Gaposchkin & Lambeck 1971) field which only employed a very limited amount of surface data. However, in attempting to make detailed correlations between the gravity field and surface features on the Earth, as was done by Anderson *et al.* (1973) and Menard (1973), several things must be kept in mind. Despite the good general agreement between the surface and satellite fields, they do not agree in detail, which in many cases is very important for establishing the correlations. There is disagreement in both the location and amplitude of anomalies and as mentioned above, the values at a given location may differ by more than 20 mgal. We have satisfied ourselves that these differences cannot be attributed to the differences in smoothing implicit in the two kinds of fields.

3 Gravity anomalies over mid-ocean ridges

A general correlation between mid-ocean ridge crests and positive gravity anomalies is suggested by both the surface measurements in Fig. 1 and the GEM 6 global gravity solution in Fig. 2. The correlation is most pronounced in the North and South Atlantic, but can also be seen over the East Pacific Rise and the South-eastern and South-western Indian Ocean Ridges. Such a correlation has been suggested by several investigators. Talwani *et al.* (1961), in discussing the first continuous surface-ship gravity measurements over a mid-ocean ridge, noted that the anomalies are near zero over the basin on either side of the Mid-Atlantic Ridge and are constantly positive over the ridge in the range of 0 to +50 mgal. Kaula (1972a, b) noted a general pattern of gravity anomaly highs over mid-ocean ridges and lows over basins on the Gaposchkin & Lambeck (1971) SE II global solution which he attributed to horizontal accelerations and decelerations in the asthenospheric flow pattern (Kaula 1972a).

Representative profiles across various portions of the mid-ocean ridge system are shown in Fig. 4. The locations of the profiles in Fig. 4 and of other profiles discussed later are shown in Fig. 3. The free–air gravity anomalies show a relative maximum over the mid-ocean ridge on each profile. This is a general observation. We have examined more than 100 crossings of the mid-ocean ridge system in this study and the only portion of the ridge system which we did not find to be associated with a relative gravity maximum is an area on the East Pacific Rise extending a few degrees on either side of the Galapagos triple junction where the field appears to show a slight minimum.

The difference in morphology of the various mid-ocean ridges is reflected in the gravity anomalies. The gravity anomalies over the East Pacific Rise (profiles G and H; Fig. 4) mirror the topography in having a broad high centred over the ridge crest. Comparisons of $1 \times 1^{\circ}$ averages over the ridge crest and over the flanks and basins show a consistent relative high

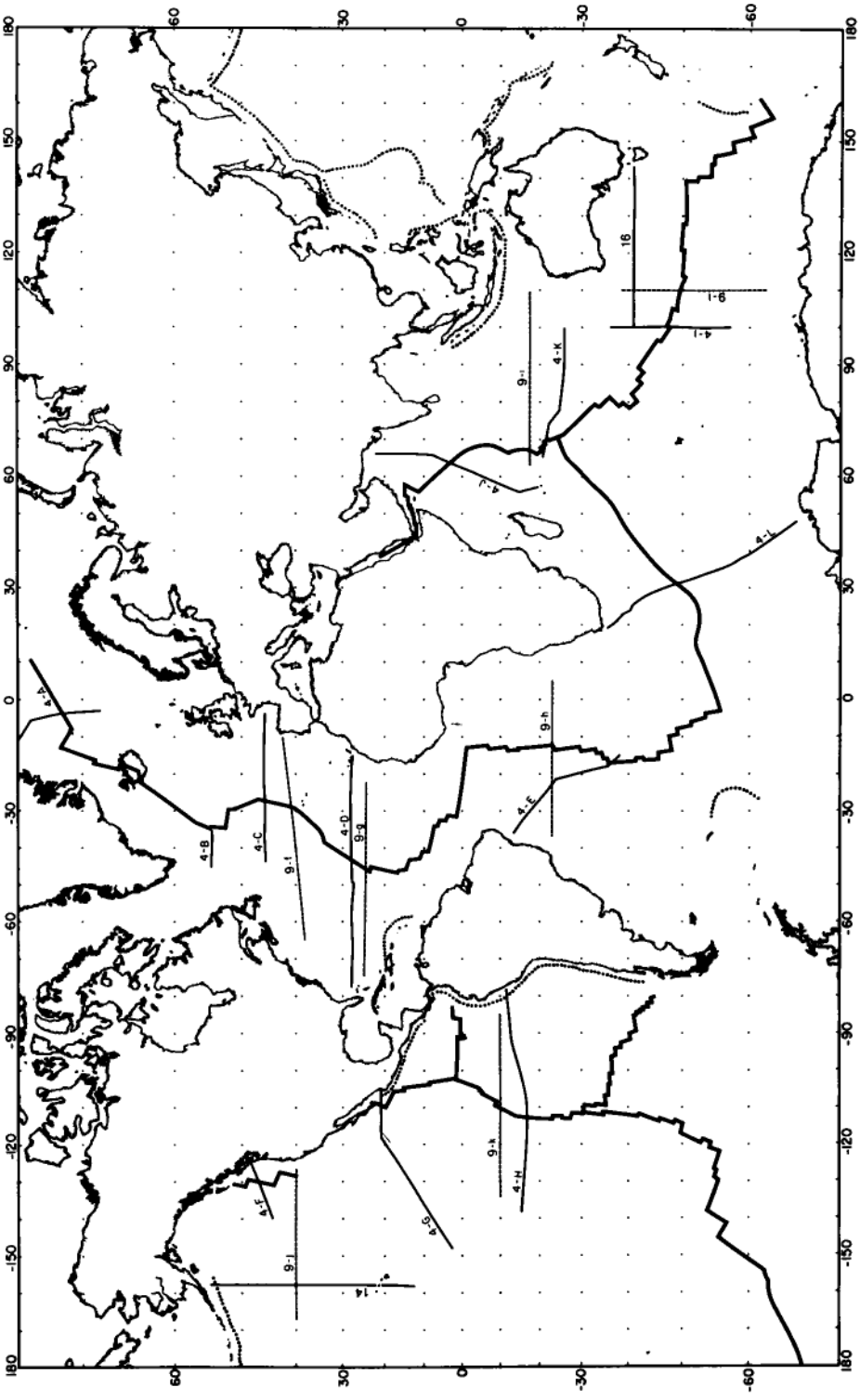

Figure 3. Location chart for profiles presented in this paper. Solid lines show ship tracks and dashed lines location of 5 × 5° average profiles. The number next to each profile indicates the figure in which the profile is shown.

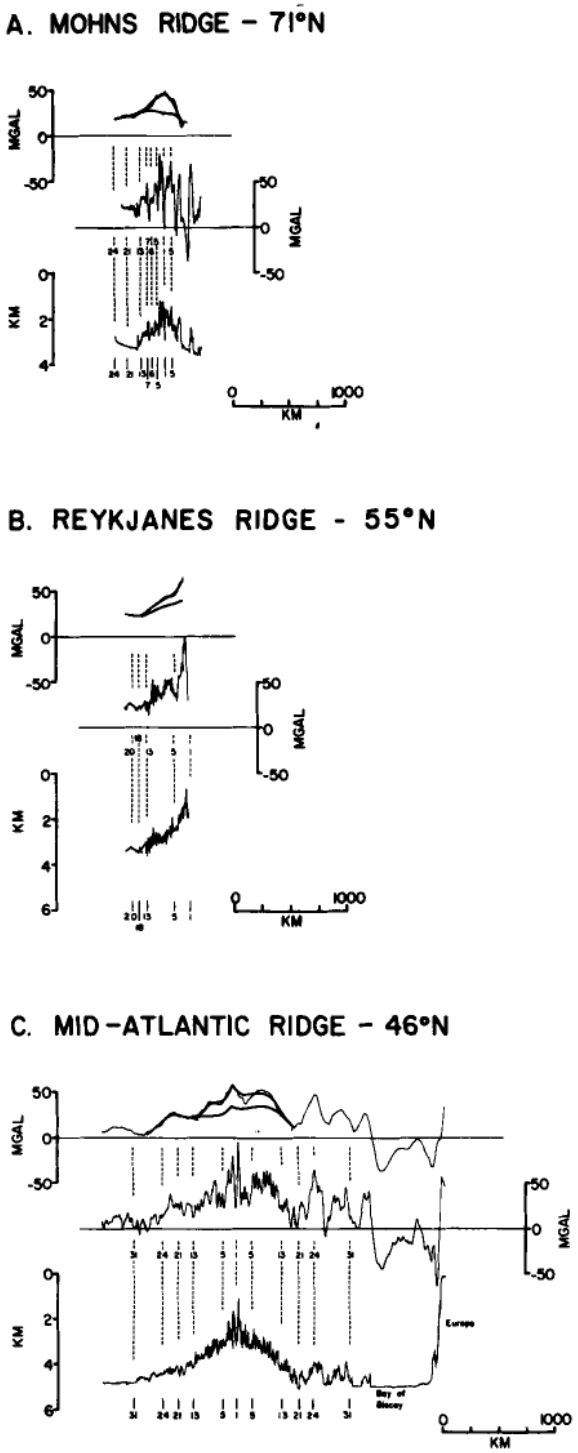

Figure 4. Projected bathymetry, free–air gravity and $1 \times 1^\circ$ average free–air gravity profiles across the mid-ocean ridge system. The profiles shown were chosen as typical of that portion of the ridge system. Vertical lines show the location of sea floor spreading magnetic anomalies identified along the ship's track. The $1 \times 1^\circ$ average free–air gravity anomalies shown here are 110 km running means of the observed gravity anomalies. The heavy lines over the $1 \times 1^\circ$ average profiles are a smoothed $1 \times 1^\circ$ average and the

D. MID-ATLANTIC RIDGE – 28°N

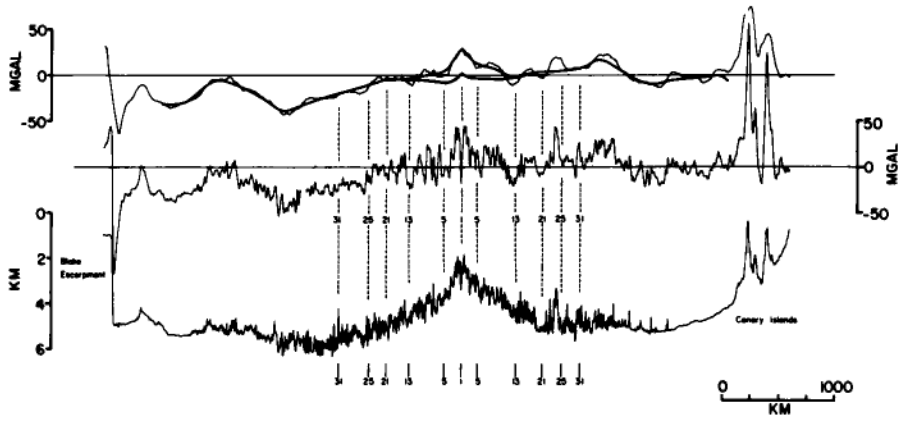

E. MID-ATLANTIC RIDGE – 36°S

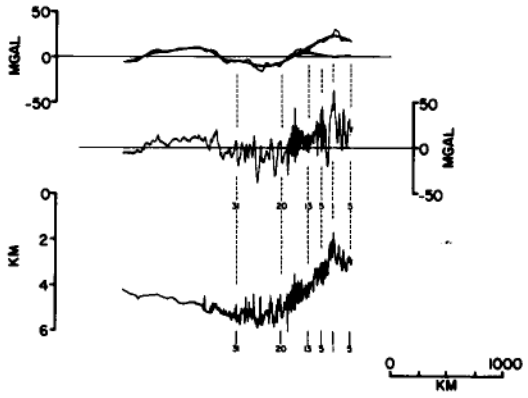

F. JUAN DE FUCA RIDGE – 48°N

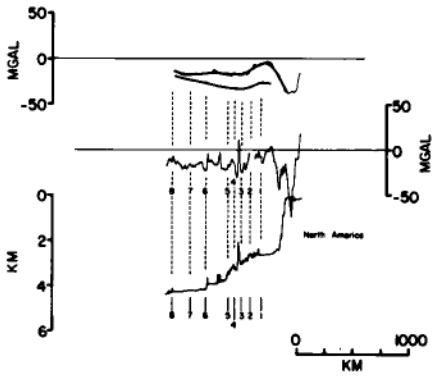

residual gravity anomaly obtained by subtracting the empirical gravity anomaly–age relationship shown in Fig. 6 from the smoothed 1 × 1° anomalies. The location of the profiles is shown in Fig. 3. All profiles have been projected perpendicular to the mid-ocean ridge. All gravity anomalies are referred to the hydrostatic figure of the Earth.

G. EAST PACIFIC RISE – 21°N

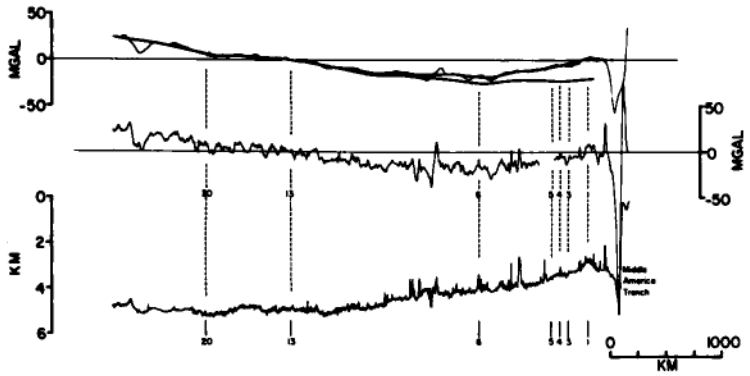

H. EAST PACIFIC RISE – 17°S

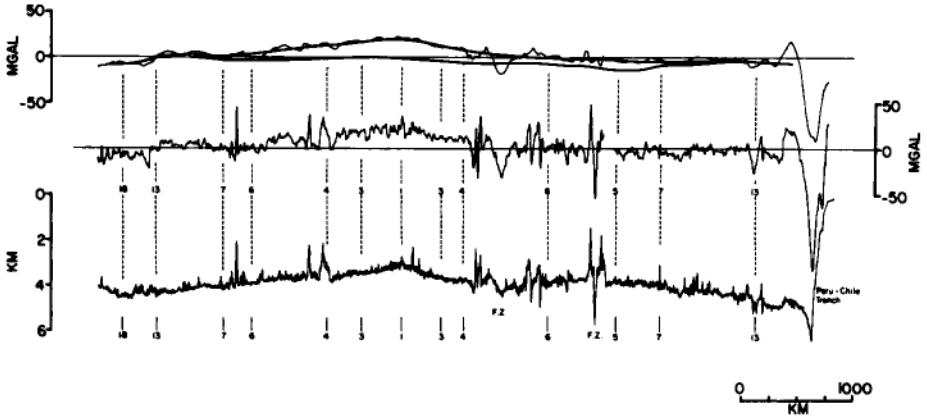

I. SOUTHEAST INDIAN RIDGE – 100°E

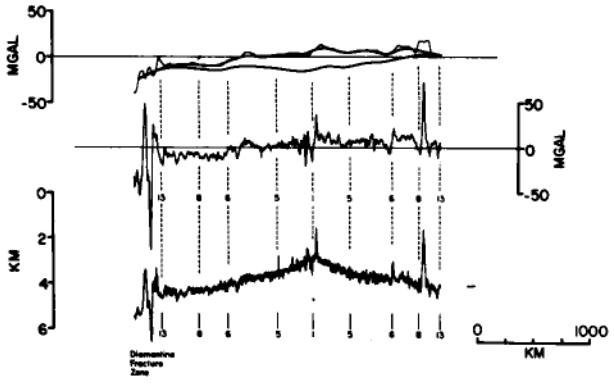

J. CARLSBURG RIDGE – 4°N

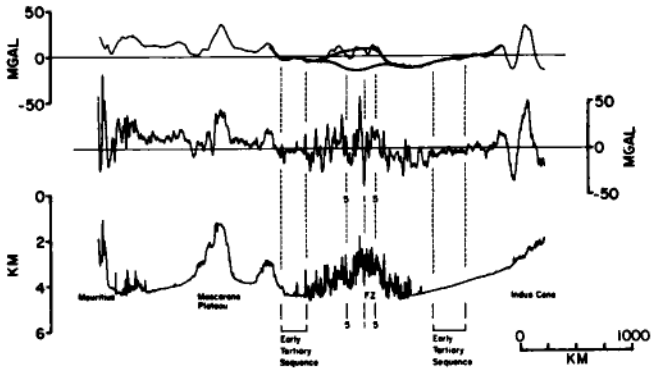

K. CENTRAL INDIAN RIDGE – 17°S

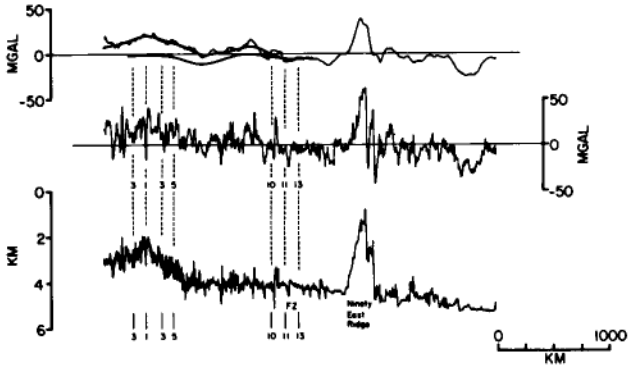

L. SOUTHWEST INDIAN RIDGE – 49°S

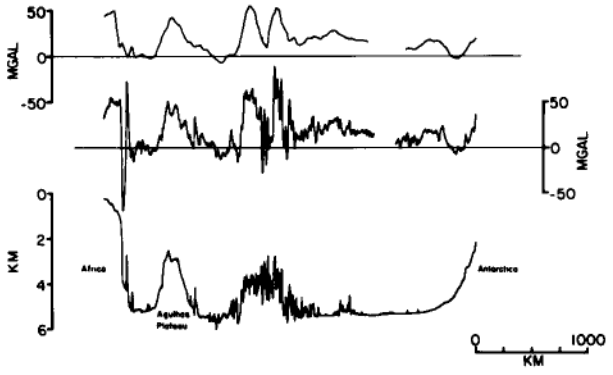

of about 20 mgal associated with the ridge crest. Anomalies associated with topography of wavelength less than about 100 km are superimposed on the broad ridge anomaly and are generally of the order of 10–15 mgal except over the major fracture zones where they can be considerably larger.

The gravity anomalies over the South-east Indian Ocean Ridge (profile I; Fig. 4) differ from those over the East Pacific Rise in that there is a marked asymmetry in the field with the southern basin much more positive than the northern basin. In some crossings the ridge crest almost appears as an inflection point in the gravity anomaly field, with the field nearly flat and near zero to the south and falling off to about −20 mgal in the north.

The ridge crest high over the Mid-Atlantic Ridge (profiles A–E; Fig. 4) is much more prominent than in the Pacific. The more rugged nature of the Mid-Atlantic Ridge is reflected in the short-wavelength gravity anomalies which are typically of the order of 25 mgal and may be 50 mgal or more. In particular, the ridge crest is marked by large-amplitude positive and negative anomalies over the rift mountains and rift valley which can have amplitudes of 75 mgal.

Both the North and South Atlantic Oceans have asymmetric gravity fields, with respect to the mid-ocean ridge system as noted by Talwani & Le Pichon (1969). This can easily be seen in Fig. 1 and is particularly marked in the North Atlantic between 15° N and 50° N.

The Mid-Ocean Ridge is steep, narrow and rugged in the Indian Ocean (profiles J, K, L; Fig. 4). This is particularly true of the south-west branch which abruptly rises 2 km from an abyssal plain and is associated with very large amplitude gravity anomalies (profile L; Fig. 4). Although there is a gravity maximum over the ridge, it does not appear to be related specifically to the ridge crest.

The gravity field in the vicinity of the Carlsberg Ridge (profile J; Fig. 4) is quite depressed because of the long-wavelength Indian Ocean gravity low, but even here the ridge crest marks a relative maximum of about 20 mgal in which the anomalies are nearly zero. The general level of the anomalies increases to the south (profile K; Fig. 4), but the relative high over the ridge is again about 20–30 mgal.

3.1 EMPIRICAL GRAVITY–AGE RELATIONSHIP

There is thus a general observation that the mid-ocean ridges are associated with a relative maximum in the gravity field. We wish to investigate whether a standard gravity anomaly can be established which describes the gravity field of all the mid-ocean ridges. There are several difficulties involved in isolating and identifying such an anomaly. One is that the general level of the field on which a ridge anomaly is superimposed varies from ocean to ocean. Secondly, the background field is not flat across the ridge. The observation that the gravity field is asymmetric with respect to the ridge in both the North and South Atlantic as well as in the Indian Ocean, demonstrates that the background field can vary considerably across the ridge.

In order, therefore, to isolate an anomaly specifically related to the ridge, we have used the following procedure. The ridge system was divided into sections in which the $1 \times 1^\circ$ average gravity values along isochrons remained relatively constant. For each isochron the $1 \times 1^\circ$ average free-air anomalies were averaged along the isochron and the averages were used to construct gravity–age profiles – Fig. 5(a). The standard deviations of the averages along isochrons were consistently in the range of 4–10 mgal.

The gravity–age profiles for the various ridge segments were overlain and adjusted to a common base level – Fig. 5(b). An empirical gravity–age relationship was constructed by drawing a smooth curve through the overlain curves. It was then adjusted by testing against observed profiles. The criteria used in testing the relationship were that the resultant regional

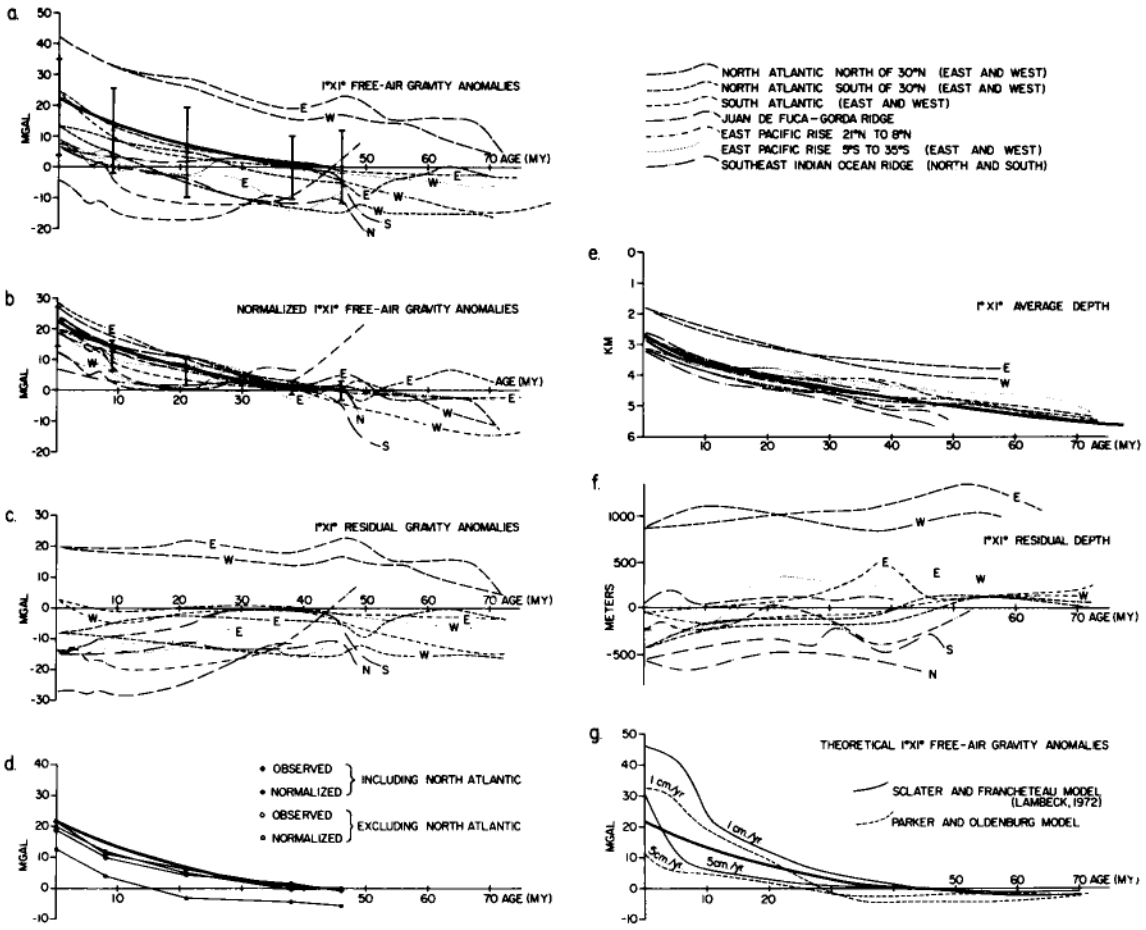

Figure 5. 1 x 1° free–air gravity anomalies across segments of the mid-ocean ridge system used in determining the empirical gravity–age curve (heavy line). In (a) anomalies are referred to the hydrostatic figure of the Earth. In (b) the profiles have been vertically adjusted to match where they level off near 40 my. Also shown are the means at various isochrons, weighted for length of ridge crest, and the standard deviations. The residual anomalies resulting from subtracting the empirical gravity–age curve from the profiles in (a) are shown in (c). The weighted means from (a) and (b) both including and excluding the North Atlantic are shown in (d). Note that the curves are all parallel to each other and the empirical gravity–age relationship (heavy line). (e) and (f) show respectively the observed and residual depths from the same data set as used in constructing (a) and (b). The scale in (f) was chosen so that 1000 m is equivalent to 30 mgal in (c). That is the relationship between gravity and depth predicted by McKenzie *et al.* (1974). Theoretical 1 x 1° average gravity anomaly profiles across mid-ocean ridges spreading at various rates are shown in (g).

field obtained by subtracting the empirical ridge anomaly from the observed field must vary smoothly and that it must not show an obvious relationship to the ridge crest. The final empirical ridge anomaly curve resulting from this procedure is shown in Fig. 6 and as the heavy curve superimposed on the observed curves in Fig. 5(a) and (b). The residual 1 x 1° average field, after removal of the ridge anomaly, is shown for each surface-ship profile in Fig. 4.

The 1 x 1° average gravity–age curve consists of a 22 mgal anomaly at the ridge crest falling off to 0 mgal at about 40 my with the decrease most rapid near the ridge crest. There is some evidence of a second order spreading rate dependence such that fast-spreading ridges

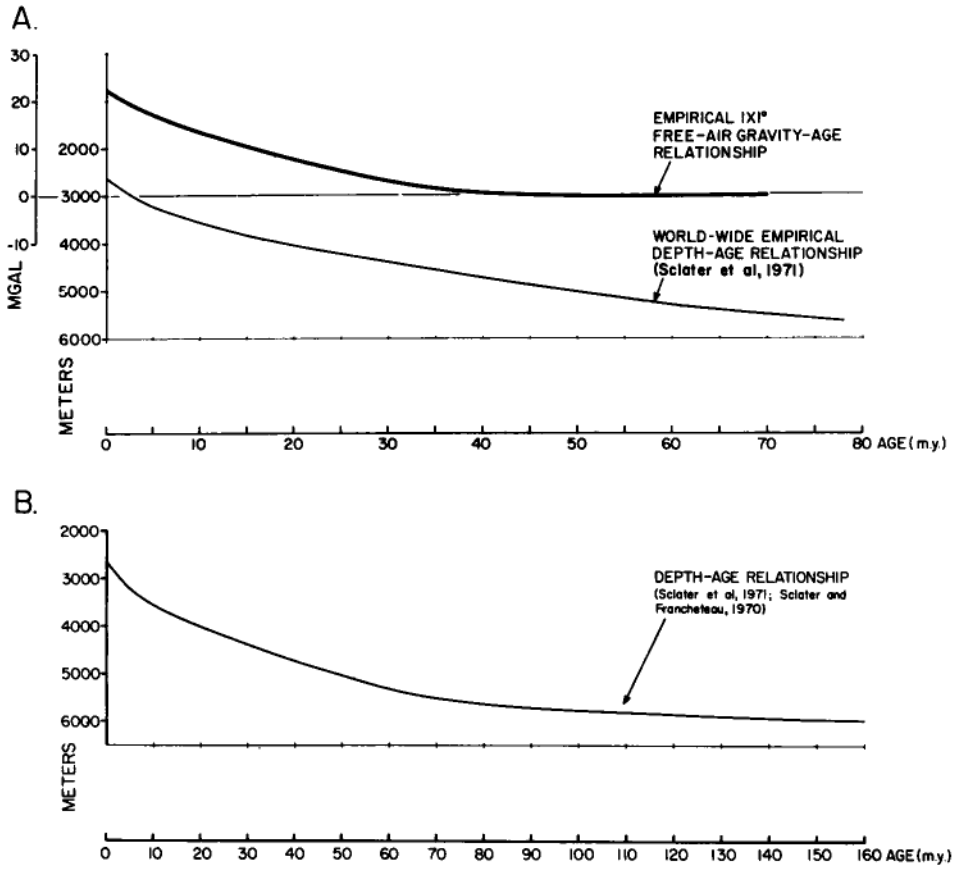

Figure 6. (A) Empirical 1 x 1° free–air gravity–age relationship. The relationship was developed through a comparison of gravity–age relationships in all of the oceans as discussed in the text. There is some evidence of a small second-order spreading rate dependence with fast-spreading ridges slightly below the curve and slow spreading ridges slightly above. An empirical depth–age relation from Sclater *et al.* (1971) is shown for comparison. The gravity anomaly–age relationship can be explained by an isostatic distribution of mass – that is by the separation of the excess mass of the ridge from its compensation– and is compatable with present thermal models of the lithosphere.

(B) Depth–age relationship used in calculating depth anomalies. For age of less than 80 my the curve is an empirical curve determined from data given by Sclater *et al.* (1971), The older portion of the curve is obtained from the Sclater & Francheteau (1970) theoretical relationship.

are associated with an anomaly of about 20 mgal and slow spreading ridges a somewhat larger anomaly of about 25–30 mgal.

Fig. 5(a) shows the gravity age curves for the different ridge segments and the mean values at various isochrons. In determining the means shown in Fig. 5, the values were weighted by the amount of ridge crest which they represent. The bars extend one standard deviation above and below the mean. It can be seen that the weighted means fall close to the empirically determined ridge anomaly, but that the standard deviations are quite large.

The weighted means determined from the vertically adjusted gravity–age curves – Fig. 5(b) – are almost identical to those of the observed anomalies but with greatly reduced standard deviations. This indicates that much of the scatter in Fig. 5(a) is simply a DC shift in level of the gravity field over the ridge in the various oceans.

The average values for isochrons near the ridge crest fall 2–3 mgal below the empirical curve. This is largely the result of several ridge segments, notably the southern flank of the

South-west Indian Ridge, the Gorda–Juan de Fuca Rise and portions of the East Pacific Rise. The residual gravity anomaly curves – Fig. 5(c) – for these ridge segments show a smooth long-wavelength gradient.

The unusual nature of the North Atlantic is clearly demonstrated in Fig. 5. Both the gravity–age (Fig. 5(a and c)) and depth–age (Fig. 5(e and f)) curves are considerably above those of the other oceans. The gravity–age curves for the North Atlantic are separated by 20 mgal from the other ridge segments and the depth–age curves by 800–1000 m.

In considering the anomalies associated with the mid-ocean ridge system, we wish to determine to what extent our conclusions are dependent upon this unusual area. Fig. 5(d) shows the weighted means of the observed and vertically adjusted average gravity anomalies both including and excluding the North Atlantic north of 30° N. The adjusted values excluding the North Atlantic are very similar to the values which include it. The observed values excluding the North Atlantic are lower but parallel to the other curves. We thus conclude that our results are not dependent on the values from the North Atlantic and also that the gravity anomaly associated with the Mid-Atlantic Ridge is similar to that of other ridge segments with a baseline shift.

The free–air gravity anomalies which have been found to be associated with mid-ocean ridges are relatively small, being of the order of 20–25 mgal compared to the 250 mgal anomaly which would be expected if the ridge was uncompensated. It is therefore reasonable to assume that mid-ocean ridges are compensated and that the anomalies arise from an isostatic mass distribution; that is as a result of the separation of the excess mass represented by the ridge and its compensation. Compensated models of mid-ocean ridges produce broad bands of slightly negative anomalies as well as a gravity high over the ridge crest – see Fig. 5(g). These negative anomalies, which are difficult to separate from the background field, can be included in Fig. 6(A). We have not done so simply for the sake of simplicity.

We computed that $1 \times 1^\circ$ gravity anomalies resulting from compensation of the ridge at various depths using a simple two-dimensional model and a cylindrical approximation to the Earth's curvature (Takin & Talwani 1966). The resulting anomalies depend on the spreading rate, but for all spreading rates found in the oceans, the calculations imply that most of the compensation must be shallower than 150 km. For slow spreading ridges, the depth of compensation must be shallower than 100 km. If the compensation is deeper, the anomalies become much larger than is observed.

Lambeck (1972) used the Sclater–Francheteau thermal model to calculate densities throughout the lithosphere and then used the densities to compute free–air gravity anomalies. His calculations showed a sharp positive anomaly over the ridge crest decreasing to 0 mgal near 45 my. The $1 \times 1^\circ$ average gravity anomalies computed from Lambeck's curves are similar to the empirical ridge anomaly except that they are considerably larger than the obseved anomalies over the ridge crest – Fig. 5(g). This is perhaps not unexpected since the Sclater & Francheteau (1970) model also predicts elevations much greater than observed in the immediate vicinity of the ridge crest.

Parker & Oldenberg (1973) modified the Sclater & Francheteau (1970) model by changing the boundary conditions to require finite heat flow at the ridge crest and by allowing the cooling to extend to unlimited depth. They calculated the ridge elevation by assuming a mean density for the lithosphere and assuming that it is compensated by a density inversion of constant magnitude in the upper asthenosphere. We have calculated the $1 \times 1^\circ$ gravity anomalies resulting from this simple model and obtained results similar to those obtained by Lambeck (1972) for the Sclater & Francheteau model, but without as large a peak at the ridge crest – Fig. 5(g).

Preliminary three-dimensional calculations on a spherical Earth using the Parker & Oldenburg model gives a $1 \times 1^\circ$ gravity high of 25–35 mgal over a ridge spreading at 1.2 cm/yr

(Cochran & Talwani, in preparation). This is in good agreement with our observations at slow-spreading ridges (Fig. 4).

It is not useful to try to obtain more than a general fit between the observed free–air gravity anomalies associated with the ridge and those predicted by the various thermal models. There are too many parameters that are poorly known in those models. The important point is that a good quantitative explanation of the observed gravity anomalies can be obtained from the same models of the thermal evolution of the lithosphere which provide quantitative fits of the same order to the observed heat flow and topography. The gravity anomalies which would be expected from the Sclater & Francheteau (1970) and Parker & Oldenberg (1973) thermal models are similar and it is not possible to use the observed gravity anomalies over the ridge crest to distinguish between them.

4 Residual gravity anomalies and residual depths

In the previous section, we isolated and identified a component of the Earth's gravity field associated with the mid-ocean ridge system and expressed the anomaly quantitatively in terms of an empirical gravity–age curve. The ridge anomaly, which probably has its origin within the lithosphere, can be removed from the observed free–air gravity field allowing the residual anomaly pattern to be examined.

We obtained $1 \times 1^\circ$ average residual gravity anomalies in the North Atlantic and Indian Oceans by assigning an age to each $1 \times 1^\circ$ square from magnetic isochron maps and then subtracting the $1 \times 1^\circ$ average gravity anomaly appropriate for that age from the observed $1 \times 1^\circ$ average free–air anomaly. Only areas less than 40 my old were affected by this procedure. The residual $1 \times 1^\circ$ average anomalies were then summed and averaged to form residual $5 \times 5^\circ$ averages. In the oceans where the anomalies were determined by averaging along tracks, the locations where the tracks crossed various isochrons were noted on the profiles and smoothed residual averages obtained at those locations. The residual gravity anomaly map constructed in this fashion is shown in Fig. 7.

The sources of age data are the magnetic isochron maps of Pitman & Talwani (1972), Larson & Pitman (1972) and Talwani & Eldholm (in press) for the North Atlantic; Larson & Ladd (1973) and Ladd (1974) for the South Atlantic; Atwater & Menard (1970) and Herron (1972) for the Eastern Pacific; Weissel & Hayes (1972) for the South-east Indian Ocean; and McKenzie & Sclater (1971), Markl (1974a), Schlich (1974), Sclater & Fisher (1974), Whitmarsh (1974), Larson (1975) and Sclater, Luyendyk & Meinke (1976) for the Indian Ocean. We made no age correction to the observed anomalies in the Indonesia–Melanesia area where the lithospheric ages are not well known. We have also determined $5 \times 5^\circ$ residual depth anomalies for much of the world's oceans and show a map of them in Fig. 8. The term residual depth anomaly is defined as the difference between the depth expected for ocean floor of a given age and the observed basement depth corrected for sediment loading (Menard 1973). Areas shallower than expected have positive depth anomalies, those deeper than expected have negative depth anomalies. The corrected basement depths were obtained by adding half of the sediment thickness to the water depth, which is equivalent to assuming local compensation and a sediment density of 2.2 g/cm^3. The depth anomalies were referred to the age–depth curve shown in Fig. 6(B). The predicted depths were taken from an empirical relationship for ocean floor less than 80 my old obtained by averaging Sclater *et al.*'s (1971) data from the various oceans and a curve obtained from the Sclater & Francheteau theoretical relationship for older ocean floor. This curve gives depths slightly shallower, but within 100 m of the empirical curve for old oceanic areas given by Parsons & Sclater (1977).

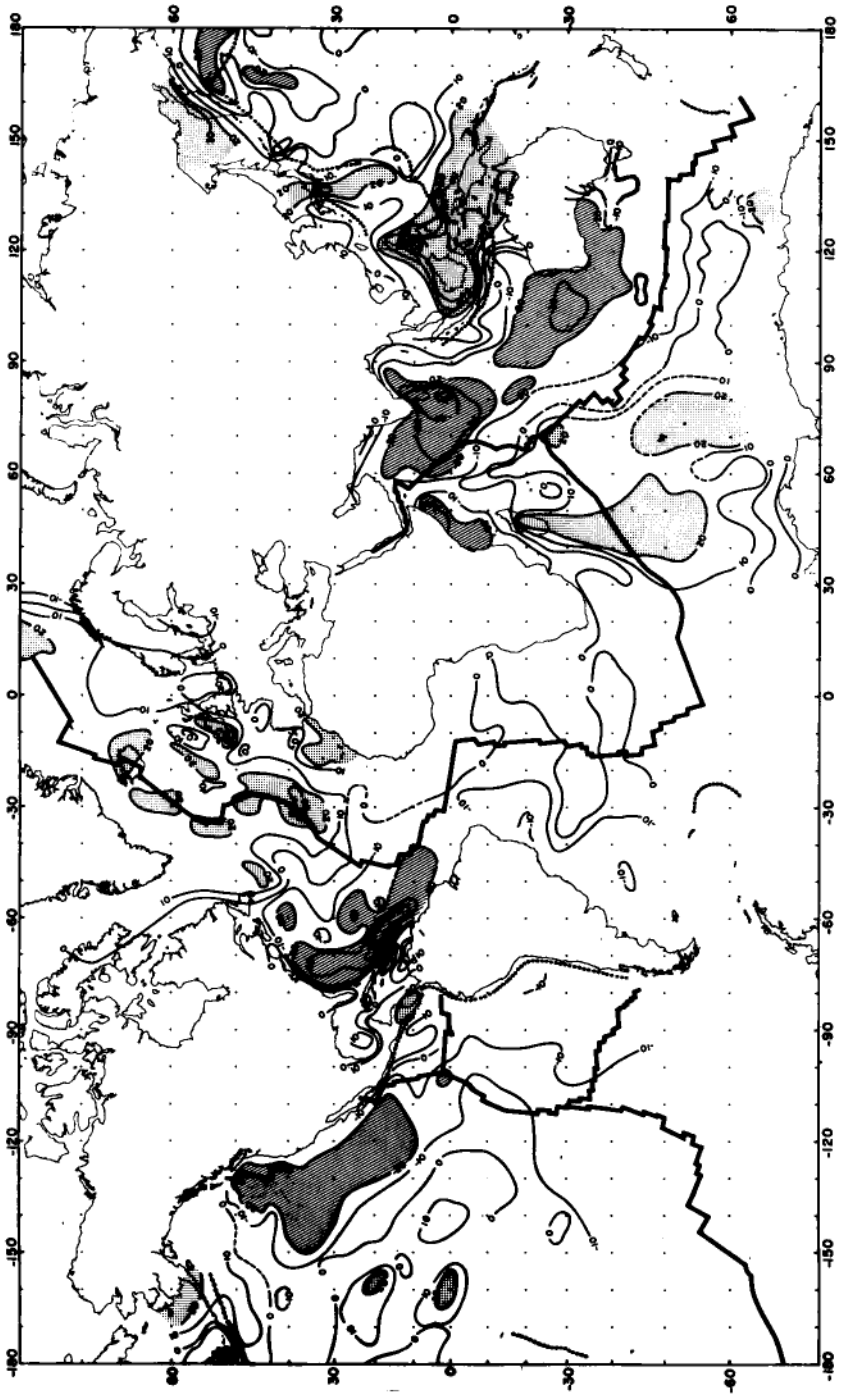

Figure 7. 5 × 5° average residual gravity anomalies over the world's oceans determined by removing the empirical gravity anomaly–age relation from the anomalies shown in Fig. 1. Note how this procedure has, with the exception of the North Atlantic, made the gravity anomalies independent of the mid-ocean ridge. Also note asymmetry in the gravity field of most oceans and tendency for large areas to have anomalies of one sign. Areas with residual anomalies greater than 20 mgal are stippled; areas with anomalies more negative than −20 mgal are ruled. The gravity anomalies are referred to the hydrostatic figure of the Earth (flattening = 1/299.7).

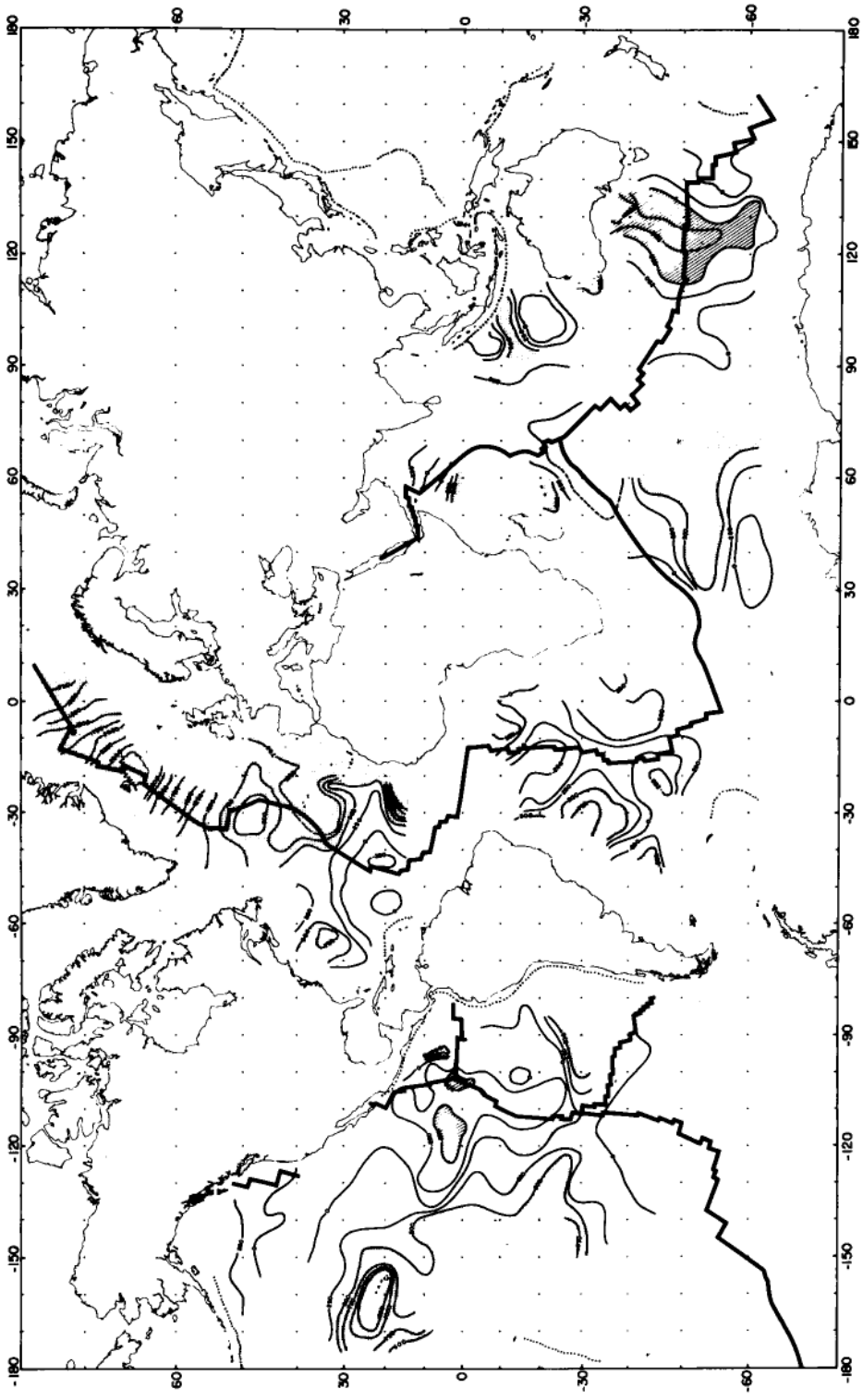

Figure 8. 5 x 5° average residual depth anomalies over the world's oceans. Residual depth anomalies are defined as the difference between the observed basement depth corrected for sediment loading and an empirical depth–age curve. Shallow areas have positive depth anomalies, deep areas have negative depth anomalies. Sources of data and method of calculating averages are discussed in the text. Contour interval is 250 m. Areas with anomalies greater than +500 m are stippled, areas with anomalies more negative than −500 m are ruled.

The observed depths for a region were obtained in the same manner as were the gravity anomalies except in the north-eastern Pacific where 5 x 5° averages were determined from Menard's (1973) 1 x 1° average depth anomalies. The 1 x 1° average depths were obtained in the North Atlantic from the bathymetric maps of Uchupi (1971) and an unpublished map of the Norwegian–Greenland Sea. Sediment thicknesses were determined from isopach maps of Eldholm & Windisch (1974) and Ewing *et al.* (1973). In the Indian Ocean, bathymetric maps of Fisher, Sclater & McKenzie (1971) and Sclater & Fisher (1974) were used to obtain 1 x 1° average depths to the west of 103° E and Markl (1974b) and the bathymetric map in the International Indian Ocean Atlas (Fisher, Laughton & Roberts 1975) were used in the Wharton Basin. Sediment thicknesses were determined from the International Indian Ocean Atlas isopach map (Ewing *et al.* 1975). It was considered desirable to calculate depth anomalies slightly to the east of the area in which magnetic anomalies were mapped by Sclater & Fisher (1974) in order to include the deepest portion of the Wharton Basin. Ages determined from magnetic anomalies identified by Sclater & Fisher (1974) between the Investigator Fracture Zone (98° E) and the Java trench were extrapolated to the south and the extrapolated ages used to determine predicted depths between the Investigator Fracture Zone and 103° E. Between 103° E and 110° E, a predicted depth of 5800 m was assumed.

In the areas where the gravity anomalies were obtained from averaging along tracks, the depths were obtained in the same manner as the gravity. Sediment thicknesses were determined from isopach maps. Those used were Ewing *et al.* (1973) for the South Atlantic, Houtz & Markl (1972) in the south-east Indian Ocean, and a revised version of the isopach map in Ewing *et al.* (1968) (G. Carpenter, private communication) for the Eastern Pacific. Sediment thicknesses were determined from published and unpublished Lamont-Doherty seismic profiler records in areas where isopach maps were not available. The 1 x 1° average depth anomalies are tabulated in Appendix 2 and the 5 x 5° averages in Appendix 3.

For the remainder of this study, the terms 'residual gravity' and 'residual depth' will refer to 5 x 5° averages constructed in the manner described above unless specifically stated otherwise.

4.1 RESIDUAL GRAVITY ANOMALIES

Except in the North Atlantic where a very broad, flat high is centred at the ridge, the residual gravity anomalies in Fig. 7 show no obvious relationship to the location of the mid-ocean ridge system. The general lack of an anomaly associated with the mid-ocean ridge system in the residual anomaly field supports the validity of the worldwide empirical mid-ocean ridge gravity anomaly.

Mid-oceanic areas of large positive gravity anomalies not associated with subduction zones are found in two locations. One is the North Atlantic where, as noted before, a broad high is centred at the ridge crest to the north of 30° N (Fig. 9, profile f). The other is in the south-western Indian Ocean. There, an area in which the regional gravity field is greater than 20 mgal is found to the south of the south-western Indian Ocean Ridge on the Antarctic Plate. It extends across the ridge and along the Madagascar Ridge into the island of Madagascar. It thus overlies oceanic portions of two plates and the continental crust of Madagascar.

There are also smaller areas of quite positive gravity anomalies. These are generally found over areas of extensive volcanism away from the mid-ocean ridges. Examples include Hawaii, Kerguelen, and the Canary Islands.

Wide areas of negative gravity anomalies are quite common in oceanic regions. The largest area of negative anomalies is the Indian Ocean Gravity Low which extends from the area of the Great Australian Bight, around the western end of Australia, and across the northern

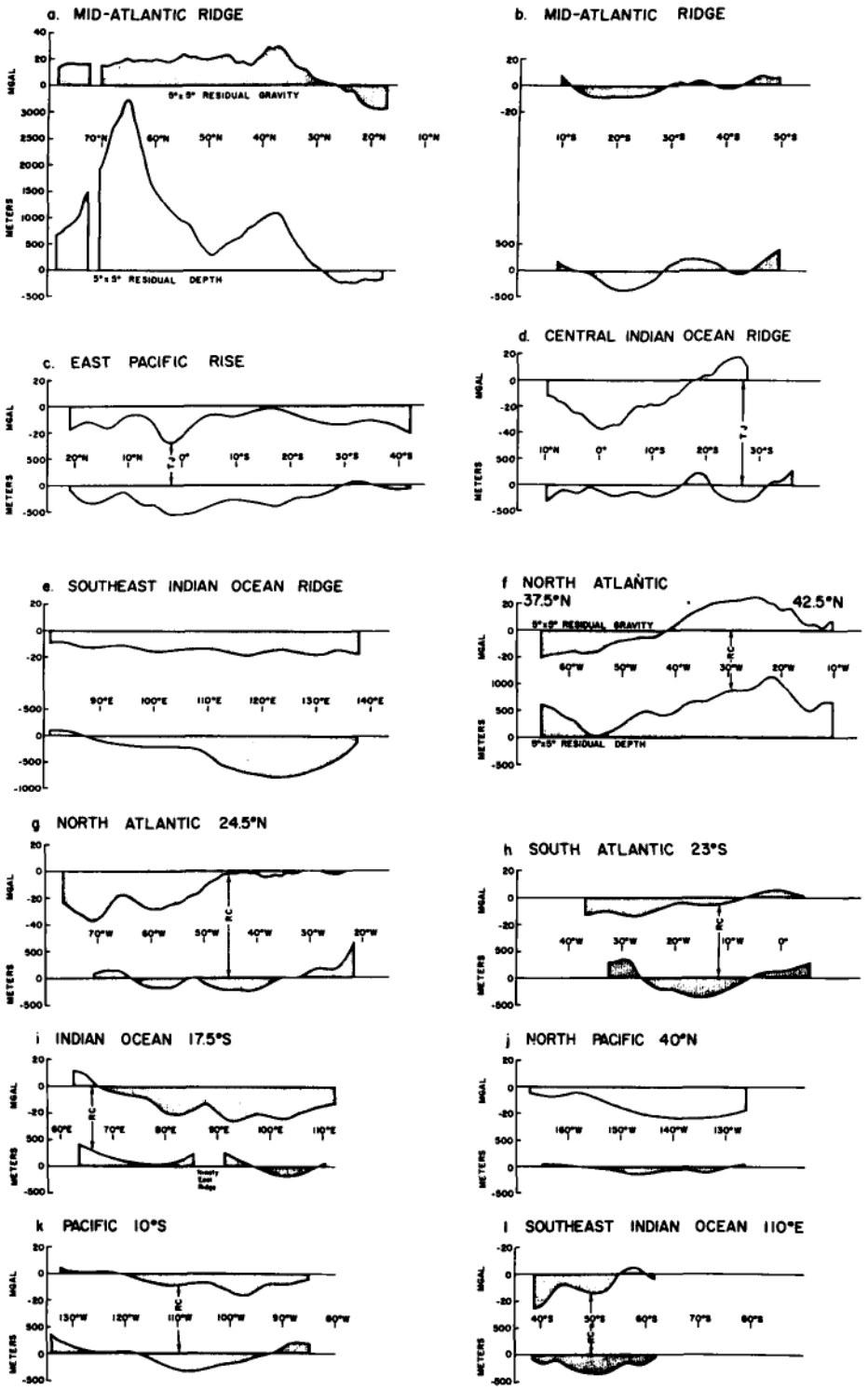

Figure 9. Profiles of 5 X 5° residual gravity and depth anomalies along (a–e) and across (f–l) the mid-ocean ridges. The locations of triple junctions are indicated by 'TJ' and the points at which profiles cross the mid-ocean ridge crest are marked by 'RC'. The location of the profiles is shown in Fig. 3.

part of the Indian Ocean (Fig. 9, profiles d and i). The anomalies are of the order of −20 to −30 mgal through most of that region and reach a maximum south of Ceylon where the 5 x 5° averages have values which are more negative than −50 mgal. An area of large negative anomalies is found in the western North Atlantic along the eastern margin of the Americas from Nova Scotia to Brazil. The gravity anomalies are more negative than −30 mgal throughout much of that area. This anomaly is quite apparent in Fig. 9, profiles f and g. Another important area of negative anomalies extends from 50° N to 10° N off the western coast of North America (Fig. 9, profile j) and much of the interior of the North and East Pacific is associated with negative gravity anomalies of up to about −10 mgal.

A general asymmetry in the gravity fields of most oceans is evident in Fig. 7 and in the profiles across the various ridges in Fig. 9. The western basins of both the North and South Atlantic are considerably more negative than the eastern basins (Fig. 9, profiles f, g and h). The same situation exists in the south-eastern Indian Ocean where the South Australian Basin has free–air anomalies of about −20 mgal while the anomalies are near zero throughout most of the Antarctic Basin (Fig. 9, profile l). The most dramatic example of asymmetry is found in the Indian Ocean where the Indian Ocean Gravity Low is in juxtaposition to the gravity high in the south-western Indian Ocean.

The asymmetry shows an interesting geographical relationship. In a reference frame in which Africa and Antarctica are considered to be nearly fixed and Australia, India, and the Americas moving away from them, the sense of the asymmetry is such that the more negative anomalies are found on the moving plate.

In this section we will examine the relationship between residual gravity anomalies and residual depths. We will begin by examining the relationship between the two parameters in the individual oceans and then consider the correlations on a world-wide scale. We will show that (1) a good correlation does exist in some areas, which is dominated by relatively short-wavelength positive topographic features associated with areas of extensive off-ridge volcanism. (2) No correlation between gravity and topography exists over negative topographic features (i.e. deeps). (3) On a longer wavelength scale, no simple relationship exists between gravity and depth and, in particular, no relationship exists which can be universally applied.

Finally, we will consider the implications of the relationship of gravity anomalies and topography to flow in the asthenosphere.

4.2 NORTH ATLANTIC OCEAN

We show, in Fig. 10, the residual gravity and depth anomalies in the North Atlantic and Norwegian–Greenland Seas.

Three observations can be immediately drawn from Fig. 10. First, there is an important boundary at about 30° N. The boundary is marked by steep gradients in both the gravity and topography and is clearly demonstrated in Fig. 11 which shows a profile of the 1 x 1° average free–air gravity and depth along the ridge crest and a plot in which the gravity anomaly and depth for each point are plotted against each other. (Since age is constant along the ridge crest these curves, with shifts in scales, also represent residual depth and residual gravity curves.) Points to the north and to the south of 32° N fall into two distinct groups without any overlap. The same result would have been obtained for profiles along other isochrons on either side of the ridge crest. The ridge crest 1 x 1° averages to the south of 32° N in Fig. 11 show large, relatively uniform depths and 1 x 1° average free–air gravity anomalies which range from 0 to 30 mgal. The northern points show greatly variable, but consistently shallower depths and higher gravity anomalies with no apparent relationship between gravity and depth.

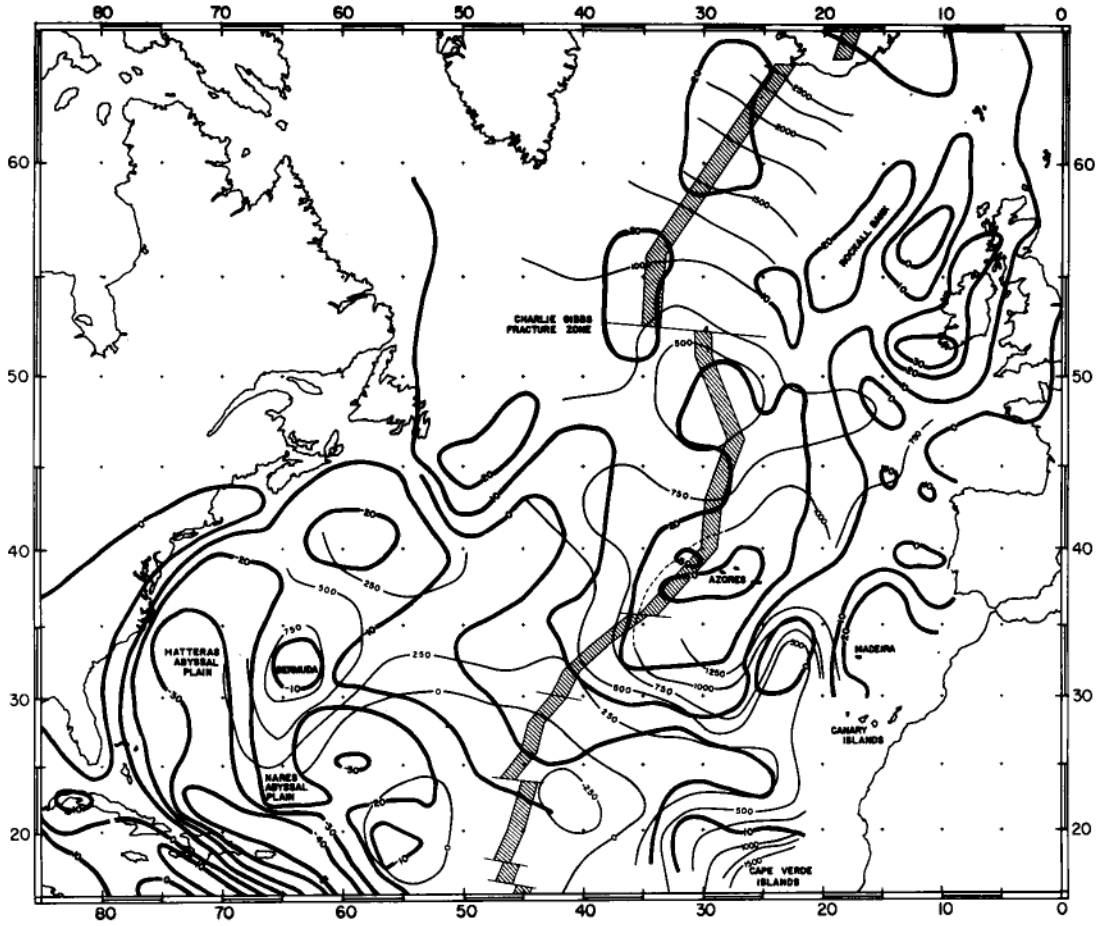

Figure 10. (a) Map of 5 × 5° residual gravity and depth anomalies in the North Atlantic. The gravity is contoured at 10 mgal and the depth at 250-m intervals. Note the gradient in the gravity anomalies near 30° N and the general smoothness of the field north of there in a region in which the depth anomalies vary greatly. Also notice the correlation of gravity and topographic highs in the vicinity of Bermuda, Azores, the Canaries and the Cape Verde Islands.

The second observation which can be drawn from Figs 10 and 11 is the lack of any very large variations in the residual gravity field over oceanic areas to the north of about 40° N. The residual gravity field in that region consists of a very broad high centred at the ridge crest. There is very little latitudinal variation in the gravity field, in marked contrast to the depth anomalies which vary from about 300 m just south of the Charlie Gibbs Fracture Zone to about 3000 m at Iceland (Fig. 9, profile a). The largest regional change in depth along the ridge axis is thus not reflected in the gravity field. Our results, which employ more extensive gravity data than was available for earlier studies, contradicts the conclusions which Anderson *et al.* (1973) drew from the SE II combination field. The SE II and GEM 6 fields are also shown on Fig. 11.

A third observation which can be made from Fig. 10 is that there are locations at which there are some striking visual correlations between residual gravity and depth anomalies. Specifically, shallow depths and large positive gravity anomalies are associated with the areas around the Azores, the Cape Verde Islands and the Canary Islands. Greater depths

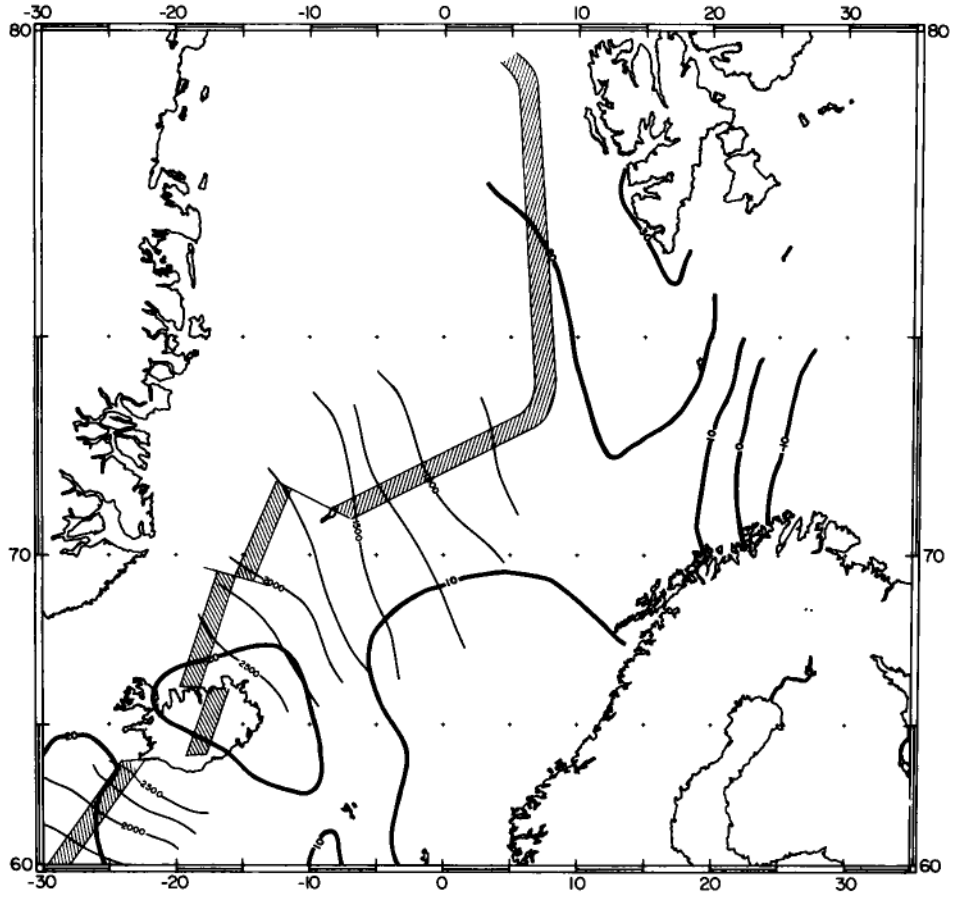

Figure 10. (b) Map of 5 × 10° residual gravity and depth anomalies in the Norwegian–Greenland Sea. The gravity is contoured at 10 mgal and the depth at 250-m intervals.

and lower residual gravity anomalies are associated with the areas between these features and to the west of the Azores and the Cape Verde Islands. It is this general area, between 10° N and 50° N to the east of 50° W, that the data used by Sclater *et al.* (1975) was drawn and these local areas of unusual elevation and positive gravity anomalies appear to contribute largely to the correlation between gravity and residual depth which they noted.

We note that the Azores, Cape Verde Islands and Canary Islands are all areas in which extensive amounts of volcanism have occurred away from the Mid-Atlantic Ridge. The association of extreme volcanism and shallow depths with higher than normal gravity anomalies is further demonstrated at Bermuda which is at the crest of a topographic swell and at the centre of a local relative gravity high over the regional low. The main difference is that Bermuda is characterized by much older (30 my bp) volcanism (Aumento & Sullivan) 1974).

Although there is a correlation between residual gravity and depth anomalies in the special locations noted above (clearly seen in profile f, Fig. 9 in which an east–west profile passes near the Azores) there is no correlation over much of the North Atlantic. For example, look at profile g, Fig. 9 which runs east–west across the North Atlantic at 24.5° N. In that

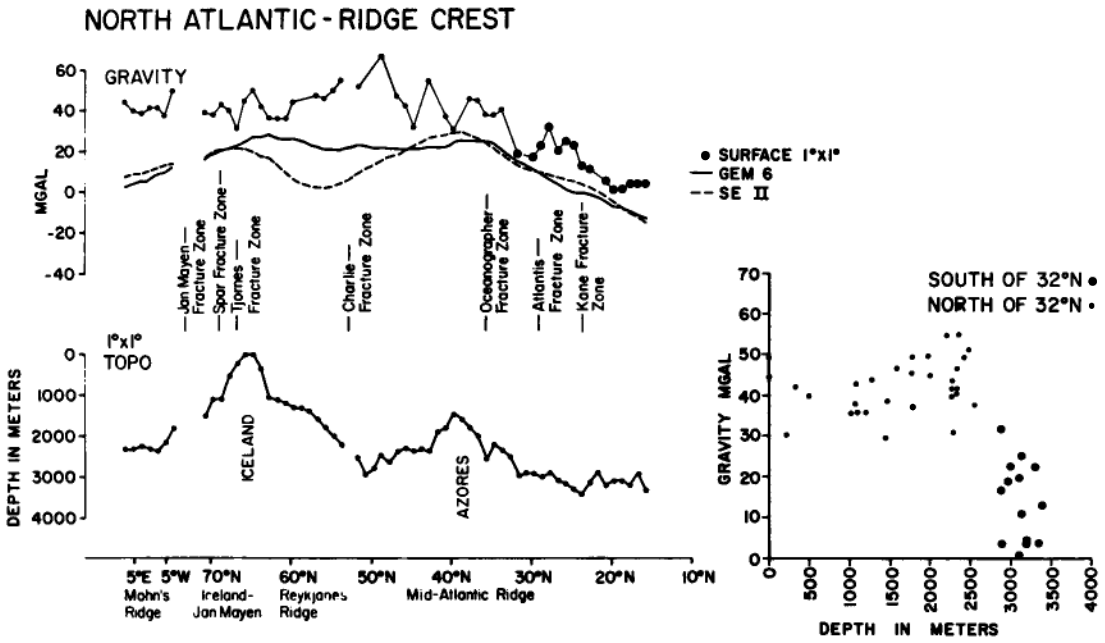

Figure 11. Profile along the Mid-Atlantic Ridge of 1 x 1° depth, 1 x 1° average free–air gravity and satellite derived gravity field. The solid line is the GEM 6 solution (Lerch *et al.* 1974) and the dashed line the SE II solution (Gaposchkin & Lambeck 1971). Also shown is a plot of surface 1 X 1° free–air gravity anomalies against 1 x 1° depth. Since the ridge crest is an isochron these anomalies correspond to residual anomalies with an appropriate shift in the baseline.

profile the residual gravity anomalies, which are near zero in the eastern basin, fall off west of 47° W reaching values more negative than −30 mgal without any substantial change in the residual depths.

The entire North American Basin of the North Atlantic is characterized by negative 5 x 5° average residual gravity anomalies which are more negative than −20 mgal over an area 4000 x 1500 km encompassing the Hatteras, Nares and Demerara Abyssal Plains. The 5 x 5° average residual depth anomalies, on the other hand, have positive values ranging up to several hundred metres west of Bermuda and values close to zero south of Bermuda. Thus, although small areas such as Bermuda show a correlation between residual gravity and residual topography, the most important observation is that the very prominent negative gravity values in the western Atlantic basin are not associated with correspondingly negative residual depth values.

The principal facts in the North Atlantic can be summarized as follows:

(i) At about 32° N in the area of the Mid-Atlantic Ridge there is a step in depths which corresponds to a step in residual gravity. North of there the gravity values over the ridge are uniformly high and within the northern region there is no correlation between depth and gravity, as examplified by the contrasts between the area around the Charlie Gibbs Fracture Zone and Iceland.

(ii) Gravity highs in the North Atlantic, south of about 45° N, are associated with topographic highs at specific areas such as the Azores, Canaries, Cape Verde Islands, and Bermuda. The deeper areas between and around these topographic highs have associated relative negative anomalies. This is the correlation noted by Sclater *et al.* (1975).

(iii) The important negative gravity anomaly in the western North Atlantic has no counterpart in residual negative depth anomalies.

4.3 SOUTH ATLANTIC

The most notable features of the South Atlantic gravity field are the small magnitudes of the residual gravity anomalies and the conspicuous asymmetry of the gravity field (Figs 9 and 12). The only area in which positive 5 x 5° residual gravity anomalies are found in the western basin is in a band which follows the Rio Grande Rise, Tristan da Cunha group and Walvis Ridge before widening out to include most of the eastern basin north of 35° S. Limited areas of positive gravity anomalies also extend toward the western basin in the very north near the equatorial fracture zones and the south near the Falkland Plateau. The residual gravity field thus has positive values in the north, in the centre over the aseismic ridges, and again in the far south. This pattern is roughly reproduced in the residual depths. Depths are shallower than predicted in the north near Ascension Island and the Guinea Ridge, in the central part of the ocean over the aseismic ridges and again in the south toward Bouvet and the Falkland Plateau. Between these features, depths fall to near or somewhat deeper than the predicted

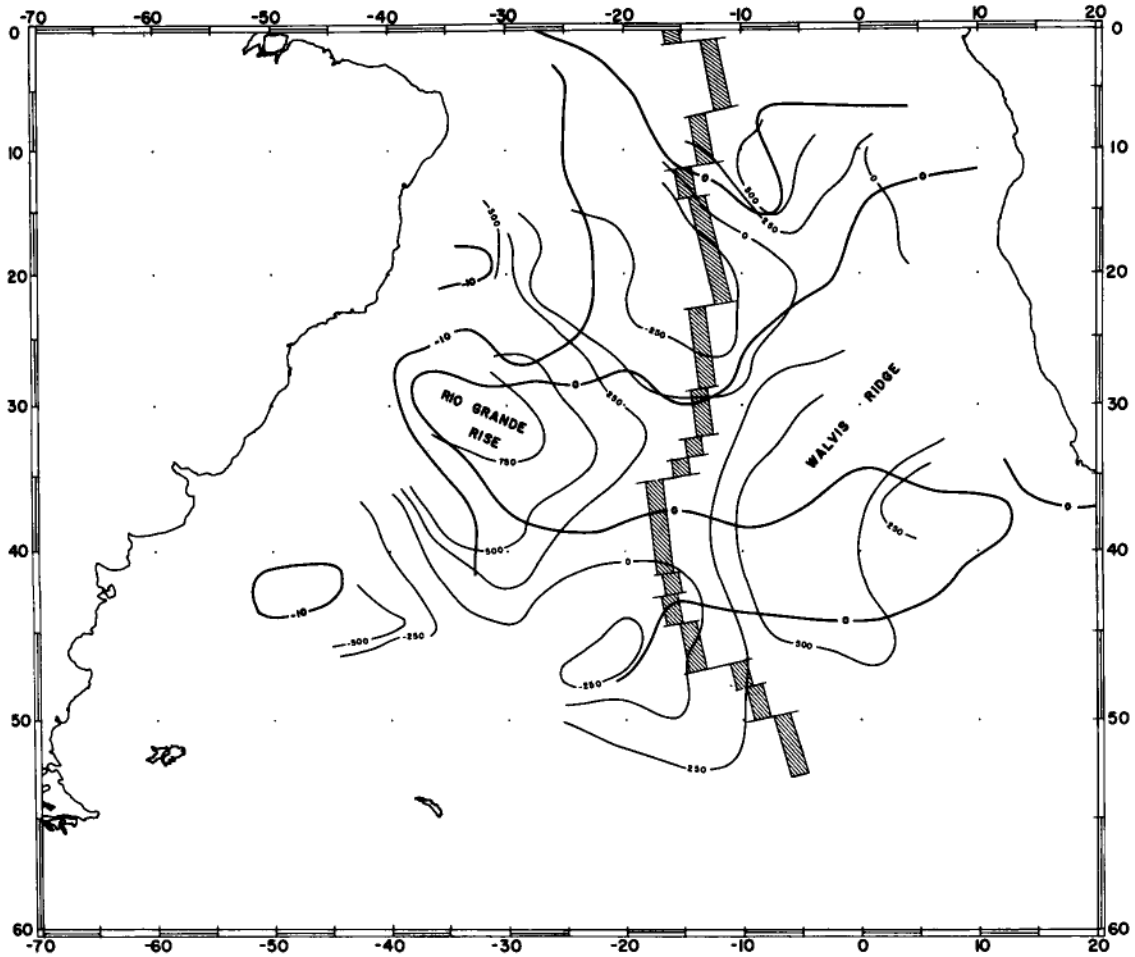

Figure 12. Map of 5 x 5° average residual gravity and depth anomalies in the South Atlantic. The gravity is contoured at 10 mgal and the depth at 250-m intervals.

depths except in the Cape Basin where the average residual basement depths are positive. As a result, the residual gravity and depth profiles along the ridge crest both have a somewhat sinusoidal appearance (Fig. 9, profile b).

Thus there is a rough visual correlation between the residual gravity and depth anomalies along a north–south profile (Fig. 9, profile b) in the South Atlantic with a half wavelength of about 1000 km. The correlation results, as in the case of the North Atlantic, from the presence of gravity highs over topographic highs of limited extent. In this case, these are the Rio Grande and Walvis aseismic ridges and the Tristan da Cunha Island Group. However, no correlation is evident on an east–west profile (Fig. 9, profile h, west of 20° W) since the asymmetry of the gravity field is not seen in the depths.

4.4 NORTHERN AND EASTERN PACIFIC

Menard (1973) constructed $1 \times 1^\circ$ average depth anomalies for a portion of the north-eastern Pacific Ocean. He noted a pattern in which local anomalies of a few hundred metres amplitude are superimposed on longer wavelength regional anomalies. The $5 \times 5^\circ$ averages (Figs 8 and 32) completely suppress the short-wavelength anomalies and bring out the regional pattern, the $5 \times 5^\circ$ residual depths decrease from a maximum of about 1400 m near Hawaii to slightly negative values at about 40° N and then increase to the north. The minimum values are small, between −50 and −150 m. The northward shallowing represents the outer rise off the Aleutian Trench which Watts & Talwani (1974) showed to be unusually wide off the eastern Aleutian Arc. There is a good general correlation between depth and gravity to the north of Hawaii, as shown in the map in Fig. 13 and in Fig. 14 which presents a gravity and bathymetry profile from Watts, Talwani & Cochran (1976). The profile shows the large local gravity anomalies associated with the Hawaiian ridge and moat superimposed on a broad gravity high over the Hawaiian swell. Beyond the swell, residual depth and free–air gravity anomalies decrease gradually to the north and then increase again toward the Aleutian trench. The qualitative correlation between gravity and depth is thus caused by two features, the Hawaiian swell and the Aleutian outer rise. Due to their different origin, there is a different relationship between gravity and depth over each feature. This can easily be seen in Fig. 14, where the gravity effect of the outer rise is roughly the same as that of the Hawaiian swell even though the outer rise has a topographic amplitude of only about half that of the swell. The outer rise is the result of the mechanical bending of the plate as it is consumed in the Aleutian trench (Hanks 1971; Watts & Talwani 1974) while the Hawaiian swell apparently results from thermal processes beneath the lithosphere which also produce the great amount of volcanic activity resulting in the Hawaiian ridge (Dietz & Menard 1953; Watts 1976a).

Away from the influence of the Hawaiian swell and the Aleutian Outer High, the residual depth anomalies in the north-eastern Pacific are small and relatively constant in the range of +50 to −150 m. The residual gravity anomalies, however, decrease from about −10 mgal in the west to more negative than −20 mgal in the east, as shown in profile j, Fig. 9 along 40° N.

Menard (1973) attributed depth anomalies to 'asthenospheric bumps' over which the lithosphere moves. He used the Gaposchkin & Lambeck (1971) SE II field to demonstrate that volcanic activity occurs on the updrift side of the 'asthenospheric bump', and that older islands are elevated as they drift over the 'bump' with maximum depth anomalies and gravity anomalies downdrift of the active volcanism. More recent data do not fit this pattern. Watts (1976a) calculated $5 \times 5^\circ$ depth anomalies and gravity anomalies around Hawaii. He showed that the maximum gravity anomalies and depth anomalies both occur over the south-eastern end of the Hawaiian ridge and appear to be related to the area of recent volcanism.

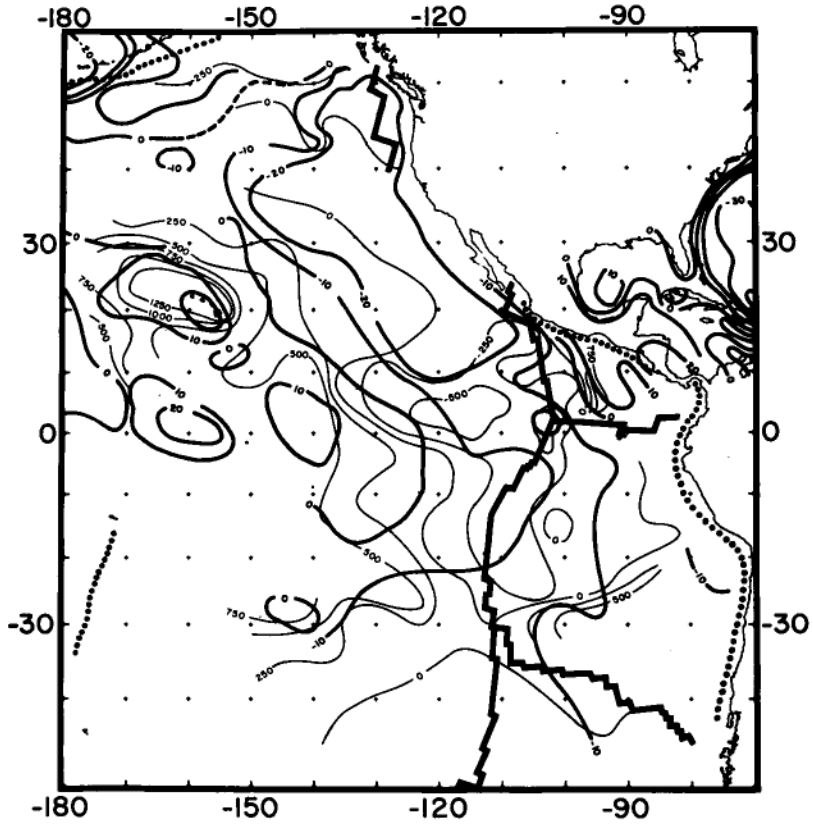

Figure 13. Map of 5 x 5° average residual gravity and depth anomalies in the Eastern Pacific. The gravity is contoured at 10 mgal and the depth at 250-m intervals.

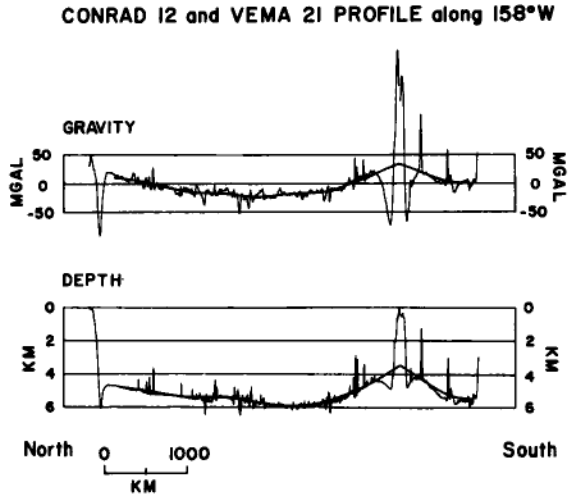

Figure 14. Free–air gravity and bathymetric profile from south of the Hawaiian ridge to the Aleutian trench. The heavy solid line over the profile is a 5° (555 km) average along the track.

The central Pacific southwest of Hawaii to about 30° S is characterized by positive residual depths while those in the eastern Pacific are generally negative. The residual gravity anomalies also show a west to east gradient, as shown in profile k, Fig. 9 at 10° S.

There is thus evidence of a relationship between gravity anomalies and depth anomalies at some locations in the northern and eastern Pacific, specifically in the area of Hawaii and the Aleutian Outer Gravity High. There is also a pronounced west to east gradient in both fields to the south-east of Hawaii.

However, there is no correlation evident on profile c, Fig. 9, along the crest of the East Pacific Rise where the residual depth and gravity anomalies appear to vary independent of each other, or on the east–west profile along 40° N (profile j, Fig. 9). Here, not only do the depth and gravity anomalies vary independently, but also a large gravity anomaly is associated with nearly average depths. Watts (1976a) noted that near Hawaii, where a correlation was observed, zero depth anomalies were associated with gravity anomalies of about −20 mgal.

4.5 INDIAN OCEAN

The residual depths and gravity anomalies in the South-east Indian Ocean both show simple, although contrasting, patterns, as shown in Fig. 15. The residual gravity anomaly contours are parallel to the mid-ocean ridge and reflect the asymmetry of the free–air gravity field. They are characterized by positive values of 5–10 mgal to the south of the ridge falling off toward the north to values more negative than −20 mgal in the South Australian Basin (profile l, Fig. 9).

The depth anomaly contours, on the other hand, are nearly perpendicular to the South-east Indian Ridge and although, as Weissel & Hayes (1974) note, the southern flank of the ridge is systematically shallower than the northern flank by up to a few hundred metres (Fig. 5(f)), the depth anomalies are dominated by a great depression centred at the Australian–Antarctic Discordance. This depth anomaly has an amplitude of almost 1 km and a half wavelength of about 2000 km (Hayes & Weissel 1974), and is associated with rough, chaotic topography and asymmetric sea floor spreading (Hayes & Connolly 1972; Weissel & Hayes 1974).

The lack of correlation between the gravity field and regional depth across the Discordance can be seen both in profile e, Fig. 9 along the ridge crest and in Fig. 16, which shows free–air gravity and depth profiles along 41° S gathered by USNS *Eltanin* . The gravity anomalies reflect the short-wavelength topographic relief up to wavelengths of a few hundred kilometres, but do not mirror the 1000-m regional change in depth along the isochron.

The residual gravity anomaly low in the South Australian Basin extends around the western end of Australia and across the northern Indian Ocean nearly to the Gulf of Aden (Fig. 17). The Indian Ocean Gravity Low, as delineated by the −20 mgal contours, is divided into two portions by a relative 5 x 5° residual gravity high over the Ninetyeast Ridge (Fig. 9, profile i). The residual gravity anomalies throughout most of the area are in the range of −20 to −35 mgal, except between the Ninetyeast and Chagos-Laccadive ridges immediately south of Ceylon where the 5 x 5° average anomalies reach −51 mgal.

The depth anomalies in the area of the extreme negative gravity anomalies south of Ceylon are slightly positive. The only area of markedly negative depth anomalies within the entire Indian Ocean Low is from about 15° S to 20° S in the Wharton Basin where the 5 x 5° depth anomalies are between −200 m and −300 m. However, other than this one deep area, the depth anomalies are either near zero or positive. We have calculated 1 x 1° average depth anomalies for all of the 1 x 1° squares in the Indian Ocean for which we

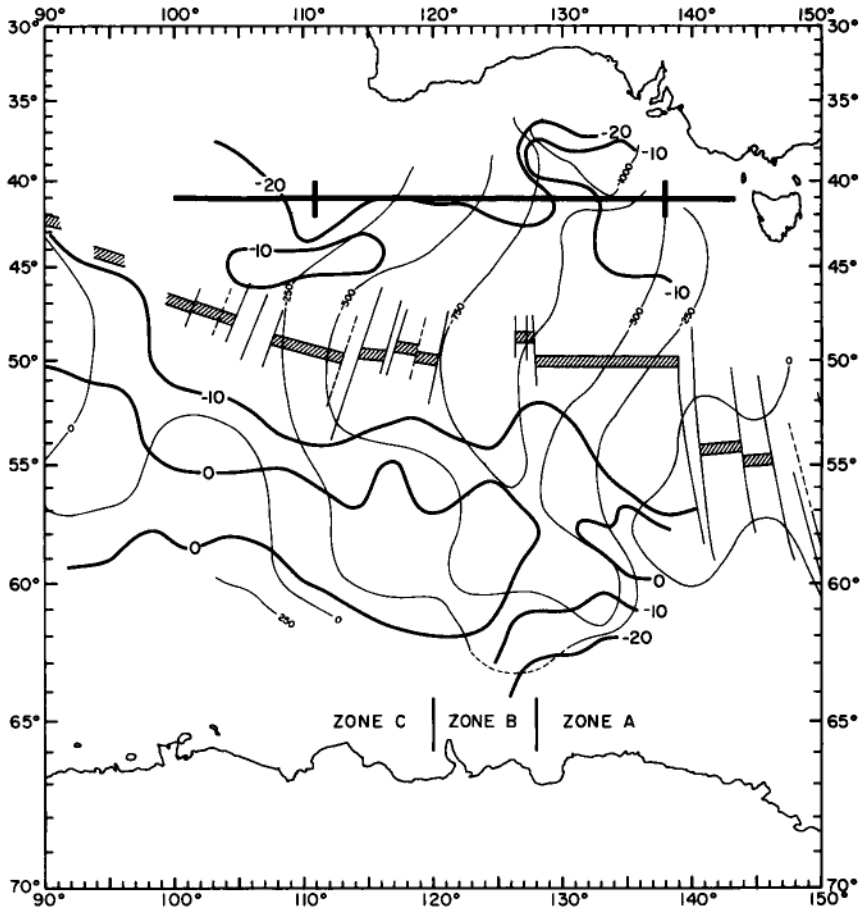

Figure 15. Map of 5 × 5° average residual gravity and depth anomalies in the South-east Indian Ocean. The gravity is contoured at 10-mgal and the depth at 250-m intervals. Note that the gravity and depth anomaly contours are nearly perpendicular to each other. The heavy solid line shows the location of the profile in Fig. 15. Zones A, B, and C are the tectonic zones of Weissel & Hayes (1971).

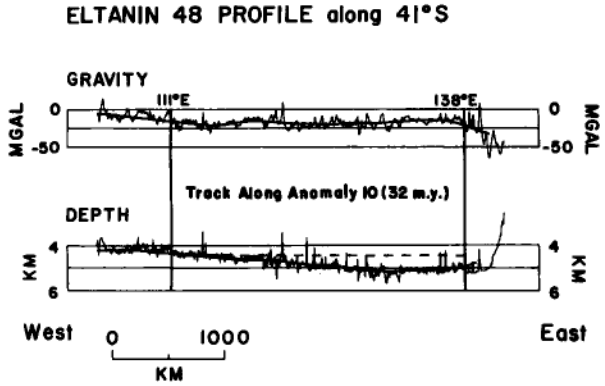

Figure 16. Free–air gravity and bathymetric profile along 41° S in the South-east Indian Ocean. Heavy solid line over the profiles is a 5° (550 km) average along the track. The heavy vertical lines are at 111° E and 138° E. Between these longitudes, the profile is very nearly along anomaly 10 (32 my bp). The dashed line on the bathymetric profile marks the predicted depth for 32-my old crust. Note that the gravity anomalies are nearly constant across the large depth anomaly.

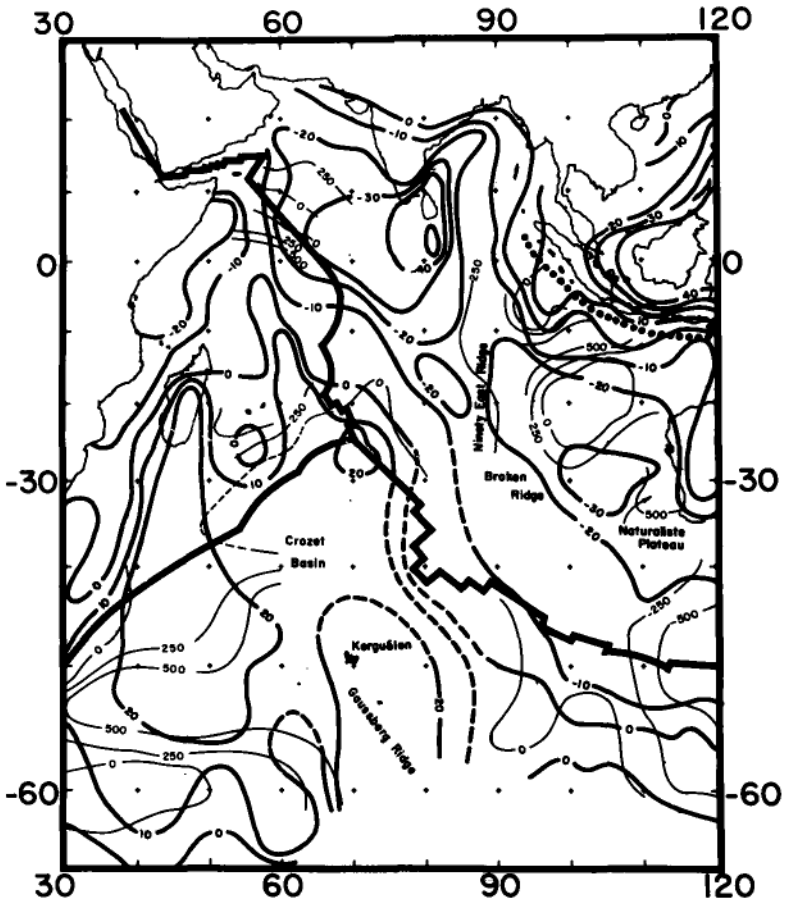

Figure 17. Map of 5 x 5° average residual gravity and depth anomalies in the Indian Ocean. The gravity is contoured at 10-mgal and the depth at 250-m intervals. Note lack of very deep depths in the region of large negative gravity anomalies in the north-eastern Indian Ocean.

could reasonably assign an age. The average of the 373 1 x 1° depth anomalies contained within the −20 mgal contour north of Broken Ridge and the Naturaliste Plateau (about 32° S) is +158 m. The average of 508 1 x 1° depth anomalies within the −10 mgal contour is +146 m.

The south-western Indian Ocean is characterized by positive gravity anomalies which appear to be centred in two locations. The first area is Kerguelen and the Gaussberg Ridge, which have been proposed to be, respectively, a hot spot and the aseismic ridge marking its trace (Morgan 1972).

The second area which positive residual gravity anomalies are found is near 45° E, principally to the south of the South-west Indian Ocean Ridge, but also extending northwards into Madagascar. Schlich (1974, 1975) has identified magnetic anomalies out to anomaly 32 in the Crozet Basin and their trend suggests that much of the South-west Indian Ocean was created during the Cretaceous epoch of uniform magnetic polarity or earlier. In order to estimate the depth anomalies in the areas where the age of the sea floor is not well known, we have chosen a predicted depth of 5800 m, equivalent to an age of about 105 my. Since the depth–age curve has a small slope at these ages, errors due to a wrong age are

small. The depth anomalies are positive through most of the basin with maximum values of about 700 m near 55° S over a very pronounced east–west trending arch in the acoustic basement. There is thus an agreement between the residual depth and gravity anomalies in this region, at least to the extent that both are of the same sign.

With the exception of the above mentioned areas in the South-west Indian Ocean, there is no general correlation between residual gravity anomalies and depth anomalies. Thus, in the North–east Indian Ocean which is characterized by large negative gravity anomalies, the depth anomalies are small, generally less than 500 m in amplitude and show no apparent relationship with the residual gravity anomalies. In the South-east Indian Ocean important changes in depth anomalies are not correspondingly present in the gravity anomalies (Figs 15, 16; Fig. 9, profile j). Thus one can draw the general conclusion that no simple and general relationship is evident between residual gravity and residual depth anomalies in the Indian Ocean

5 Discussion

Three broad scales of anomalies are prominent in the gravity field over the ocean basins:

5.1 SHORT-WAVELENGTH STRUCTURAL ANOMALIES

These anomalies, with wavelengths of up to a few hundred kilometers, are in large part directly related to uncompensated topographic relief (Talwani *et al.* 1972). Although in this study we have treated the short-wavelength anomalies as noise and attempted to average them out, this scale of anomaly contains most of the information used in crustal gravity studies.

5.2 INTERMEDIATE WAVELENGTH ANOMALIES

The survey of the gravity fields of the various oceans in the previous sections showed locations where a good correlation between intermediate wavelength anomalies (a few hundred to a few thousand kilometres) in residual gravity and depth appear to exist. Of particular importance are two groups of locations – (i) mid-ocean ridges and (ii) areas away from mid-ocean ridges, some of them with extensive volcanism. We review these areas more fully in the following:

(i) Mid-ocean ridges – A consistent anomaly does exist *across* mid-ocean ridge systems (Figs. 5 and 6), which is a function of the age of the ridge crust and appears to result from the thermal evolution of a compensated lithosphere as it is transported away from the spreading centre.

Gravity and depth both vary greatly *along* the mid-ocean ridge system (Fig. 9, profiles a–e). However, the variations in two parameters are not, in general, correlated along the ridge. The most obvious place where they do vary together is at the pronounced gradient in the gravity and depth anomalies near 30° N in the North Atlantic (Fig. 9, profile a). This gradient coincides with the boundary between 'normal' ocean to the south and the anomalous portion of the North Atlantic to the north. Within the anomalous area, gravity and depth are not correlated since the gravity anomalies are nearly constant from 30° N to 70° N across the Iceland topographic anomaly. They also appear to vary together in the South Atlantic (Fig. 9, profile b) where the gravity and depth anomaly profiles both have a sinusoidal appearance. However the significance of this observation may not be great,

since the amplitude of the variations along the ridge in the South Atlantic is small. On the other hand, the prominent 1000 m depression in the ridge at the Australian–Antarctic Discordance (Fig. 9, profile e) is not reflected in the gravity field. Similarly, the $5 \times 5^{\circ}$ gravity anomalies vary by about 50 mgal along the central Indian Ocean Ridge (Fig. 9, profile d) while the depths remain nearly constant.

(ii) Areas away from the mid-ocean ridge crests – Many of the correlations observed between residual gravity and depth anomalies arise from unusually shallow depths and positive gravity anomalies surrounding areas of extensive intraplate volcanism. Examples of this type of area are the Azores, Canaries, Cape Verde Islands and Hawaii.

The classical explanation for these regions of free–air gravity highs has been given by invoking regional and deep isostatic compensation. Watts (1976a) estimated that the compensation for the Hawaiian swell extends to a depth of 100–200 km. Sipkin & Jordan (1975) and Okal & Anderson (1975) have studied *ScS* travel-time residuals and found that shear-wave velocities are anomalously low in the upper mantle directly beneath oceanic islands.

A problem with the model of deep compensation embodied in density inhomogeneities is that they imply large shear stresses which the asthenosphere is unable to support. Flow must result and this flow has been associated with phenomena such as mantle plumes (Morgan 1972) which are able to maintain the topographic and gravity highs. One problem that the plume hypothesis raises, however, is that the observed correlation between gravity and topography is observed not only for areas of recent volcanism but also at Bermuda, which has not been active for 30 my (Aumento & Sullivan 1974), and aseismic ridges such as the Rio Grande Rise and Walvis Ridge and, in fact, probably for all large topographic features formed off the ridge axis.

Richter & Parsons (1975) have argued that convection in the Earth's mantle occurs at two distinct scales. A mass transport from ridge to trench occurs through the motion of a lithospheric plate and a large-scale return flow is required to conserve mass. They argued that the relatively constant heat flow in the old ocean basins and the tendency of thermal convection cells in both laboratory and numerical experiments to have dimensions of the order of their depth suggest that a second smaller scale of convection exists which is responsible for the major portion of heat transfer. They assumed that both forms of convection extend to the 650–700 km discontinuity and studied their interaction in a constant viscosity fluid.

There is at least one location in which intermediate wavelength gravity and depth anomalies are related to each other in a manner suggestive of Richter & Parson's hypothesis. This is over the elongated high which extends south-west from about 10° N, 150° W toward the East Pacific Rise. It is evident on the maps in Figs 7 and 8 and the relationship between the residual gravity and depth anomalies can be seen in profile k, Fig. 9. Also, as argued by Richter & Parsons (1975), the areas of extensive off-ridge volcanism which are associated with correlated gravity and depth anomalies can be explained either as modulations on the amplitude of convection along a roll or as upwelling spouts under slow moving plates. However, these features are not necessarily compatible with only one particular convection pattern and could as readily be explained as the result of plumes of either deep or shallow origin.

However, in general, intermediate wavelength residual depth and gravity anomalies are not correlated except at specific locations as can be readily seen from the profiles in Fig. 9. In particular see profile c along the East Pacific Rise. Also in some of the locations where a correlation is observed, such as over the Bermuda Rise and aseismic ridges, the correlation has remained long after the active volcanism has ceased and as the plate has moved over great distances. Thus the entire data set do not agree with a simple relationship between intermediate wavelength gravity and depth anomalies.

5.3 LONG-WAVELENGTH ANOMALIES AND CONVECTION IN THE MANTLE

A conspicuous feature of the Earth's gravity field is that large areas (several thousand kilometres on a side) are characterized by gravity anomalies that are consistently of one sign and of significant magnitude (Figs 1 and 7). Perhaps the most spectacular feature is the Indian Ocean Gravity Low which forms a trough in the gravity field 2000 km wide and more than 7500 km long in which the 5 x 5° average gravity anomalies are frequently more negative than −30 mgal and reach −50 mgal just south of Ceylon. Other large areas of significant negative anomalies are found in the western North Atlantic and off the western margin of North America in the Pacific. Equally large areas of positive gravity anomalies of the order of 20 mgal are found in the South-west Indian Ocean and over the central part of the North Atlantic north of about 30° N. The only ocean in which such large long-wavelength anomalies are not found is the South Atlantic. Even here though, 5 x 5° average gravity, anomalies of −10 to −20 mgal are found over much of the western basin. In addition, as noted by Watts *et al.* (1976), the interior of the northern and western Pacific is generally associated with gravity anomalies of the order of −10 mgal.

Areas in which depth anomalies of one sign occur are, in general, much smaller in extent than are such areas in the gravity anomaly field, and the 5 x 5° depth anomalies quite often vary from several 100 m positive to several 100 m negative within the area enclosed by one of the large long-wavelength gravity anomalies. One example of this pattern is in the Indian Ocean where the depth anomalies range from more than +500 m to about −250 m within the Indian Ocean Gravity Low. An exception is north of the 30° N boundary in the North Atlantic where there is a large area of consistently positive depth anomalies. Here the depth anomalies are all positive although they vary greatly in magnitude, from +300 to +3000 m, in an area in which the gravity anomalies are nearly constant (Fig. 10). With the exception of the North Atlantic, the 5 x 5° depth anomalies are generally less than about 500 m, with larger values confined to regions of extensive past or present volcanism away from the mid-ocean ridge.

As has been known for some time, the long-wavelength gravity field is not related in any obvious manner to surface tectonic features (Cook 1963) and the anomalies cut across plate boundaries and ocean–continent boundaries. This observation has been used to argue that the source of the anomalies must be located beneath the lithosphere. In addition, if such large, long-wavelength gravity anomalies have their source in the lithosphere, their presence implies that the lithosphere can support very large stresses. Fig. 18 shows the shear stresses which would occur within a 100-km thick lithosphere from supporting the anomalous masses implied by a three-dimensional harmonic gravity anomaly of a given wavelength and given peak-to-peak amplitude. The stresses were calculated following Lambeck (1972) and McKenzie (1967). Basically, the method is to calculate the stresses and gravity anomalies resulting from the harmonic deformation of an elastic lithosphere overlying an inviscid liquid asthenosphere. The two equations are combined to eliminate the deformation and give the stress, σ, as a function of the amplitude, $|\Delta g|$, and wavelength, λ, of the gravity anomaly.

The relationship between maximum sheer stress and the gravity anomalies is given by Lambeck (1972) as

$$\sigma \max = \sqrt{\tfrac{2}{3}}\, \bar{\rho} r\, |\Delta g|\, [(0.67 + 0.27\sqrt{k'^2})/(1-\sqrt{2h}\, k' R)]$$

where $\bar{\rho}$ and R are the Earth's mean density and radius; $2h$ is the thickness of the lithosphere and k' is a non-dimensional wave number defined as $k' = 2\pi h/\lambda$.

It is extremely difficult to make an accurate estimate of the strength of the lithosphere. Most laboratory experiments have been designed to study processes in the lower continental crust and have been carried out under temperature and pressure conditions appropriate to

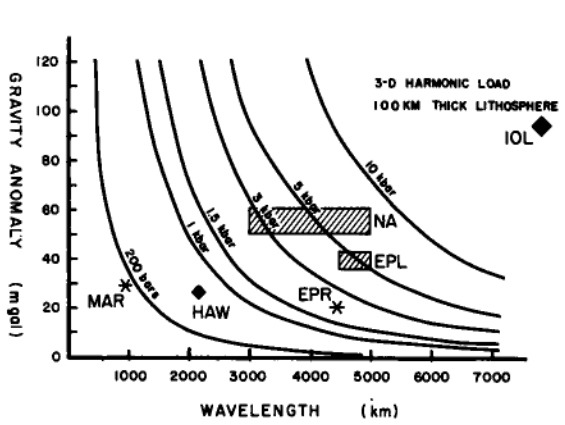

Figure 18. Shear stresses within a 100-km thick lithosphere resulting from support of the anomalous masses implied by harmonic gravity anomalies of a given wavelength and peak-to-peak amplitude. The shaded areas show the position of features in Earth's gravity field. IOL – Indian Ocean Low, EPL – gravity low off North America in the East Pacific, NA – North Atlantic High, HAW – Hawaiian Swell. Also shown are the stesses implied by the gravity anomalies associated with a fast-spreading (East Pacific Rise) and slow-spreading (Mid–Atlantic Ridge) mid-ocean ridge.

depths of less than about 30 km and at strain rates of at least several orders of magnitude greater than those present in the Earth (Griggs, Turner & Hoard 1960; Handin 1966). These tests give failure in shear at stresses of several kilobars. McKenzie (1967) estimated that the actual strength of the lithosphere was perhaps an order of magnitude less and picked a value of 200 bar, which roughly agrees with the stress release of large earthquakes. Lambeck (1972) argued that the strength of the lithosphere is four to five times as great as the apparent average stress reached in earthquakes and that a value of 1000 to 1500 bars was more representative. Jeffreys (1970) estimated the stress difference resulting from the static support of the Himalayas as 1200–1600 bar from an order-of-magnitude calculation. Although Wyss (1970) suggested that local shear stresses of 3 kbar might be reached beneath trenches, none of the available data suggest that the lithosphere could support the stresses of 4–5 kbar implicit in several of the features of the Earth's gravitv field (Fig. 18).

If the origin of the gravity anomalies is within the asthenosphere, as has been widely suggested (Kaula 1972a; McKenzie *et al.* 1974; Sclater *et al.* 1975), then they must be maintained in some manner, presumably by a convective flow pattern, since the asthenosphere has no long term finite strength. McKenzie *et al.* (1974) and Sclater *et al.* (1975) have argued that flow within the asthenosphere will exert stresses on the base of the lithosphere causing it to be deformed, and McKenzie *et al.* (1974) calculated that there should be a direct relationship between depth anomalies, gravity anomalies and the asthenospheric flow pattern.

In Fig.5, we have chosen the vertical scale in the plots of the residual gravity and depth anomalies across the ridges (Fig. 5(c) and (f)) so that 30 mgal is the same distance above the origin as 1000 m, since the slope of the relationship predicted by McKenzie *et al.* (1974) is 30 mgal/km. It can be seen that similar envelopes can be drawn around the majority of residual depth and gravity profiles, but that the position of individual ridge segments within the two envelopes is considerably different.

If a particular relationship were found between gravity and bathymetry other than that predicted by a particular model, then it could be argued that the disagreement arises from the drastic simplifications necessary to formulate and carry out numerical calculations and

by the fact that the values of many of the relevent parameters are poorly known. However, we are unable to find any overall relationship between the long-wavelength gravity field and residual ocean depths.

This result does not imply that convection is not occurring in the mantle or that it is not possible to learn anything regarding the form of the convection pattern. If the large observed long-wavelength gravity anomalies have their source within the asthenosphere, then they contain information on the distribution of mass within the asthenosphere. The fact that the residual depths are not related to the gravity anomalies must then necessitate that the lithosphere is in effect decoupled from the main body of the asthenosphere.

A possible qualitative explanation of how this necessary decoupling might occur comes from consideration of the effects of a strongly depth-dependent effective viscosity on the small-scale convection in the upper mantle.

Models of the viscosity structure of the upper mantle from glacial isostatic rebound generally involve either a uniform mantle viscosity or a low-viscosity channel in the upper asthenosphere. Walcott (1973) reviewed the arguments and concluded that because of the large increase in the relaxation time with increase in size of the glaciated region, the thin channel rather than half space model is the closest approximation to the real Earth. His analysis suggests that the structure most consistent with the data is a 110-km thick lithosphere, a low-viscosity channel 100–500 km thick with a viscosity of 10^{19}–10^{21} P depending on thickness and a lower mantle with a viscosity greater than 10^{23} P. Artyushkov (1971) concluded that a low-viscosity channel about 150 km thick with a viscosity of about 10^{21} P exists beneath the Canadian shield with much higher viscosities found below.

Turcotte & Oxburgh (1969, 1972) calculated viscosity profile for the mantle based on the assumption that deformation occurs by diffusion creep. They found a strong minimum of about 10^{21} P located directly beneath the lithosphere. The viscosity increased greatly with depth reaching 10^{24} P at a depth of about 700 km. Effective viscosity profiles determined by Weertman (1970) for dislocation creep also increase with depth although not nearly as dramatically as for diffusion creep.

The presence of a pronounced zone of low viscosity in the upper part of the asthenosphere could help to isolate the lithosphere from the mass inhomogeneities causing the long-wavelength gravity anomalies in two ways. First, the normal stress exerted by a viscous fluid is given by

$$\sigma_{zz} = 2\eta\,(dv/dz)$$

where η is the coefficient of viscosity and v is the vertical velocity. Thus, for a given flow pattern, the stresses are directly dependent on the viscosity. Since the surface deformation is determined by balancing the vertical stress, a decrease in the viscosity near the base of the lithosphere will result in a corresponding decrease in the deformation for a given flow pattern.

Second, and probably more important, is the effect that a variable viscosity has on the flow pattern. Torrance & Turcotte (1971) systematically investigated convection in a fluid layer heated from below with a viscosity which is strongly temperature and/or depth dependent. They found that the fluid motion tends to concentrate in the region of lowest viscosity and that as the viscosity gradient increases, this tendency becomes more pronounced. Using a temperature and pressure dependent expression determined by Turcotte & Oxburgh (1969) for the diffusion creep viscosity of the mantle, Torrance & Turcotte (1971) found that active circulation was confined to the upper few hundred kilometres and that most of the mantle was characterized by extremely sluggish flow. Other investigators (Foster 1969; Peltier 1972; Houston & DeBremaecher 1975; Parmentier, Turcotte & Torrance 1975) obtained similar results for fluids heated from within and/or below.

The numerical experiments cited above show a strong tendency for the convective flow in a fluid with a highly variable viscosity to be concentrated in the area of low viscosity in the form of nearly equidimensional cells or rolls. If a low-viscosity layer exists beneath the lithospheric plates, then the small-scale flow of Richter & Parsons (1975) would tend to be concentrated within the low-viscosity channel.

The observed long-wavelength gravity anomalies cover areas much greater than the proposed size of the small-scale convection cells. Thus, if their source is within the asthenosphere, they apparently arise from inhomogeneities resulting from the large-scale circulation. The inhomogeneities would be expected to interact with the small-scale convection and modify its intensity by, for example, modifying the amount of heat available to the small scale cells, and thus might be expected to effect the ocean depths.

However, the finite strength of the lithosphere cannot be ignored for small-scale convection cells. The surface deformation computed by McKenzie *et al.* (1974) is for a free surface. Sclater *et al.* (1975) and McKenzie & Weiss (1975) considered the effect an elastic lithosphere on the deformation. Their results imply that for a stress system with a half wavelength of 600 km, corresponding to convective cells extending from the base of the lithosphere to the 700-km discontinuity, the deformation is 60–70 per cent that of a free surface. However, if the half wavelength is 350 km, the surface deformation is only about 20 per cent and for a half wavelength of 250 km, less than 10 per cent that of a free surface. This, combined with the lower viscosity layer in the upper part of the asthenosphere, could reduce the surface deformation due to convection to within the noise level of averaged depth measurements.

Although this discussion does not provide an explanation for the large long-wavelength anomalies, it suggests that their source is located in the lower portion of the asthenosphere between depths of about 350 and 650 km and that they contain information on the large-scale circulation of the upper mantle. It could then be speculated that the shallow depths and positive gravity anomalies in the northern half of the North Atlantic are due to high temperatures at shallow depths in the low-viscosity asthenosphere. This is also suggested by the heat-flow study of Langseth & Zielinski (1974) who found uniformly high heat flow in the Norwegian–Greenland Sea and on the Reykjanes Ridge. The North Atlantic will be considered in detail in another study (Cochran & Talwani, in preparation).

Alternatively, the sources of the observed gravity anomalies could be in the lower mantle, beneath the asthenosphere. However, the density fluctuations necessary to produce anomalies of a given wavelength increase greatly as their source is placed deeper (Cook 1967) and the sources of the main portion of the global gravity field are probably at depths of less than 1000 km (Bott 1971).

Conclusions

We have compiled $5 \times 5^\circ$ free–air gravity anomalies over much of the world's oceans. The study of the gravity data allows the following conclusions to be made:

(1) Satellite and combination gravity field. Analysis of satellite orbits can accurately determine the Earth's gravity field at wavelengths of greater than about 4000 km. The higher order terms in combination solutions are largely dependent on surface data. Comparison of the combination solutions with our surface data shows that the recent GEM 6 field (Lerch *et al.* 1974) is in much better agreement with the surface data than is the older, widely used SE II field (Gaposchkin & Lambeck 1971) for which only a limited amount of surface data was available. Recent combination solutions are in reasonable agreement with the surface data concerning the general location and amplitude of major features in the Earth's gravity field. There is, however, significant disagreement in the exact location of extrema and in the

value of the gravity field at a given location. It is, therefore, necessary to use surface data to make detailed studies of the relationship of the intermediate and long wavelength components of the gravity field to surface features and phenomena.

(2) Mid-ocean ridges. Surface-ship gravity profiles across the mid-ocean ridge system show that the ridge crest is consistently associated with a maximum in the free–air gravity field when compared to gravity anomalies over the ridge flanks. We were able to quantify the ridge anomaly in terms of an empirical $1 \times 1^\circ$ average gravity–age relationship. This curve shows a positive gravity anomaly of between 20 and 25 mgal falling off to zero at about 40 my. There is some evidence of a second order spreading rate dependence such that fast spreading ridges are associated with $1 \times 1^\circ$ average gravity highs of about 20 mgal over the crest while the high over slow spreading ridge axes is of the order of 25–30 mgal. The observed mid-ocean ridge gravity anomalies are generally compatible with current thermal models of the lithosphere (Sclater & Francheteau 1970; Parker & Oldenberg 1973) although the spreading rate dependence is less than might be predicted from those models. It is not possible to distinguish between the two thermal models on the basis of observed and predicted gravity anomalies. The gravity anomalies associated with the mid-ocean ridge can thus be explained by processes operating at the plate boundary and the subsequent thermal evolution of the lithosphere. They thus do not provide direct information on deeper processes.

(3) Residual gravity anomalies and residual depths. We removed the empirical gravity–age relationship from the observed free–air gravity anomalies to produce $5 \times 5^\circ$ residual gravity anomalies which, in general, showed no relationship to the location of the mid-ocean ridges and which showed the gravity fields of most oceans to be asymmetric. We then examined in detail the relationship between the residual gravity anomalies and depth anomalies in the various oceans. This study showed that there are regions in which a good correlation does exist. These areas are intermediate wavelength positive features often associated with areas of extensive volcanism away from mid-ocean ridges. Not only does such a correlation exist over active hot spots, but it is also found over such relict features as Bermuda and the South Atlantic aseismic ridges. Areas of unusual elevation and volcanic activity located at a mid-ocean ridge crest do not, however, have a coresponding gravity anomaly associated with them suggesting that new lithosphere is created in isostatic equilibrium and the gravity anomalies associated with 'hot spots' arise from disturbing the already existing lithospheric plate.

The long-wavelength component of the Earth's gravity field is characterized by large areas in which significant anomalies of constant sign are found. There is apparently no relationship between the long-wavelength gravity field and oceanic depths. If the long-wavelength gravity anomalies have their origin within the asthenosphere, their presence implies the presence of a convective flow system. The lack of correlation between the long-wavelength gravity field and the residual depths implies that the lithosphere and asthenosphere are decoupled in some manner, at least as far as the propagation of vertical stress is concerned. Such decoupling could be the result of a region of low viscosity immediately beneath the lithosphere below which the viscosity increases rapidly with depth.

Acknowledgments

R. N. Anderson, P. Dehlinger, D. W. Forsyth, D. E. Hayes and A. B. Watts reviewed the manuscript and offered helpful criticisms and suggestions. This research was suported by National Science Foundation grants GA–312, GA–668, GA–894, GA–1434, GA–1523, GP–5392, GA–17761, GV–23334, GA–12825, GV–27472, GA–27281, OPP–74–02238

and DES–71–00214 and by Office of Naval Research contracts NONR 266 (48), NONR 266 (79), N00014–67–A0108–0004 and N00014–75–C–0210. This study would not have been possible except for the efforts of the officers, scientists and gravity observers on *R/V Vema, R/V Robert D. Conrad* and *USNS Eltanin* who contributed greatly to the collection of the large amount of gravity data on which this study is based.

References

Anderson, R. N., McKenzie, D. & Sclater, J. G., 1973. Gravity, bathymetry and convection in the Earth, *Earth planet. Sci. Lett.*, **18**, 391–407.

Artyushkov, E. V., 1971. Rheological properties of the crust and upper mantle according to data on isostatic movements, *J. geophys. Res.*, **76**, 1376–1390.

Atwater, T. & Menard, H. W., 1970. Magnetic lineations in the northeast Pacific, *Earth planet. Sci. Lett.*, **7**, 445–450.

Aumento, F. & Sullivan, K. D., 1974. Deep drill investigations of the oceanic crust in the North Atlantic, *Geodynamics of Iceland and the North Atlantic Area*, pp. 83–108, ed. Kristjansson, L., D. Reidel, Dordrecht, Holland.

Bott, M. H. P., 1971. The mantle transition zone as possible source of global gravity anomalies, *Earth planet. Sci. Lett.*, **11**, 28–34.

Cochran, J. R., 1973. Gravity and magnetic investigations in the Guiana Basin, Western Equatorial Atlantic, *Bull. geol. Soc. Am.*, **84**, 3249–3268.

Cochran, J. R. & Talwani, M., 1977. Long-wavelength gravity anomalies and the deep structure of the North Atlantic Ocean, *in preparation.*

Cook, A. H., 1963. Sources of harmonics of low order in the external gravity field of the Earth, *Nature*, **198**, 1186.

Cook, A. H., 1967. Gravitational considerations, *The Earth's Mantle*, ed. Gaskell, T. F., pp. 63–87, Academic Press, New York.

Coron, S., 1973. Sur les anomalies moyennes de la pesanteur, Tests et Resultants – Anomalies a L'air Libre par $1^\circ \times 1^\circ$, *Bureau Grav. Inter. Bull. D'info.*, **31**, 118–149.

Dietz, R. S. & Menard, H. W., 1953. Hawaiian swell, deep and arch, and the subsidence of the Hawaiian Islands, *J. Geol.*, **61**, 99–113.

Eldholm, O. & Windisch, C. C., 1974. Sediment distribution in the Norwegian–Greenland Sea, *Bull. geol. Soc. Am.*, **85**, 1661–1676.

Elvers, D., Potter, K., Siedel, D. & Morley, J., 1971. *I.D.O.E. 1971 Surveyor Seamap*, N.O.A.A. National Ocean Survey, Washington.

Ewing, J., Ewing, M., Aitken, T. & Ludwig, W. J., 1968. North Pacific sediment layers measured by seismic profiling, *The Crust and Upper Mantle of the Pacific Area*, eds L. Knopoff, C. L. Drake & P. J. Hart, *Am. geophys. Un. Monogr.* **12**, 147–173.

Ewing, M., Carpenter, G., Windisch, C. & Ewing, J., 1973. Sediment distribution in the oceans; the Atlantic, *Bull. geol. Soc. Am.*, **84**, 71–88.

Ewing, M., Eittreim, S., Truchan, M. & Ewing, J., 1975. Sediment isopach map of the Indian Ocean, *International geophysical – geological atlas of the Indian Ocean*, ed Udintsev, G., Moscow.

Fisher, R. L., Sclater, J. G. & McKenzie, D., 1971. The evolution of the Central Indian Ridge, Western Indian Ocean, *Bull. geol. Soc. Am.*, **82**, 553–562.

Fisher, R. L., Laughton, A. S. & Roberts, D. G., 1975. Bathymetric map of the Indian Ocean, *Internationl geophysical – geological atlas of the Indian Ocean*, ed. Udintsev, G., Moscow.

Fleischer, U., 1971. Gravity surveys over the Reykjanes Ridge and between Iceland and the Faeroe Islands, *Mar. geophys. Res.*, **1**, 314–327.

Foster, T. P., 1969. Convection in a variable viscosity fluid heated from within, *J. geophys. Res.*, **74**, 685–693.

Gaposchkin, E. M. (ed.), 1973. 1973 Smithsonian Standard Earth III, *Smithson. astrophys. Obs., Spec. Rept. 353.*

Gaposchkin, E. M., 1974. Earth's gravity field to the eighteenth degree and geocentric coordinates for 104 stations from satellite and terrestrial data, *J. geophys. Res.*, **79**, 5377–5411.

Gaposchkin, E. M. & Lambeck, K., 1970. 1969 Smithsonian Standard Earth II, *Smithson. astrophys. Obs., Spec. Rept. 315.*

Gaposchkin, E. M. & Lambeck, K., 1971. Earth's gravity field to the sixteenth degree and station coordinates from satellite and terrestrial data, *J. geophys. Res.*, **76**, 4855–4883.

Griggs, D. T., Turner, F. J. & Hoard, H. C., 1960. Deformation of rocks at 500 to 800° C, *Rock deformation.*, eds Griggs, D. & Handin, I., *Geol. Soc. Am. Mem.*, **79**, 39–104.

Handin, J., 1966. Strength and Ductility, *Handbook of physical constants*, ed. Clark, S. P., *Geol Soc. Am. Mem.*, **97**, 223–290.

Hanks, T. C., 1971. The Kuril Trench – Hokkaido rise system: large shallow earthquakes and simple models of deformation, *Geophys. J. R. astr. Soc.*, **23**, 173–189.

Hayes, D. E. & Conolly, J. R., 1972. Morphology of the southeast Indian Ocean, *Antarctic Oceanology II: The Australian – New Zealand Sector*, ed. Hayes, D. E., *Antarctic Res. Ser.*, **19**, 125–145.

Hayes, D. E. & Weissel, J. K., 1974. Depth anomalies in the Southeast Indian Ocean (abstract), *Abstr. Prog. Geol. Soc. Amer.*, **6**, 784.

Heiskanen, W. A. & Vening Meinesz, F. A., 1958. *The Earth and its gravity field*, 470 pp., McGraw-Hill, New York.

Herron, E. M., 1972. Sea-floor spreading and the Cenozoic history of the East-Central Pacific, *Bull. geol. Soc. Am.*, **83**, 1671–1692.

Houston, M. H. & DeBremaecker, J.-Cl., 1975. Numerical models of convection in the upper mantle, *J. geophys. Res.*, **80**, 742–751.

Houtz, R. E. & Markl, R. G., 1972. Seismic profiler data between Antarctica and Australia, *Antarctic Oceanology II: The Australian–New Zealand Sector*, ed. Hayes, D. E., *Antarctic Res. Ser.*, **19**, 147–164, Am. Geophys. Un., Washington DC.

Jeffreys, H., 1970. *The Earth*, 5th edn, 525 pp., Cambridge University Press.

Kahle, H. G. & Talwani, M., 1973. Gravimetric Indian Ocean geoid, *Z. Geophys*, **39**, 167–187.

Kaula, W. M., 1966. Tests and combination of satellite determinations of the gravity field with gravimetry, *J. geophys. Res.*, **71**, 5303–5313.

Kaula, W. M., 1969a. A tectonic classification of the main features of the Earth's gravitational field, *J. geophys. Res.*, **74**, 4807–4826.

Kaula, W. M., 1969b. Interpretation of lunar mass concentrations, *Phys. Earth planet. Int.*, **2**, 123–137.

Kaula, W. M., 1972a. Global gravity and tectonics, *The nature of the solid Earth*, pp. 385–405, ed. Robertson, E. C., McGraw-Hill, New York.

Kaula, W. M., 1972b. Global gravity and mantle convection, *Tectonophys.*, **13**, 341–359.

Khan, M. A., 1974. Satellite techniques in geophysics and their relationship to marine geodesy, *Proc. Int. Symp. Applications of marine geodesy*, 87–112, Columbus, Ohio.

Ladd, J. W., 1974. Sea-Floor Spreading in the South Atlantic and Caribbean Tectonics, 152 pp., *PhD thesis, Columbia University*.

Lambeck, K., 1972. Gravity anomalies over ocean ridges, *Geophys J.*, **30**, 37–54.

Langseth, M. G. & Zielinski, G. W., 1974. Marine heat flow measurements in the Norwegian-Greenland Sea and in the vicinity of Iceland, *Geodynamics of Iceland and the North Atlantic Area*, pp. 277–295, ed. Kristjansson, L., D. Reidel, Dordrecht, Holland.

Larson, R. L., 1975. Late Jurassic sea floor spreading in the eastern Indian Ocean, *Geology*, **3**, 69–71.

Larson, R. L. & Ladd, J. W., 1973. Evidence for the opening of the South Atlantic in the Early Cretaceous, *Nature*, **246**, 209–212.

Larson, R. L. & Pitman, W. C. 1972. Worldwide correlation of Mesozoic magnetic anomalies and its implications, *Bull. geol. Soc Am.*, **83**, 3645–3662.

LePichon, X. & Talwani, M., 1969. Regional gravity anomalies in the Indian Ocean, *Deep-Sea Research*, **16**, 263–274.

Lerch, F. J., Wagner, C. A., Richardson, J. A. & Brownd, J. E., 1974. Goddard earth models (5 and 6); *Rep. X–921–74–145*, 100 pp., Goddard Space Flight Center, Greenbelt, Maryland.

Markl, R. G., 1974a. Evidence for the breakup of eastern Gondwanaland by the Early Cretaceous, *Nature*, **251**, 196–199.

Markl, R. G., 1974b. Bathymetric Map of the Eastern Indian Ocean, *Initial Reports of the Deep Sea Drilling Project*, **26**, 967–968, Davies, T. A., Luyendyk, B. P., *et al.*, Washington.

Mather, R. S., 1969. The free air geoid for Australia, *Geophys. J. R. astr. Soc.*, **18**, 499–516.

McKenzie, D. P., 1967. Some remarks on heat flow and gravity anomalies, *J. geophys. Res.*, **72**, 6261–6273.

McKenzie, D. P. & Sclater, J. G., 1971. The evolution of the Indian Ocean since the Late Cretaceous, *Geophys J. R. astr. Soc.*, **25**, 437–528.

McKenzie, D. P. & Weiss, N., 1975. Speculations on the thermal and tectonic history of the Earth, *Geophys. J. R. astr. Soc.*, **42**, 131–174.

McKenzie, D. P., Roberts, J. M. & Weiss, N. O., 1974. Convection in the Earth's mantle: towards a numerical simulation, *J. Fluid Mech.*, **82**, 465–538.

Menard, H. W., 1973. Depth anomalies and the bobbing motion of drifting islands, *J. geophys. Res.*, **78**, 5128–5137.

Morgan, W. J., 1972. Deep mantle convection plumes and plate motions, *Am. Ass. Petr. Geol. Bull.*, **56**, 203–213.

Okal, E. A. & Anderson, D. L., 1975. A study of lateral inhomogeneities in the upper mantle by multiple *ScS* travel-time residuals, *Geophys. Res. Lett.*, **2**, 313–316.

Parker, R. L. & Oldenberg, D. W., 1973. A thermal model for oceanic ridges, *Nature*, **247**, 137–139.

Parmentier, E. M., Turcotte, D. L. & Torrance, K. E., 1975. Numerical experiments on the structure of mantle plumes, *J. Geophys. Res.*, **80**, 4417–4424.

Parsons, B. & Sclater, J. G., 1977. An analysis of the variation of ocean floor bathymetry and heat flow with age, *J. geophys. Res.*, **82**, 803–827.

Peltier, W. R., 1972. Penetrative convection in the planetary mantle, *Geophys. Fluid Dyn.*, **5**, 47–88.

Pitman, W. C. & Talwani, M., 1972. Sea-floor spreading in the North Atlantic, *Bull. geol. Soc. Am.*, **83**, 619–646.

Rabinowitz, P. D. & Cochran, J. R., 1977 Free-air gravity anomaly map of the continental margin of Brazil, *Am. Ass. Petr. Geol. Special Map Series*, in press.

Rapp, R. H., 1968. Gravitational potential of the Earth determined from a combination of satellite, observed, and model anomalies, *J. geophys. Res.*, **73**, 6555–6562.

Richter, F. M., 1973. Convection and the large scale circulation of the mantle, *J. Geophys. Res.*, **78**, 8735–8745.

Richter, F. M. & Parsons, B., 1975. On the interaction of two scales of convection in the mantle, *J. geophys. Res.*, **80**, 2529–2541.

Schlich, R., 1974. Sea floor spreading history and deep sea drilling results in the Madagascar and Mascarene Basins, Western Indian Ocean, *Initial Reports of the Deep Sea Drilling Project*, **25**, 663–678, Simpson, E. S. W., Schlich, R., *et al.*, US Govt. Printing Office, Washington.

Schlich, R., 1975. Structure et age de L'Océan Indian Occidental, *Mém. horssérie Soc. Geol. de France, no. 6*, **102.**

Sclater, J. G. & Fisher, R. L., 1974. Evolution of the East-Central Indian Ocean, with emphasis on the tectonic setting of the Ninetyeast Ridge, *Bull. geol. Soc. Am.*, **85**, 683–702.

Sclater, J. G. & Francheteau, J. 1970. The implications of terrestrial heat flow observations on current tectonic and geochemical models of the crust and upper mantle of the Earth, *Geophys. J. R. astr. Soc.*, **20**, 509–542.

Sclater, J. G., Anderson, R. N. & Bell, M. C., 1971. The elevation of ridges and the evolution of the Central Eastern Pacific. *J. geophys. Res.*, **76**, 7888–7915.

Sclater, J. G., Lawver, L. A. & Parsons, B., 1975. Comparison of long wavelength residual elevation and free–air gravity anomalies in the North Atlantic and possible implications for the thickness of the lithospheric plate, *J. geophys. Res.*, **80**, 1031–1052.

Sclater, J. G., Luyendyk, B. P. & Meinke, L., 1976. Magnetic lineations in the southern part of the Central Indian Basin, *Bull. Geol. Soc. Am.*, **87**, 371–378.

Sipkin, S. A. & Jordan, T. H., 1975. Lateral inhomogeneity of the upper mantle determined from the travel times of *ScS*, J. Geophys. Res., **80**, 1474–1484.

Takin, M. & Talwani, M., 1966. Rapid computation of the gravitational attraction of topography on a spherical Earth, *Geophys. Prosp.*, **14**, 119–142.

Talwani, M. & Eldholm, O., 1977. Evolution of the Norwegian–Greenland Sea, *Bull. geol. Soc., Am.*, in press.

Talwani, M. & Grønlie, G., 1976. Free–air gravity field of the Norwegian–Greenland Sea, *Geol. Soc. Am., Special Map and Chart Series*, MC-15.

Talwani, M. & Kahle, H. G., 1975. Free–air gravity maps in the Indian Ocean, *International Geophysical–Geological Atlas of the Indian Ocean*, ed. Udintsev, G., Moscow.

Talwani, M. & LePichon, X., 1969. Gravity field over the Atlantic Ocean, *The Earth's Crust and Upper Mantle*, ed. Hart, P. J., *Am. geophys. Un. Monogr.* **13**, 341–351.

Talwani, M., Heezen, B. C. & Worzel, J. L., 1961. Gravity anomalies, physiography and crustal structure of the Mid Atlantic Ridge, *Publ. Bur. Cen. Seism. Inter., Ser. A, Trav. Sci. Fasc.*, **22**, 81–111.

Talwani, M., Windisch, C. C. & Langseth, M. G., 1971. Reykjanes Ridge Crust: A detailed geophysical study, *J. geophys. Res.*, **76**, 473–517.

Talwani, M., Poppe, H. R. & Rabinowitz, P. D., 1972. Gravimetrically determined geoid in the Western North Atlantic, *Sea surface topography from space*, vol. 2, NOAA Tech. Report ERL–228–AOML 7–2, pp. 1–34.

Torrance, K. E. & Turcotte, D. L., 1971. Thermal convection with large viscosity variations, *J. Fluid Mech.*, **47**, 113–123.

Turcotte, D. L. & Oxburgh, E. R., 1969. Convection in a mantle with variable physical properties, *J. geophys. Res.*, **74**, 1458–1474.

Turcotte, D. L. & Oxburgh, E. R., 1972. Mantle convention and the New Global Tectonics, *A. Rev. Fluid Mech.*, **4**, 33–68.

Uchupi, E., 1971. *Bathymetric Atlas of the Atlantic, Caribbean and Gulf of Mexico*, Woods Hole Oceanogr. Inst. Ref. 71–72, Woods Hole, Massechusetts.

Vening Meinesz, F. A., 1934. *Gravity Expeditions at Sea, 1923–1932*, vol. II, 208 pp., Netherlands Geodetic Commission, Delft, (2nd edn 1964).

Vening Meinesz, F. A., 1948. *Gravity Expeditions at Sea, 1923–1938*, vol. IV, 233 pp., Netherlands Geodetic Commission, Delft.

Vening Meinesz, F. A., 1961. Convection currents in the mantle of the Earth, *Keninkl. Nederl. Akad. Van Wettenschappen, Ser. B*, **64**, 501–511.

Walcott, R. I., 1973. Structure of the Earth from glacio-isostatic rebound, *A. Rev. Earth. planet. Sci.*, **1**, 39–62.

Watts, A. B., 1975. Gravity Field of the Northwest Pacific Ocean Basin and its Margin: Aleutian Island Arc-Trench System, *Geol. Soc. Am., Special Map and Chart Series*, MC–10.

Watts, A. B., 1976a. Gravity and bathymetry in the Central Pacific Ocean, *J. geophys. Res.*, **81**, 1533–1553.

Watts, A. B., 1976b. Gravity Field of the Northwest Pacific Ocean Basin and its Margin: Philippine Sea, *Geol. Soc. Am., Special Map and Chart Series*, MC–12.

Watts, A. B. & Kogan, M. G., 1977. Gravity Field of the Northwest Pacific Ocean Basin and its Margin: Kuril Island Arc–Trench System, *Geol. Soc. Am., Special Map and Chart Series*, in preparation.

Watts, A. B. & Talwani, M., 1974. Gravity anomalies seaward of deep-sea trenches and their tectonic implications, *Geophys. J. R. astr. Soc.*, **36**, 57–90.

Watts, A. B. & Talwani, M., 1975. Gravity Field of the Northwest Pacific Ocean Basin and its Margin: Hawaii and Vicinity, *Geol. Soc. Am., Special Map and Chart Series*, MC–9.

Watts, A. B., Talwani, M. & Cochran, J. R., 1976. Gravity field of the northwest Pacific Ocean basin and its interior, *Am. geophys. Un. Monogr.* **19**, 17–34.

Weertman, J., 1970. The creep strength of the Earth's mantle, *Rev. Geophys. Space Phys.*, **8**, 145–168.

Weissel, J. K. & Hayes, D. E., 1972. Magnetic anomalies in the Southeast Indian Ocean, *Antarctic Oceanology II: The Australian–New Zealand Sector*, ed. Hayes, D. E., *Antarctic Res. Ser.*, **19**, 165–196, Am. geophys. Un., Washington.

Weissel, J. K. & Hayes, D. E., 1974. The Australian–Antarctic Discordance: new results and implications, *J. geophys. Res.*, **79**, 2579–2587.

Whitmarsh, R. B., 1974. Some aspects of plate tectonics in the Arabian Sea, *Initial Reports of the Deep Sea Drilling Project*, **23**, 527–536, eds Whitmarsh, R. B., Weser, O. E., Ross, D. A., *et al.*, US Govt. Printing Office, Washington.

Woodside, J. M., 1972. The Mid Atlantic Ridge near 45° N XX, The Gravity Field, *Can. J. Earth Sci.*, **9**, 942–958.

Woollard, G. P., Machesky, L. & Caldera, J. M., 1969. A regional survey of northern Mexico and the relations of Bouguer anomalies to regional geology and elevation in Mexico, *Hawaii Inst. Geophys. Rept. HIG–69–13.*

Wyss, M., 1970. Stress estimates for South American shallow and deep earthquakes, *J. geophys. Res.*, **75**, 1529–1544.

Lamont-Doherty Geological Observatory Contribution No. 2522.

Appendix 1

This appendix presents $1 \times 1^\circ$ average free–air gravity anomalies in the North Atlantic Ocean, Indian Ocean and a portion of the Central Pacific Ocean surrounding Hawaii. Also given are $1 \times 2^\circ$ average free–air gravity anomalies for the Norwegian–Greenland Sea. The gravity anomalies were determined from free–air gravity anomaly maps as described earlier and are referred to the International Ellipsoid (flattening = 1/297). The anomalies in the Indian Ocean have been previously published by Kahle & Talwani (1973), those near Hawaii by Watts (1976) and some of the North Atlantic values by Talwani *et al.* (1972).

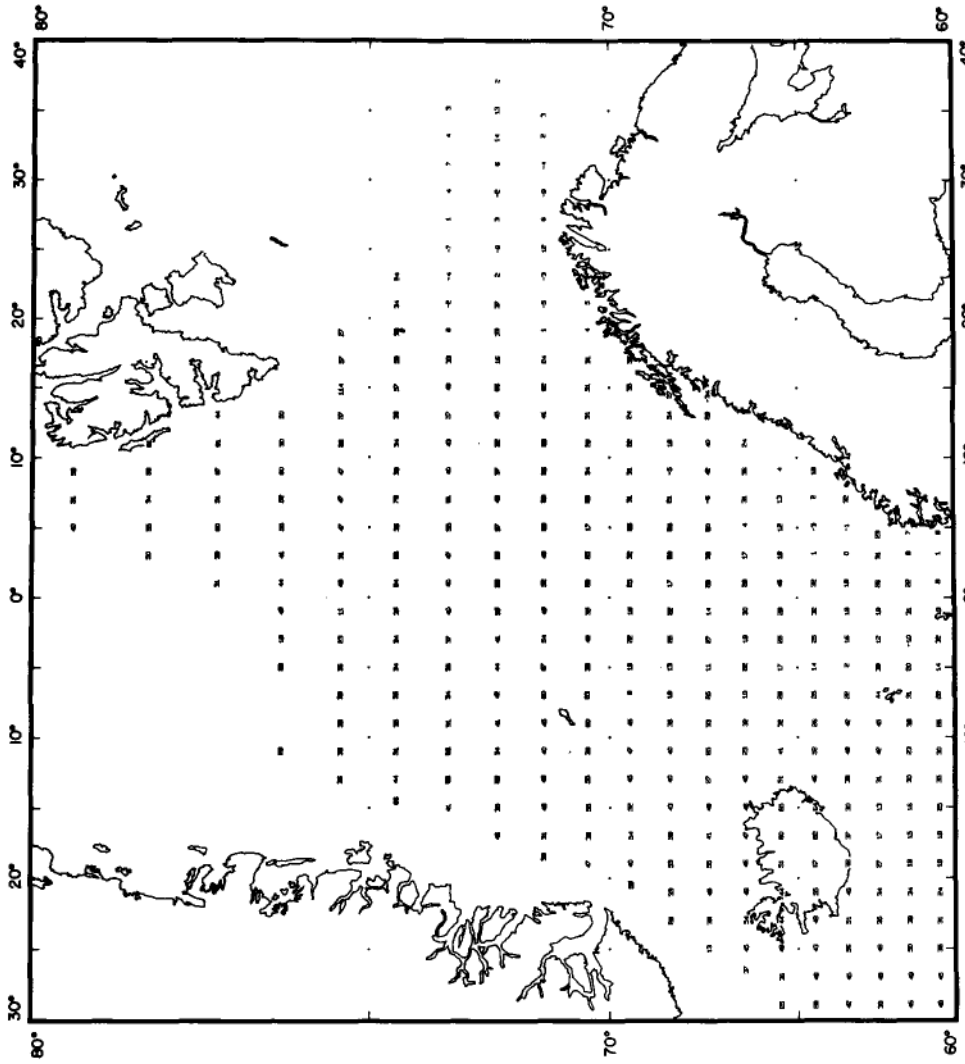

Figure 19. 1 × 2° average free-air gravity anomalies in the Norwegian–Greenland Sea referred to the International Ellipsoid (flattening = 1/297).

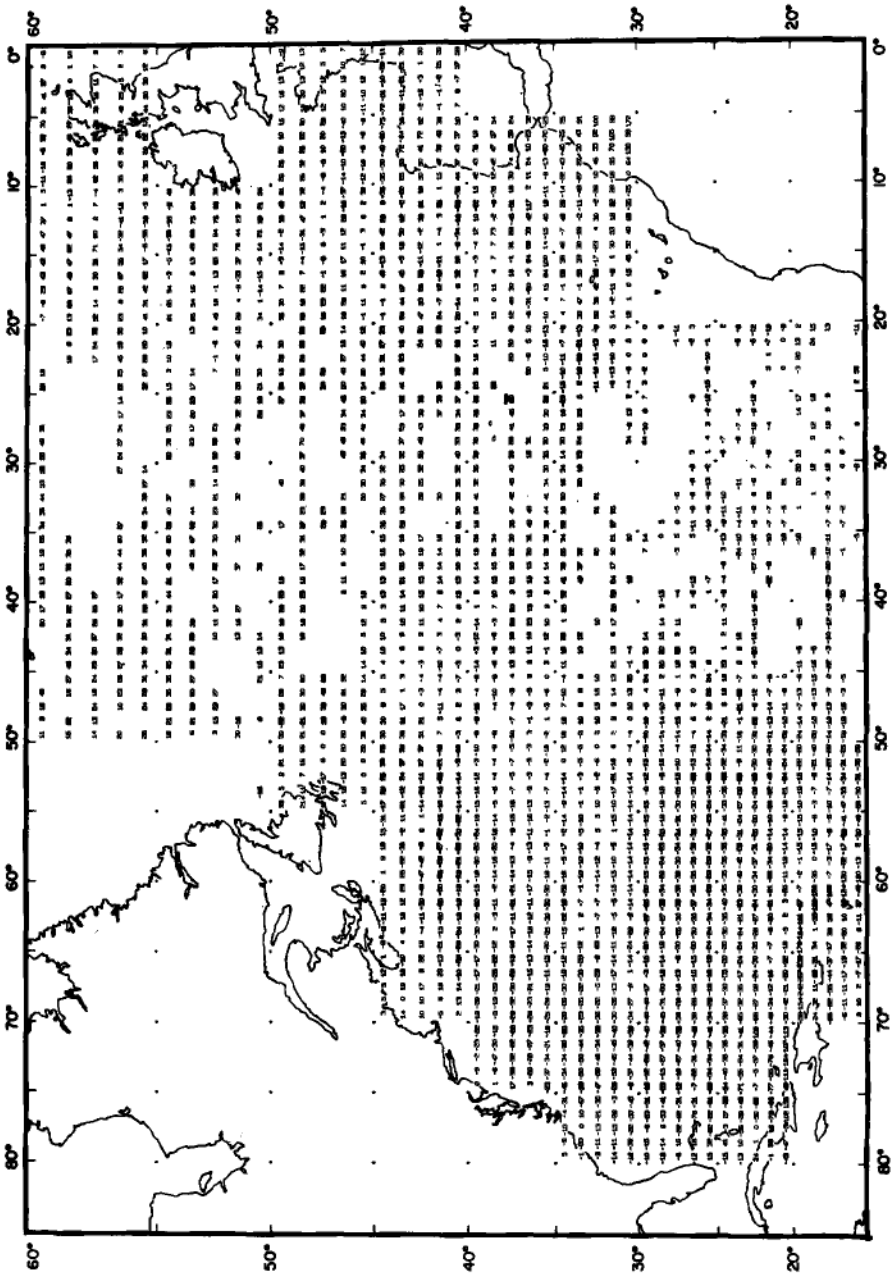

Figure 20. 1 × 1° average free–air gravity anomalies in the North Atlantic Ocean referred to the International Ellipsoid (flattening = 1/297). Many of the values to the west of about 50° are from Talwani *et al.* (1972).

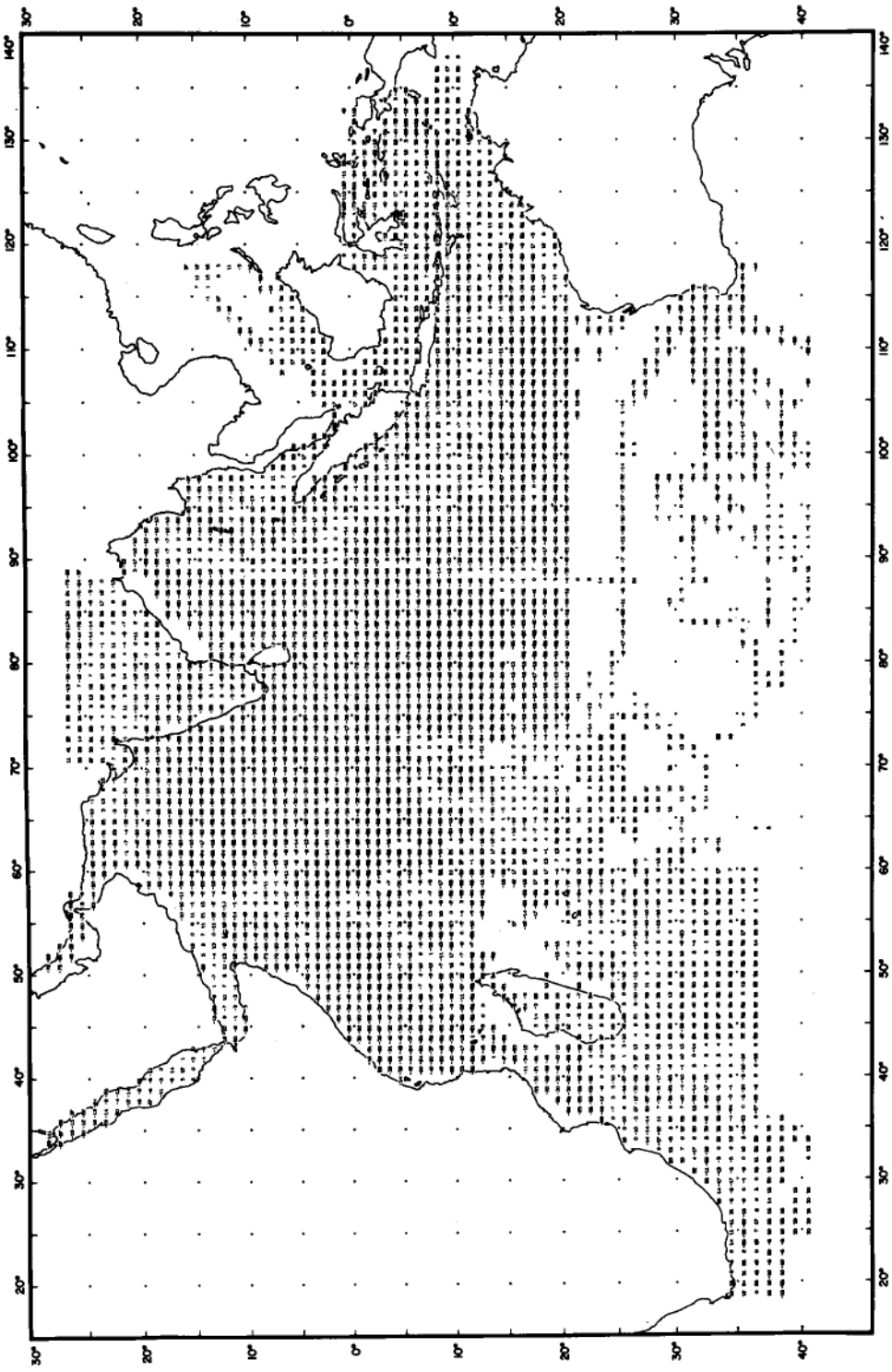

Figure 21. 1 x 1° average free–air gravity anomalies in the Indian Ocean (Kahle & Talwani 1973) referred to the International Ellipsoid (flattening = 1/297).

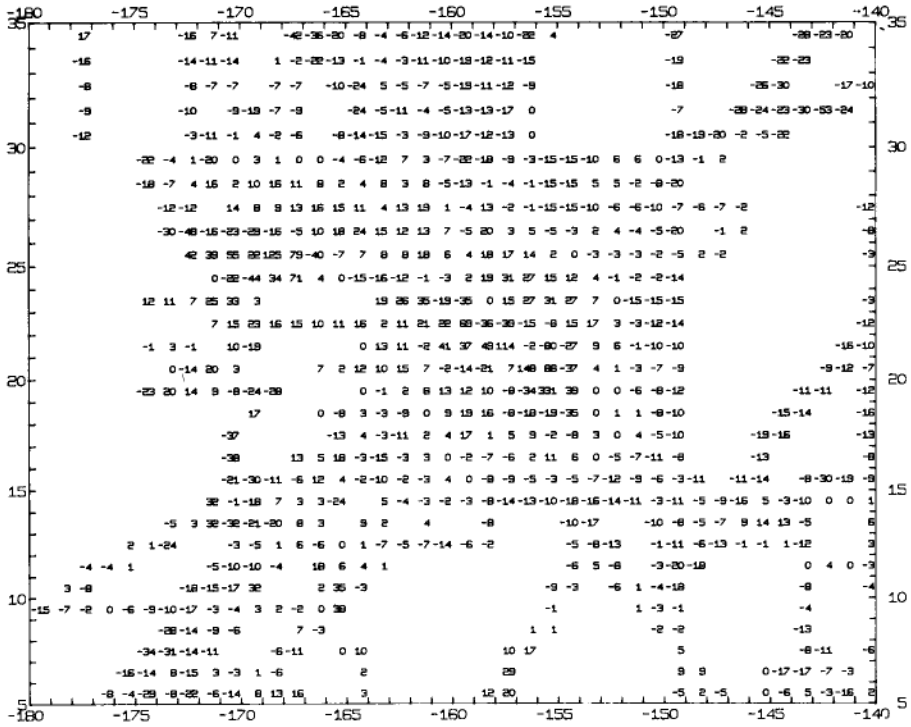

Figure 22. 1 X 1° average free–air gravity anomalies in the vicinity of Hawaii (Watts 1976a) referred to the International Ellipsoid (flattening = 1/297).

Appendix 2

This appendix presents 1 x 1° average residual depth anomalies in the North Atlantic Ocean, Indian Ocean and a portion of the Central Pacific Ocean surrounding Hawaii. Also given are 1 x 2° average residual depth anomalies for the Norwegian–Greenland Sea. Residual depth anomalies are defined as the difference between basement depth corrected for sediment loading and the predicted depth for oceanic crust of the appropriate age (Menard 1973). The depth–age relationship shown in Fig. 6 was used as a reference. Shallower areas have positive depth anomalies, deeper areas have negative depth anomalies. A sediment density of 2.2 g/cm^3 was assumed in making the corrections for sediment loading. Values near continental margins may be somewhat unreliable due to difficulties in properly accounting for sediment loading.

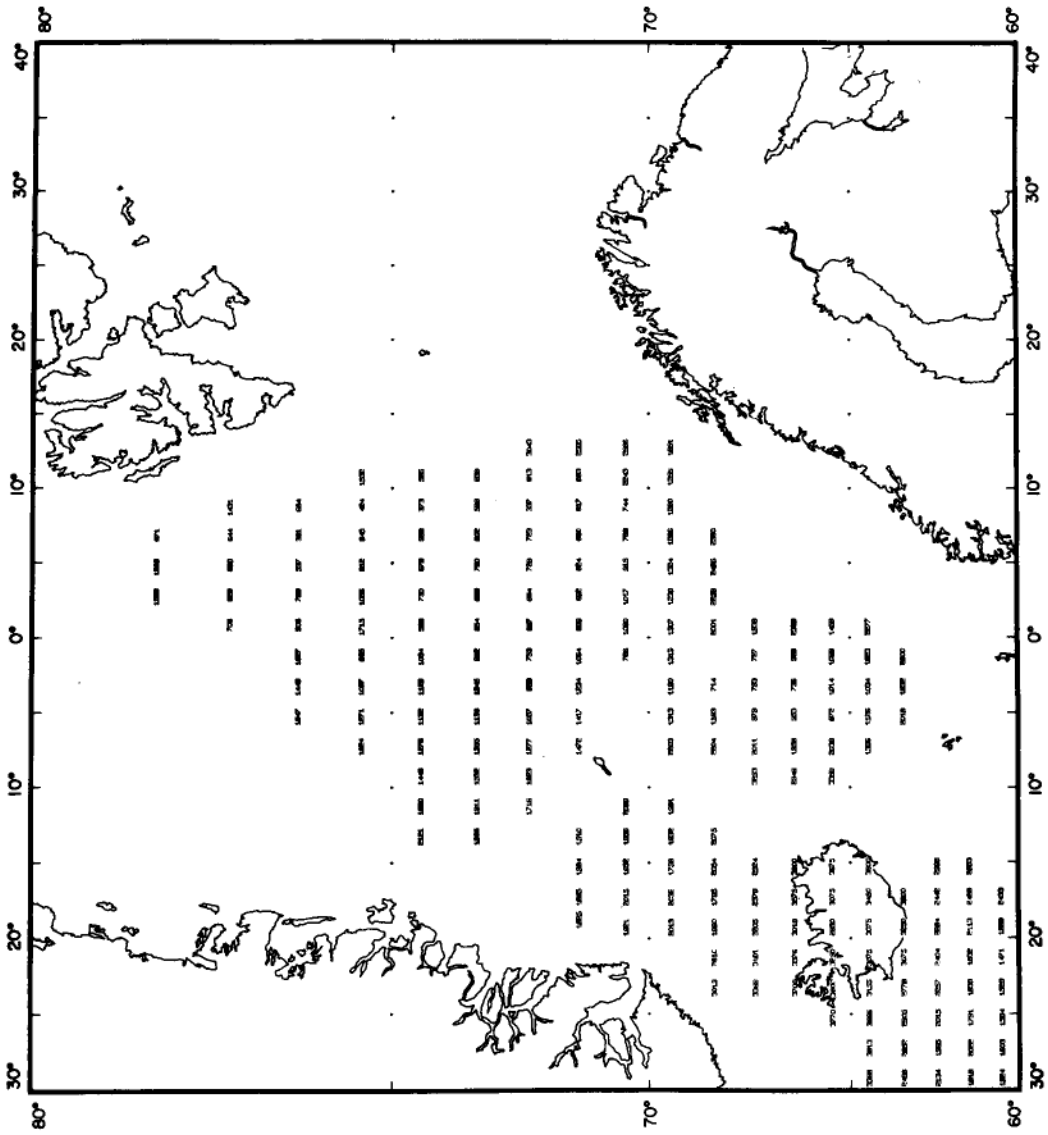

Figure 23. 1 x 2° average residual depth anomalies in the Norwegian–Greenland Sea.

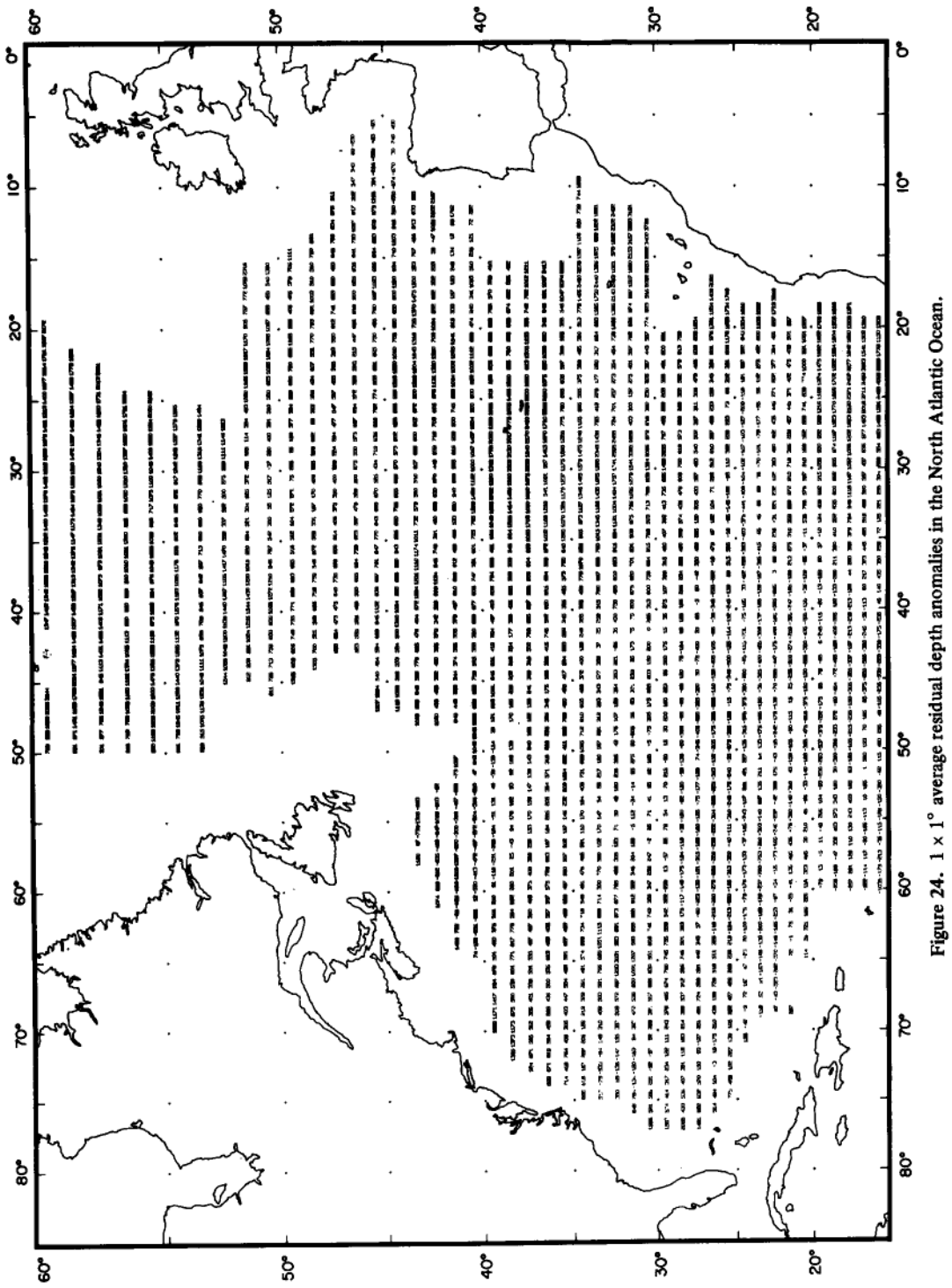

Figure 24. 1 × 1° average residual depth anomalies in the North Atlantic Ocean.

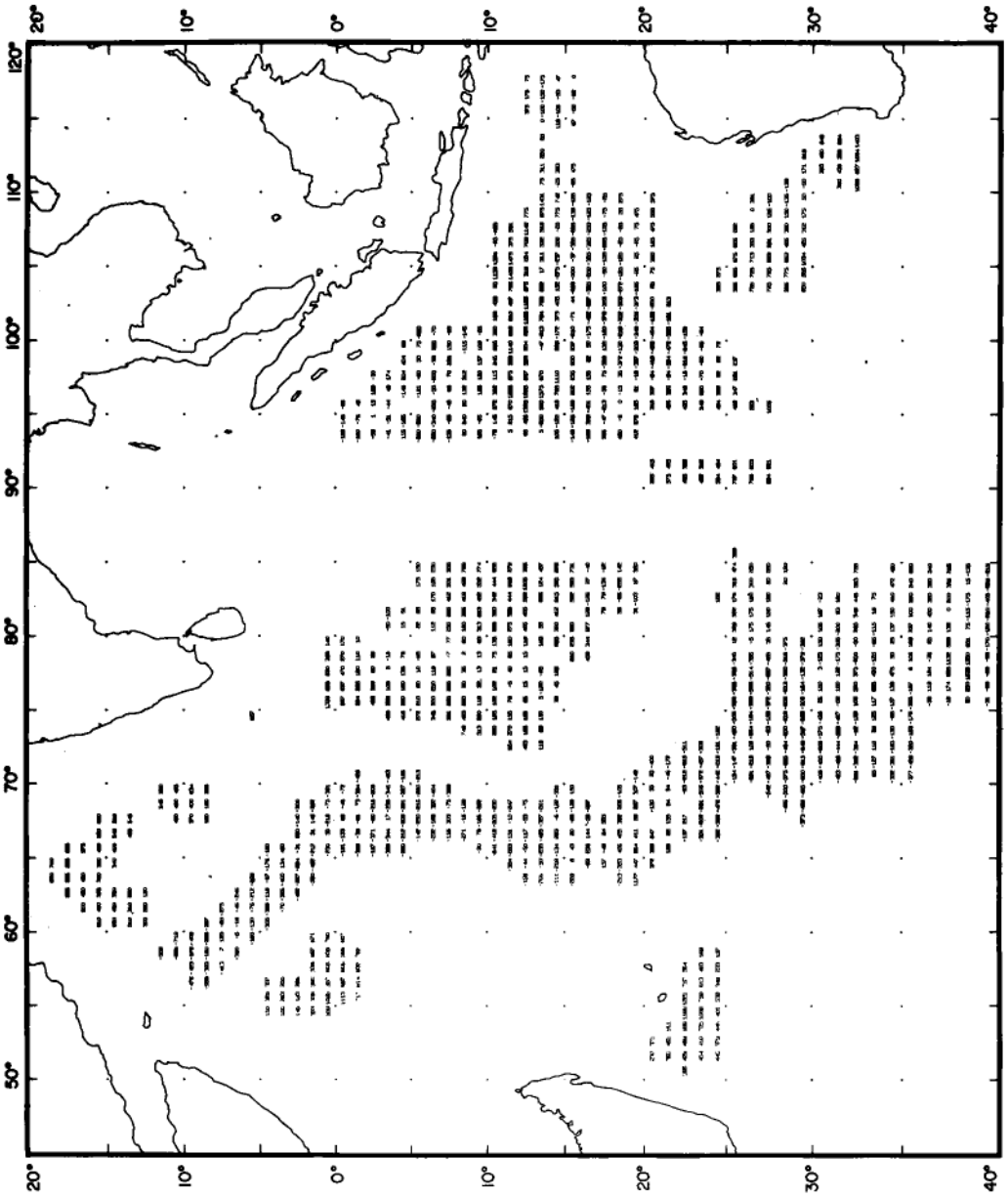

Figure 25. 1 × 1° average residual depth anomalies in the Indian Ocean.

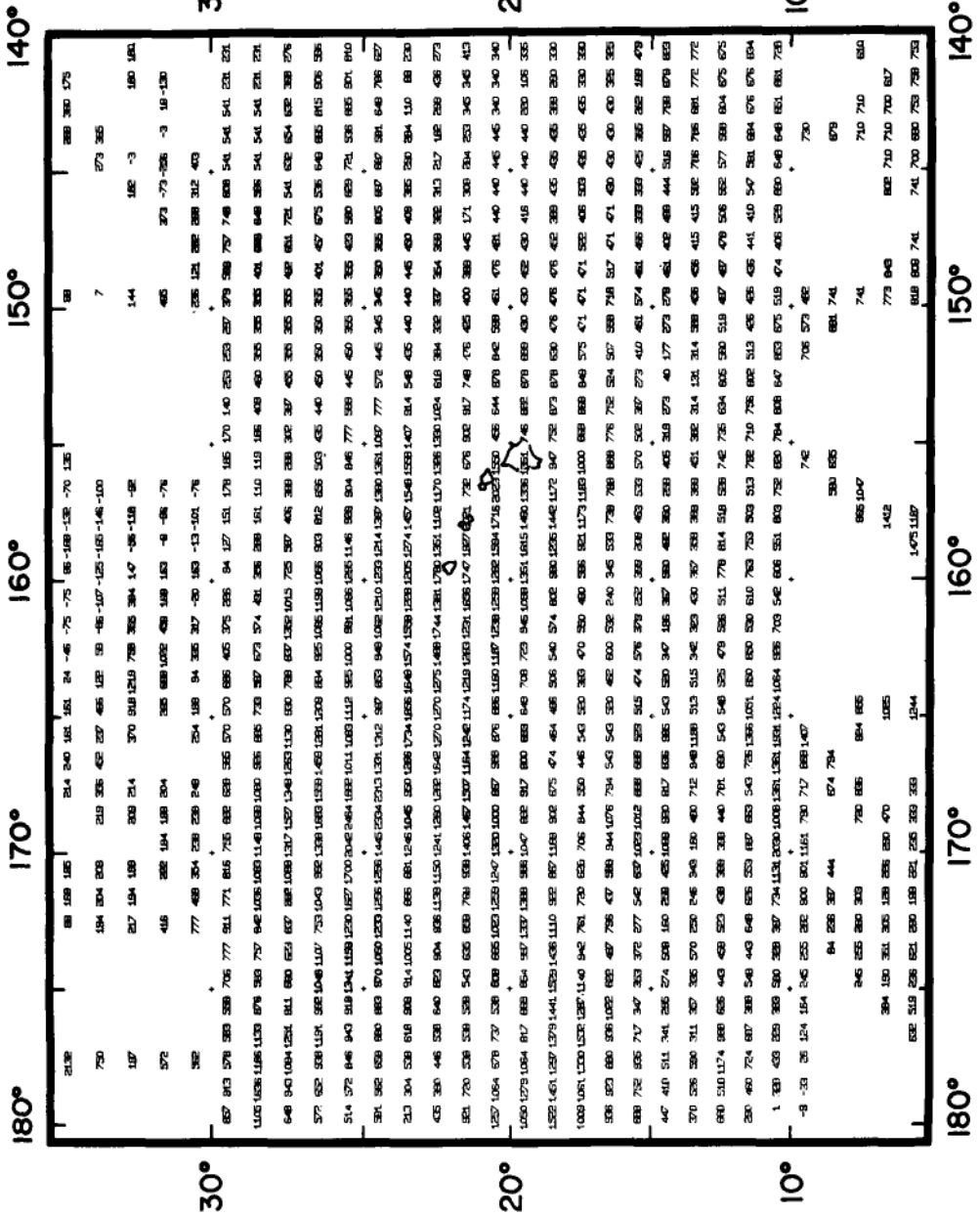

Figure 26. 1 × 1° average residual depth anomalies in the vicinity of Hawaii (Watts 1976a).

Appendix 3

This appendix presents $5 \times 5^\circ$ average free–air gravity and residual depth anomalies. The $5 \times 5^\circ$ averages in the North Atlantic Ocean, Indian Ocean and the vicinity of Hawaii, and the $5 \times 10^\circ$ averages in the Norwegian Sea were prepared from the $1 \times 1^\circ$ averages given in Appendices 1 and 2. The $5 \times 5^\circ$ averages in the South Atlantic Ocean, Southern Indian Ocean and the Eastern Pacific Ocean were prepared from averages along ships' tracks as described earlier and should be regarded as preliminary values. The manner in which they were prepared is responsible for their somewhat irregular distribution in these oceans. The $5 \times 5^\circ$ average residual depth anomalies in the north-eastern Pacific were prepared from $1 \times 1^\circ$ average anomalies given by Menard (1973).

The crosses indicate the centre of the $5 \times 5^\circ$ squares. Numbers above the crosses are depth anomalies and those below are gravity anomalies.

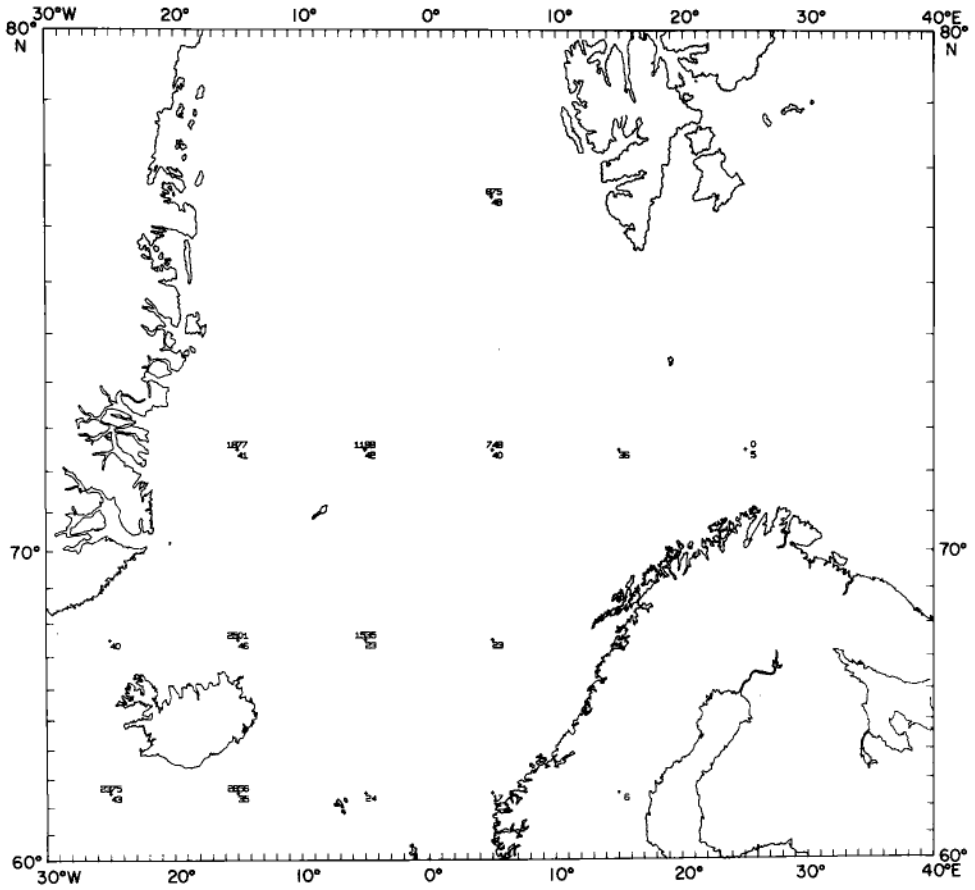

Figure 27. $5 \times 10^\circ$ average free–air gravity and residual depth anomalies in the Norwegian–Greenland Sea. Gravity anomalies are referred to the International Ellipsoid (flattening = 1/297).

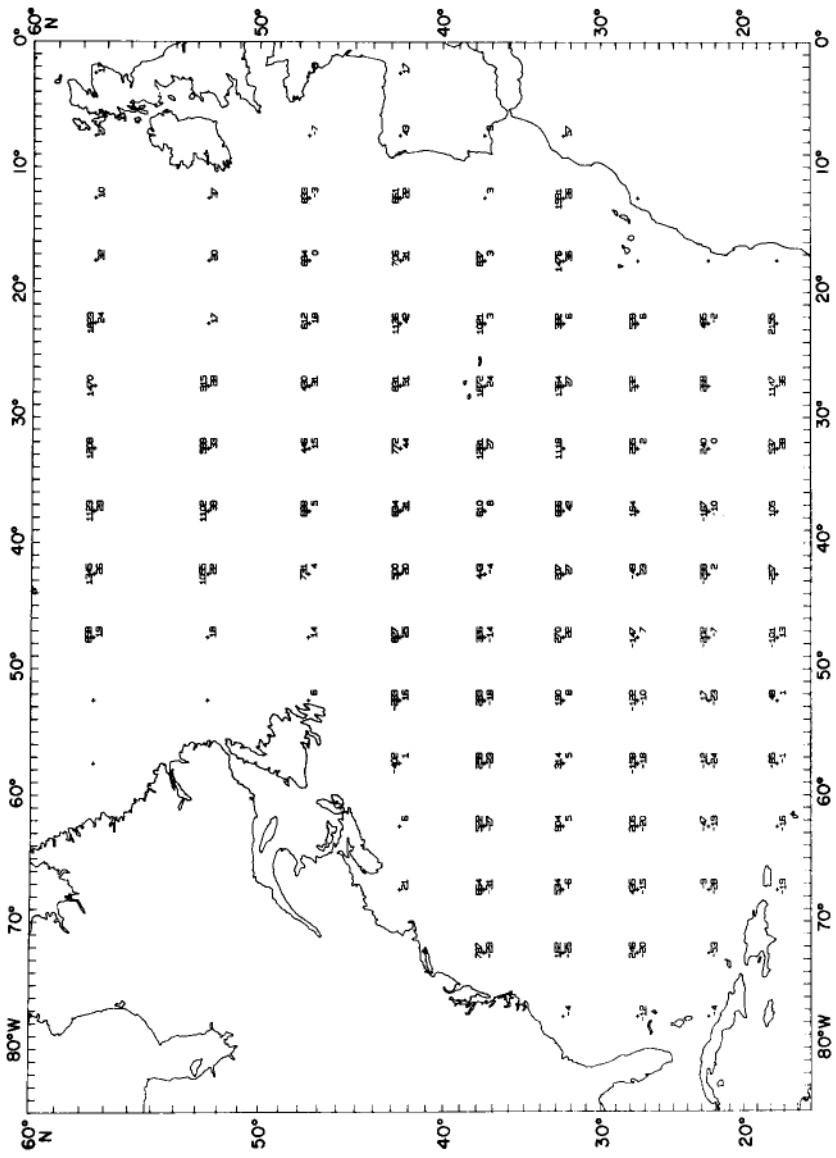

Figure 28. 5 × 5° average free–air gravity and residual depth anomalies in the North Atlantic Ocean. Gravity anomalies are referred to the International Ellipsoid (flattening = 1/297).

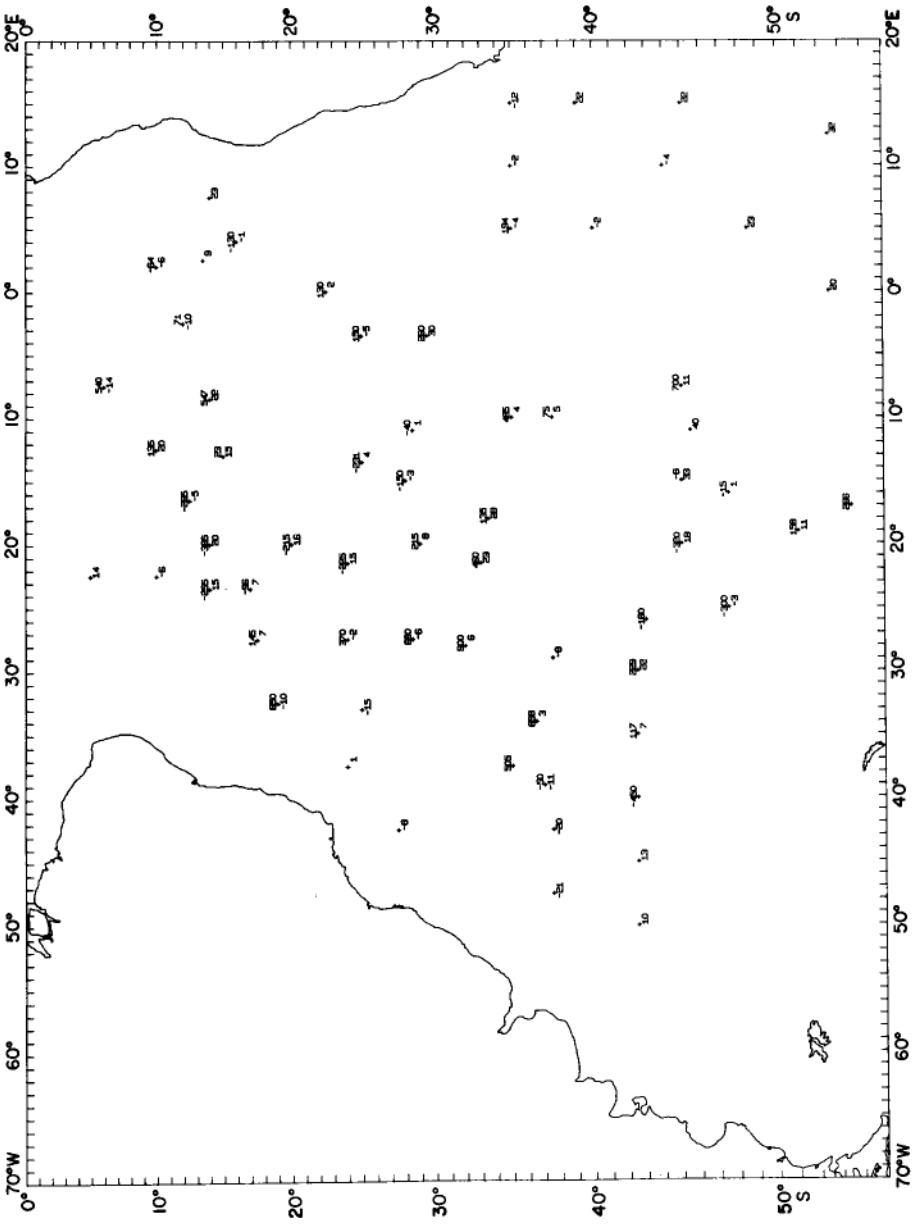

Figure 29. Preliminary 5 x 5° average free–air gravity and residual depth anomalies in the South Atlantic Ocean. Gravity anomalies are referred to the International Ellipsoid (flattening = 1/297).

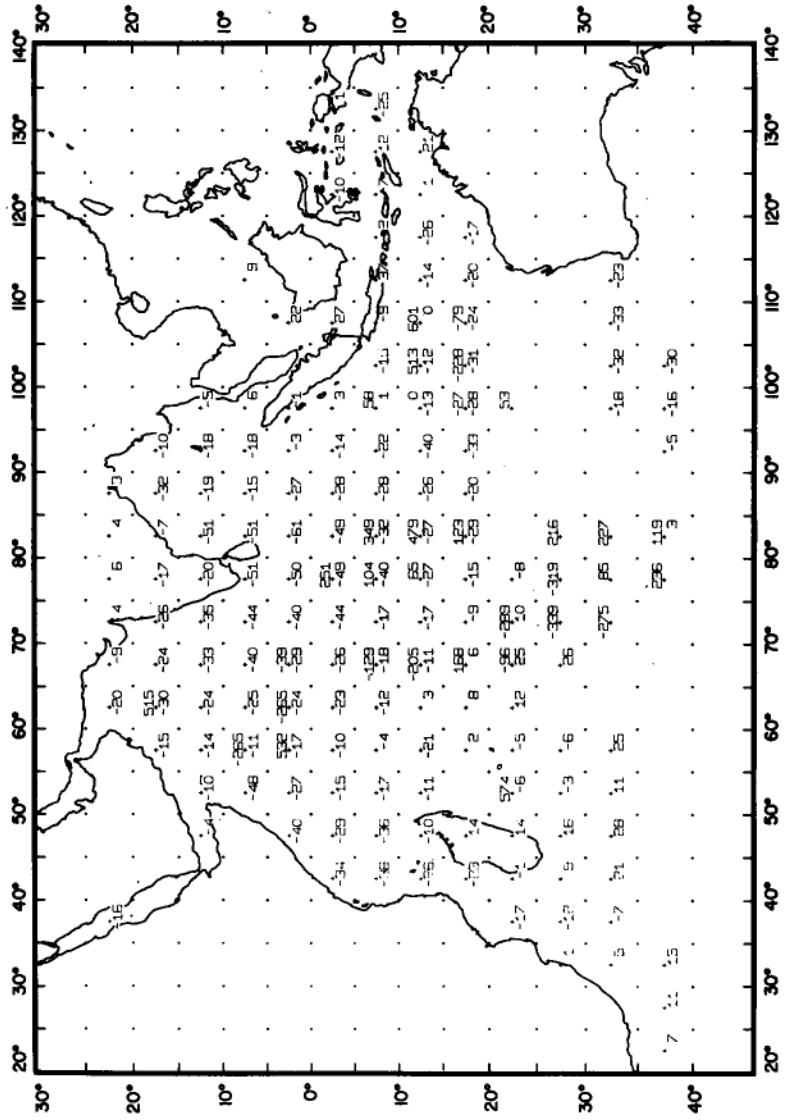

Figure 30. Preliminary 5 x 5° average free–air gravity and residual depth anomalies in the Indian Ocean. Gravity anomalies are referred to the International Ellipsoid (flattening = 1/297).

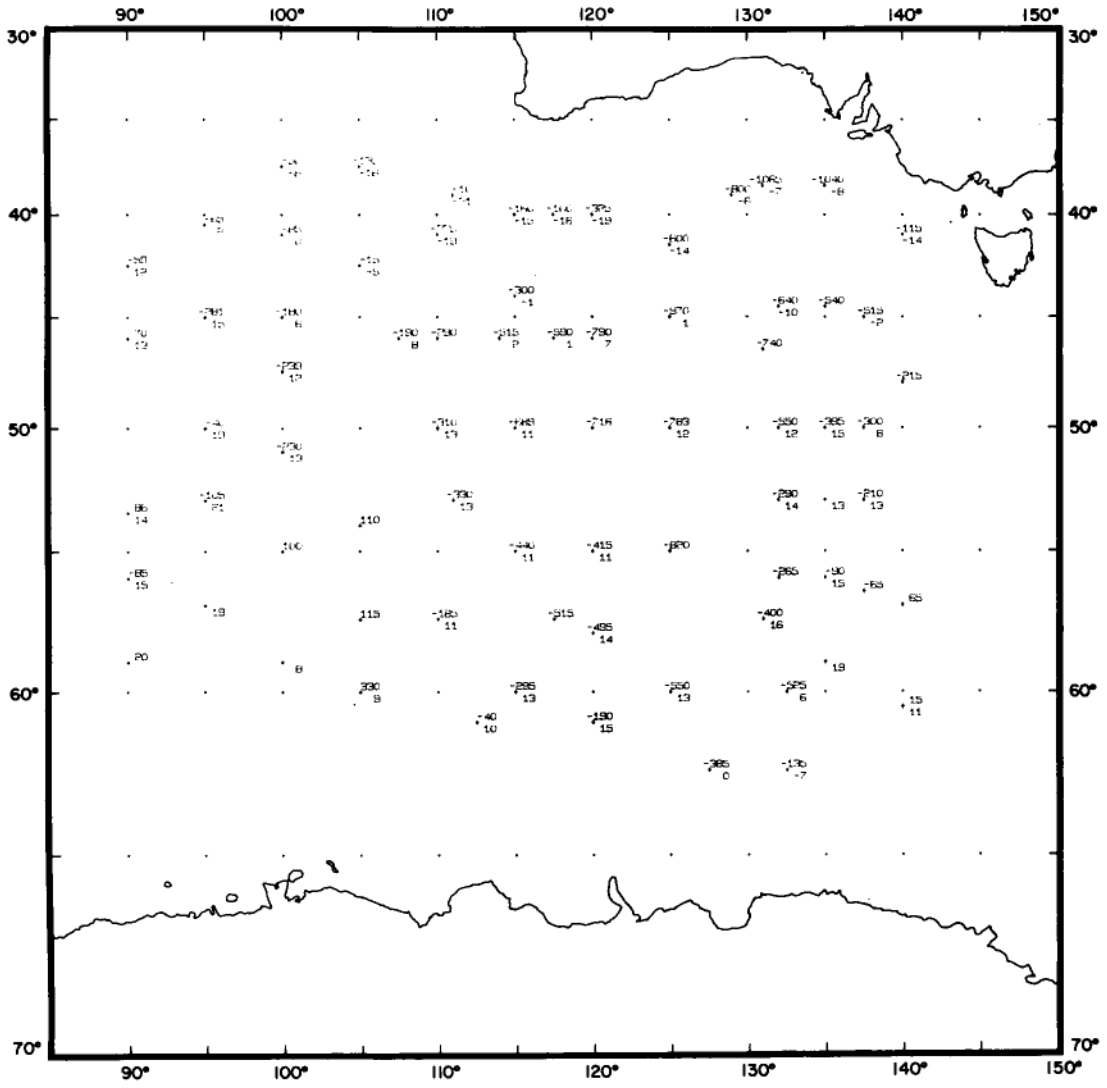

Figure 31. Preliminary 5 x 5° average free–air gravity and residual depth anomalies in the South-east Indian Ocean. Gravity anomalies are referred to the International Ellipsoid (flattening = 1/297).

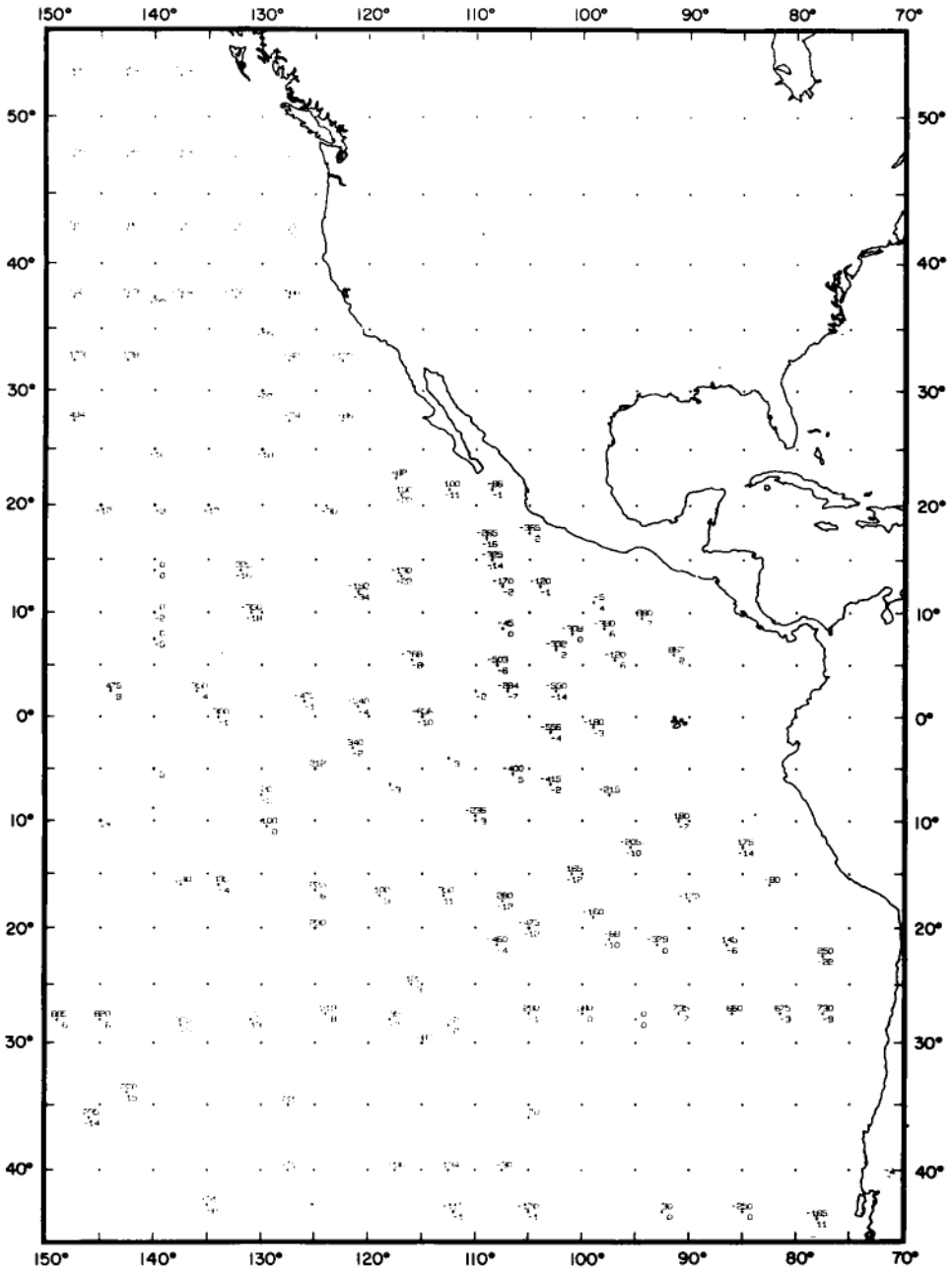

Figure 32. Preliminary 5 x 5° average free–air gravity and residual depth anomalies in the eastern Pacific Ocean. Gravity anomalies are referred to the International Ellipsoid (flattening = 1/297).

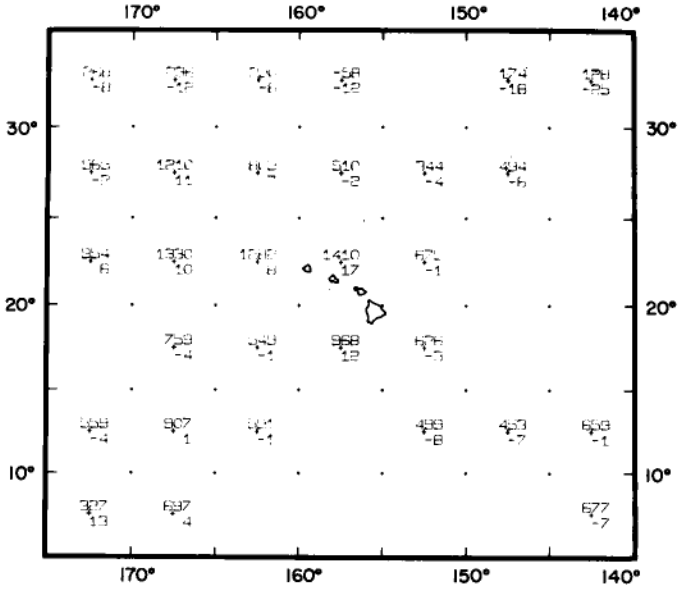

Figure 33. 5 x 5° average free–air gravity and residual depth anomalies in the vicinity of Hawaii (Watts 1976a). Gravity anomalies are referred to the International Ellipsoid (flattening = 1/297).

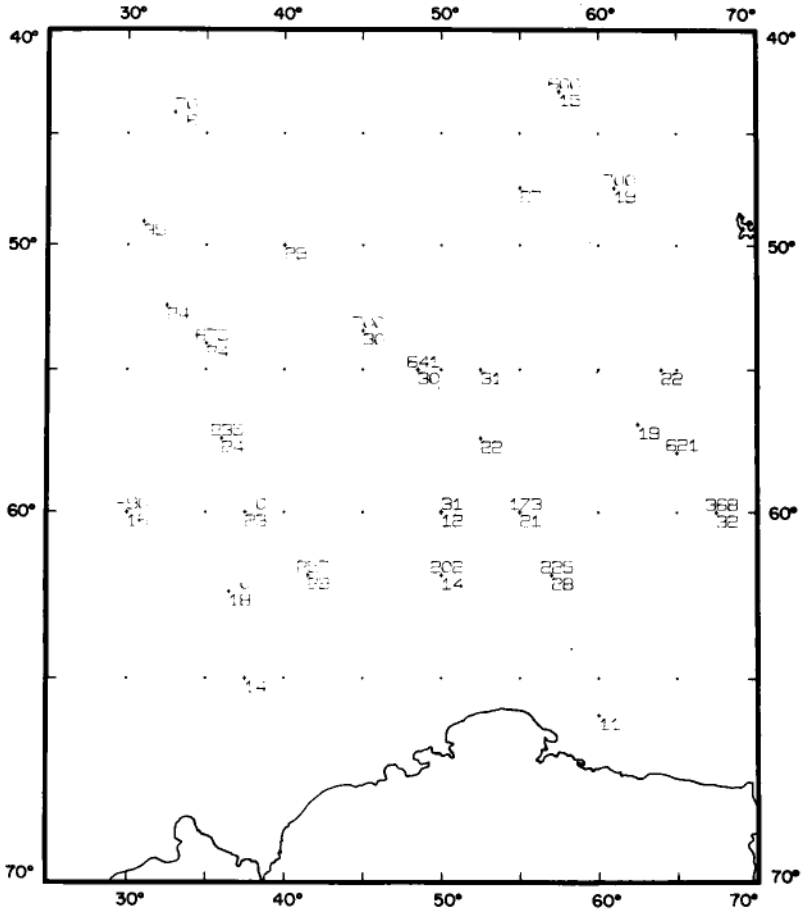

Figure 34. Preliminary 5 X 5° average free–air gravity and residual depth anomalies in the South-west Indian Ocean. Gravity anomalies are referred to the International Ellipsoid (flattening = 1/297).